

A THESIS

Molecular studies in the Gas Phase
by Microwave Spectroscopy.

Submitted to the University of Glasgow
in part fulfillment of the requirements
for the degree of Doctor of Philosophy
in the Faculty of Science

by

JOHN N. MACDONALD, B.Sc.,

Chemistry Department

August 1969.

ProQuest Number: 11011907

All rights reserved

INFORMATION TO ALL USERS

The quality of this reproduction is dependent upon the quality of the copy submitted.

In the unlikely event that the author did not send a complete manuscript and there are missing pages, these will be noted. Also, if material had to be removed, a note will indicate the deletion.



ProQuest 11011907

Published by ProQuest LLC (2018). Copyright of the Dissertation is held by the Author.

All rights reserved.

This work is protected against unauthorized copying under Title 17, United States Code
Microform Edition © ProQuest LLC.

ProQuest LLC.
789 East Eisenhower Parkway
P.O. Box 1346
Ann Arbor, MI 48106 – 1346

ACKNOWLEDGEMENT

I would like to express my sincere thanks to Dr. J. K. Tyler for guidance and encouragement throughout this work.

Thanks are due to my former colleague Dr. D. G. Lister and to the research students of the departments of physical and theoretical chemistry for many discussions and suggestions.

Thanks are also due to Dr. N.M.D. Brown of the University of Glasgow for providing the original samples of Υ - Pyrone and thiopyrone.

I am grateful to Mr. P. Carrington on whose computer program the M. O. calculations on Υ - Pyrone were carried out and to Mr. J. Hutchison for the photographic prints.

Finally I would like to thank Professor D.W.J. Cruickshank and Professor J. M. Robertson in whose Departments this work was carried out, and the Science Research Council for a maintenance grant.

SUMMARY

In this thesis an account is given of studies of the rotational spectra of γ - Pyrone, thiapyrone, cyanamide, nitramide, dideuterocyanamide and aminoacetonitrile. The spectra of these compounds were studied in the Stark modulation spectrometer which is described briefly in the introductory chapter.

γ - Pyrone and thiapyrone were studied as part of an investigation of the molecular geometries of compounds belonging to the 4 - Pyrone series. Five isotopic species of γ - Pyrone and the normal species of thiapyrone have been studied. It is concluded that both molecules are planar structures in the ground vibrational state and that there is some evidence of angular distortion of the rings to accommodate the heteroatoms in a planar structure. The Stark effect of γ - Pyrone has been found to be non-quadratic and a special treatment of the Stark effect has been carried out enabling the dipole moment of the molecule to be obtained.

A study has been made of ^{14}N - quadrupole coupling in the spectra of cyanamide and nitramide and the coupling constants obtained for these molecules. Conclusions are drawn regarding the delocalisation of the lone-pair electrons of the

amino nitrogen atom into the π - systems of the molecules. An extrapolation of these results to the more general NH_2 X system (X an electron withdrawing group) is suggested.

The energy levels of dideuteroacyanamide are highly perturbed by vibration/rotation interactions. It has been possible to locate the $K_{-1} = 2$ rotational energy levels of the ground vibrational state relative to the $K_{-1} = 1$ levels of the first excited state. It is concluded that second order perturbation theory is insufficient for the calculation of these energy levels and that a more complete calculation is required.

Some preliminary conclusions about the structure of aminoacetonitrile have been obtained. Three species have been studied and the amino hydrogen atom coordinates located exactly by isotopic substitution. The molecule exists in the conformation with the amino hydrogen atoms trans to those of the methylene group.

CONTENTS

		page
<u>Chapter 1</u>	Introduction	1
section 1	The energy levels of a rigid asymmetric rotor	2
2	The selection rules for an asymmetric rotor	4
3	The spectrometer	5
	References	8
<u>Chapter 2</u>	The microwave spectra of γ - Pyrone and thiapyrone	
section 1	Introduction	9
2	Analysis of the spectrum of γ - Pyrone	13
3	Stark effect and dipole moment of γ - Pyrone	34
4	Structure of γ - Pyrone	45
5	The spectrum and structure of thiapyrone	54
6	Discussion	62
	References	67
<u>Chapter 3</u>	Nitrogen ¹⁴ - Quadrupole Coupling in the Microwave Spectra of Cyanamide and Nitramide	
section 1	Introduction	69

		page
<u>Chapter 3</u> (cont'd.)		
section 2	Quadrupole coupling in molecules containing two Nitrogen Nuclei.	73
3	Analysis of the Spectra	82
3.1	Cyanamide	82
3.2	Nitramide	92
4	Discussion of Results	94
	References	102
<u>Chapter 4</u>	Vibration - Rotation interactions in dideutero cyanamide.	
section 1	Introduction	104
2	Stark effects in the $J = 2 - 1$ transition	109
3	The $v = 1, K_{-1} = 1, \mu_a Q$ - branch lines	116
4	The μ_c inversion transitions in ND_2CN	123
5	The Energy levels in ND_2CN	135
6	Discussion	138
	References	142
<u>Chapter 5</u>	The Conformation of Aminoacetonitrile.	
section 1	Introduction	143

	page
Chapter 5 (Cont'd.)	
section 2	145
3	159
4	160
References	164
<u>Chapter 6</u>	165
Chemical Preparations.	
References	175
<u>Appendix A</u>	177
The Secular Determinants for ^{14}N - Quadrupole Coupling Energies in molecules containing two Nitrogen Atoms.	
<u>Appendix B</u>	180
Extended Perturbation Treatment of the Stark Effect in γ - Pyrone	
<u>Appendix C</u>	182
Points on the graph of $\frac{\Delta\nu}{J+1} / (J+1)^2$ for the μ_c Q - branch series, of ND_2CN .	
<u>Appendix D</u>	183
Reprint of "Nitrogen 14 Quadrupole coupling in the microwave spectrum of Cyanamide"	

CHAPTER 1.

INTRODUCTION.

Rotational spectra of low-pressure gases are a source of a variety of information about the molecules constituting the gases. This thesis contains an account of recent studies of the microwave spectra of cyanamide (NH_2CN), nitramide (NH_2NO_2), γ - Pyrone and thiopyrone, and aminocetonitrile ($\text{NH}_2\text{CH}_2\text{CN}$).

It is convenient to divide these molecules into four groups according to the particular aspect of rotational spectroscopy which was of prime interest in the analysis of the spectra carried out in this work. These four groups are represented in the thesis by chapters 2 - 5, chapter 6 being a description of the chemical preparation of the compounds and their isotopic species.

A discussion of the classical mechanics of rotating molecules may be found in reference 1, and the corresponding quantum mechanical treatment in reference 2. For details of the experimental techniques and the standard methods of analysis of microwave spectra, references 3, 4, 5 and 6 should be consulted.

Where it was felt to be appropriate, certain aspects of the theory have been discussed in the text of the thesis. This applies particularly to the description of the anomalous Stark effect of γ - Pyrone given in chapter 2 and to the account of

nuclear quadrupole coupling in molecules containing two nitrogen nuclei in chapter 3.

The remainder of this chapter is devoted to a description of the method of calculation of rigid asymmetric rotor energy levels and to the selection rules for molecules in this class. Also included is a description of the spectrometer used in this work.

1. The energy levels of a rigid asymmetric rotor.

As for symmetric tops the rotational angular momentum quantum number J and the projection of the total rotational angular momentum on a space fixed axis M , are good quantum numbers for the asymmetric top. The projection of the total rotational angular momentum on a molecule fixed axis system K is not however constant in an asymmetric rotor with the result that K cannot be considered as a good quantum number. It is conventional to label the asymmetric rotor energy levels using the value K would have in the prolate and oblate symmetric top limit.

It can be shown² that the energy levels of an asymmetric rotor may be written in terms of Ray's asymmetry parameter κ as,

$$E = \frac{A+C}{2} J(J+1) + \frac{A-C}{2} E(\kappa) \quad (1)$$

where A and C are rotational constants defined as below and $E(\kappa)$ is the reduced energy for the molecule. The rotational constants are related to the moments of inertia along the principal molecular axes in the following way,

$$X = \frac{h}{8 \pi^2 I_x}$$

Where X is in Mc/s and I_x in a.m.u. \AA^2 then

$$X \times I_x = 5.05531 \times 10^5 \text{ Mc/s (a.m.u.}\text{\AA}^2\text{)}$$

The reduced energy $E(\kappa)$ of (1) is the energy of a molecule with rotational constants $l, \kappa, -l$. As such $E(\kappa)$ may be obtained from the matrix elements of the Hamiltonian for the rigid asymmetric rotor². In this work tables have been used giving $E(\kappa)$ accurate to eight significant figures at intervals of 0.001 in κ . In cases where κ was intermediate between two consecutive entries in the tables, linear interpolation was used to determine $E(\kappa)$ for a required energy level.

The procedure described above was used in the calculations of the energy levels of γ - Pyrone and thiapyrone described in chapter 2. In the cases of the remaining molecules which have κ values very close to the prolate limit it is more convenient to write the energies in terms of an expansion such as that due to Polo. This case is discussed in chapter 4.

2. The Selection Rules for an Asymmetric Rotor.

The selection rule for J in an asymmetric rotor is $\Delta J = 0, \pm 1$. The selection rules for the pseudoquantum numbers K can be derived from a consideration of the transformation properties of the asymmetric rotor wave functions under the operations of the four group V ,¹⁻⁶.

One aspect of the selection rules of particular interest in this work is concerned with the effects of inversion on the selection rules of a molecule like ND_2CN .

The selection rules for J and K are as above. The dipole matrix element should now however be expressed as

$$\langle n | \mu | m \rangle = \int \psi_{R,n}^* \cdot \psi_{V,n}^* \mu \psi_{R,m} \cdot \psi_{V,m} d\tau \quad (2)$$

where ψ_R is an asymmetric rotor wave function and ψ_V a vibrational wave function.

Equation (2) may be factorised into a rotational matrix element and a vibrational matrix element both of which must be non-vanishing for an inversion transition to be allowed.

Considering the inversion integral

$$\langle n | \mu | m \rangle_V = \int \psi_{V,n}^* \mu_g \psi_{V,m} d\tau$$

$\langle n | \mu | m \rangle_V$ must be totally symmetric and thus if μ_g reverses direction during the inversion then $\psi_{V,n}$ and $\psi_{V,m}$ must have opposite symmetries.

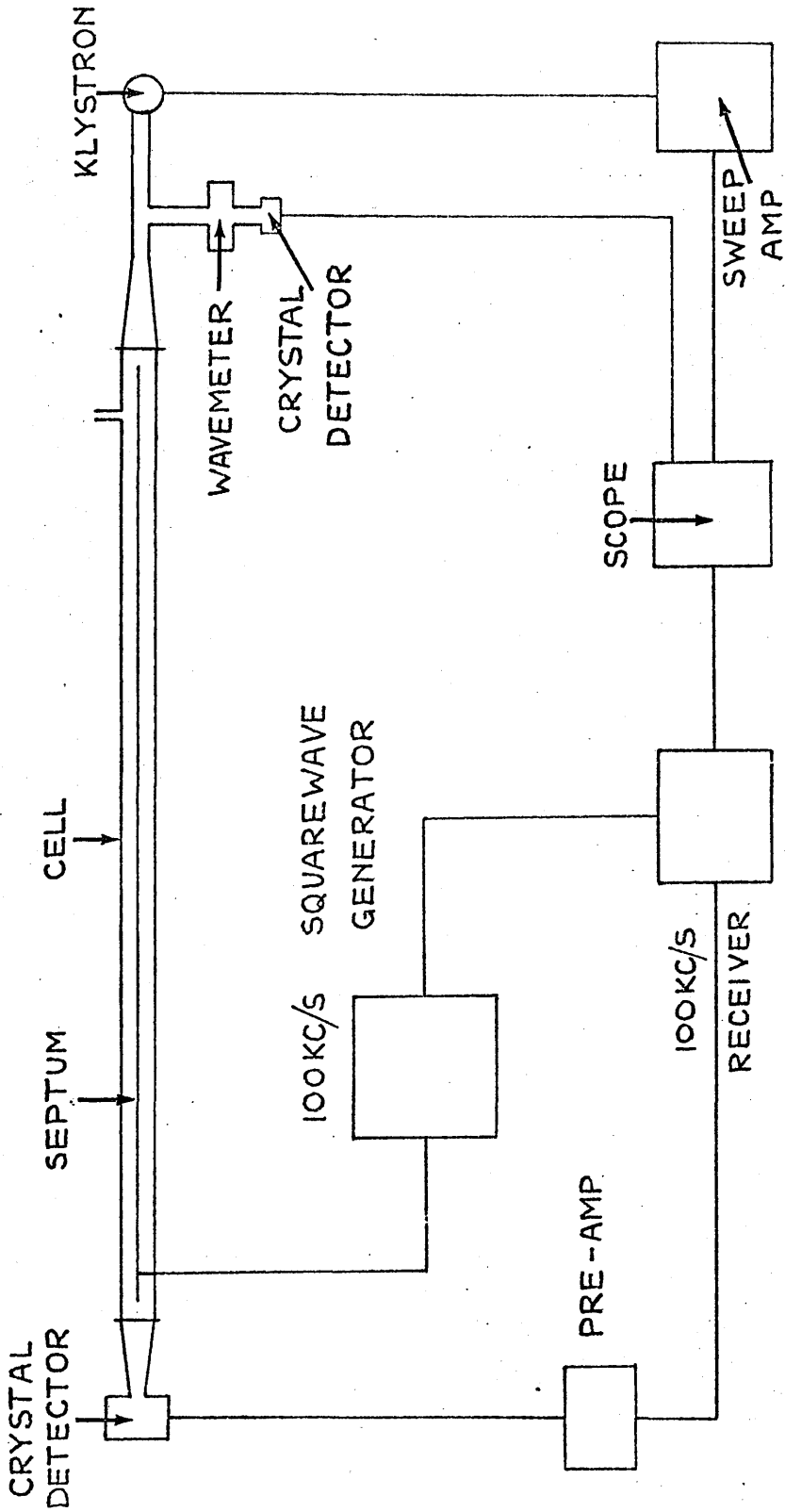
Thus for HD_2CN transitions involving the μ_c component of the dipole moment will be between rotational energy levels associated with vibrational states of opposite symmetries.

3. The Spectrometer.

All the experimental spectroscopy in this work was carried out on a conventional Stark modulation spectrometer employing square wave modulation and operating in the temperature range $0^\circ\text{C} - 50^\circ\text{C}$. A block diagram of the spectrometer is shown in fig. 1 and a general view of the instrument in the accompanying photograph.

The absorption cell is constructed from a ten foot length of copper X - band waveguide with a flange at either end and sealed by mica windows cemented to the flanges with wax. This has slight disadvantages in that the temperature of the cell cannot be raised much above 50°C without melting the wax. The method of heating the cell is described in chapter 2 section 5.

The Stark electrode is mounted parallel to the broad face of the waveguide and is supported on milled teflon strips. Modulation is applied in the form of a 100 Kc/s zero-based square wave from an Industrial Components Incorporated generator capable of producing an applied field of up to 4000 volts/cm. The square wave generator is used in conjunction with a phase



Block Diagram of the Stark Modulation Spectrometer.

fig. 1.



sensitive detection system of the same manufacture.

The low frequency range, 8 - 12 Gc/s, is covered by a low voltage E.M.I. klystron and a number of high voltage E.M.I. Klystrons extend the working range from 12 - 40 Gc/s.

The signal detected by the crystal detector is amplified in a preamplifier unit before being fed into the phase sensitive detector. It may then be presented either directly on an oscilloscope or on a pen recorder. When oscilloscope presentation is used gain in sensitivity can be obtained by using a slow sweep rate on the oscilloscope coupled with narrow band width in the receiver. When the recorder is used the klystron is driven by an electric motor attached directly to the tuning spindle of the klystron.

Direct reading cylindrical cavity wave meters are used to obtain approximate frequency measurements (± 5 Mc/s). Accurate frequency measurement is carried out using the following system. A Micro-Now frequency multiplier chain provides harmonics of 450 Mc/s, 150 Mc/s and 50 Mc/s of a 5 Mc/s fundamental variable frequency crystal oscillator. It has been found that with a simple modification to the output circuit of the Micro-Now unit it is possible to produce useful harmonics up to ~ 40 Gc/s as opposed to the 25 Gc/s specification of the standard instrument⁷.

The output from the multiplier chain is fed onto a crystal which is also receiving a small amount of the microwave power from the klystron via a directional coupler, and which serves both as a mixer and as a harmonic generator. The harmonics, spaced by 50 Mc/s are mixed with the klystron power and the beat frequency taken through a radio receiver. The result is presented on a second trace on the oscilloscope. When the beat frequency equals the radio receiver setting a sharp marker pip appears on the oscilloscope trace. Two such pips separated by twice the receiver setting emanate from each harmonic.

The frequency of the variable frequency oscillator is then tuned to set each of the markers in turn on the line to be measured. This procedure is carried out with the klystron sweeping in both forward and reverse directions and the mean of the settings taken. This technique eliminates delays.

The oscillator frequency (~ 5 Mc/s) is measured to ± 0.1 c/s using a Marconi frequency counter calibrated against the 200 Kc/s transmission of the B.B.C. Droitwich transmitter. The harmonic of the oscillator in use at a given time is determined from wave meter measurements. The method enables the frequencies of the stronger lines measured in this work to be obtained to ± 0.05 Mc/s, the majority of the weaker line measurements in the following chapters are however probably accurate to only about ± 0.1 Mc/s.

REFERENCES

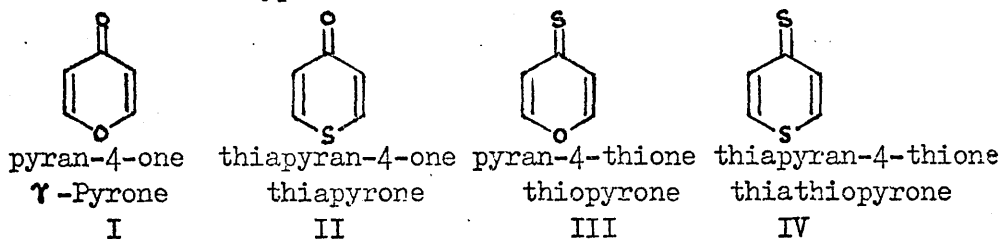
1. H. Margenau and G.M. Murphy, "The Mathematics of Physics and Chemistry", D. Van Nostrand Co., New Jersey (1956)
2. H. C. Allen Jr., and P. C. Cross, "Molecular Vib-Rotors" J. Wiley & Sons, New York (1963)
3. C. H. Townes and A. L. Schawlow, "Microwave Spectroscopy", McGraw Hill (1955)
4. T. M. Sugden and C. N. Kenney, "Microwave Spectroscopy of Gases", D. Van Nostrand Co., London (1965)
5. W. Gordy, W.V. Smith and R. F. Trambarulo, "Microwave Spectroscopy", Dover Publications Inc., New York (1953)
6. J. E. Wollrab, "Rotational Spectra and Molecular Structure", Academic Press, New York (1967)
7. J. K. Tyler, Private Communication.

CHAPTER 2.

The Microwave Spectra of γ -Pyrone and Thiapyrone.

1. Introduction.

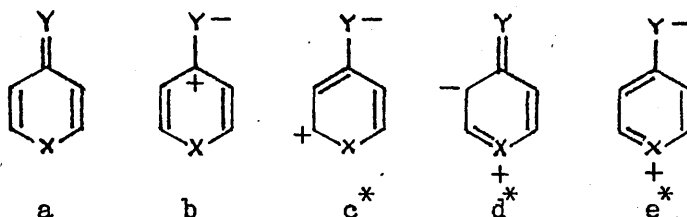
The series of compounds I - IV known as the 4-pyrone has long been known to be aromatic in the sense that the molecules comprising the series show considerable reluctance to undergo chemical reactions typical of the olefins.



The more modern definition of aromaticity is in terms of delocalisation of π - electrons over the ring system resulting in a large resonance energy and unusual stability of the ring to chemical reactions. The degree to which the 4-pyrone are aromatic by this latter definition hinges on the availability of the lone-pair electrons of the ring hetero-atom for interaction with the π - electron system of the conjugated part of the molecule. For such an interaction to take place to any significant extent it is necessary that the 4-pyrone be planar or nearly planar structures.

The chemical properties of these molecules can be understood in terms of a valence - bond description. It

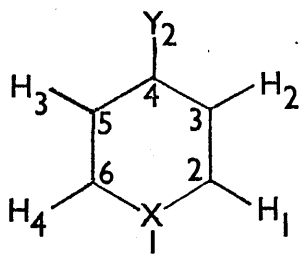
has been the usual practice to assume planarity of the systems and to describe the molecules as resonance hybrids of the canonical forms a - e.



where X and Y can be sulphur or oxygen atoms. The asterisk indicates the forms for which there are clearly two equivalent structures.

A large contribution from e* to the molecular wave functions would suggest that the molecules would be highly polar and this is indeed confirmed by solubility studies¹. The dipole moment of each member of the series has been measured in benzene solution² the experimental values ranging from ~ 3.7D for Y - Pyrone to ~ 4.4D for thiathiopyrone.

Molecular orbital calculations carried out on the series^{3,4} suggest that the molecules have a large resonance energy and that the electron density at C₃ and C₅ is higher than at C₂ and C₆ (the numbering system used here is shown in fig.1). These facts are consistent with experimental evidence that electrophilic substitution occurs at the 3 and 5 ring positions and nucleophilic attack takes place at the 2 and 6 positions.



Numbering system for 4-Pyrones
fig.1

The N.M.R. properties of the 4-pyrones support the presence of a ring current ¹. This would be expected if the rings were aromatic and the lone-pair electrons of X were delocalised into the π - systems of the molecules. The observed ring current is however very much smaller than might be expected for a fully aromatic system.

In order to definitely establish the planarity of the rings and to obtain an accurate measure of ring geometry it was decided to study the microwave spectra of these compounds. γ -Pyrone, having a high dipole moment of 3.72D and a vapour pressure of 0.2 m.m. of mercury at room temperature, is particularly suitable for study by microwave spectroscopy.

Five isotopic species of this molecule have been studied in detail,

γ - Pyrone	normal species
"	2 : 6 d_2 -species
"	3 : 5 d_2 -species
"	0 $^{18}_1$ -species
"	0 $^{18}_2$ -species

The 2 : 6 and 3 : 5 C¹³ substituted species have been tentatively assigned in natural abundance, however the reliability of the data is reduced by the weakness of the spectra.

The inertial defect for each species studied strongly suggests that in the ground vibrational state γ - Pyrone has a planar equilibrium configuration. Structural parameters for the molecule have been determined, the bond lengths showing effects which may be attributable to delocalisation of the lone-pair electrons of O₁ into the π - electron system of the molecule.

Stark effect measurements have yielded a value of $3.70 \pm 0.1D$ for the μ_a dipole moment of the normal species in the ground vibrational state. The Stark effects of the transitions studied were non-quadratic suggesting that the interactions between the ground state rotational energy levels via the μ_a dipole matrix elements are more complicated than expected thus rendering the usual second order perturbation treatment inapplicable in this case.

The normal species of thiapyran-4-one (thiapyrone) has been studied to verify that the introduction of sulphur for oxygen as the ring hetero atom does not detract from the

planarity of the system. The results obtained show that the equilibrium configuration of the ring is almost certainly planar. However, owing to the very low vapour pressure of this compound even at $\sim 50^{\circ}\text{C}$ the spectrum was very weak and no further isotopic work was attempted.

2. Analysis of the Spectrum of γ - Pyrone.

Using the structure determined by x-ray crystallographic methods for the related molecule 2 : 6 dimethyl - 4 - thiopyrone⁵ as a guide to the geometry of the pyrone ring, the structure given in table I was used as a preliminary model for predicting line frequencies for γ - Pyrone.

TABLE I

Preliminary γ - Pyrone Model (\AA)

$\text{C}_2 - \text{O}_1$	1.37	$\text{C}_6\text{O}_1\text{C}_2$	117°
$\text{C}_2 - \text{C}_3$	1.36	$\text{O}_1\text{C}_2\text{H}_1$	119°
$\text{C}_3 - \text{C}_4$	1.42	$\text{O}_1\text{C}_2\text{C}_3$	122°
$\text{C}_4 - \text{O}_2$	1.21	$\text{C}_2\text{C}_3\text{C}_4$	122°
$\text{C} - \text{H}$	1.08	$\text{C}_2\text{C}_3\text{H}_2$	119°
		$\text{C}_3\text{C}_4\text{C}_5$	114°

The model given in table I is a prolate asymmetric rotor with $\kappa = -0.569$ and rotational constants,

A = 5944.18 Mc/s B = 2758.81 Mc/s C = 1884.28 Mc/s.

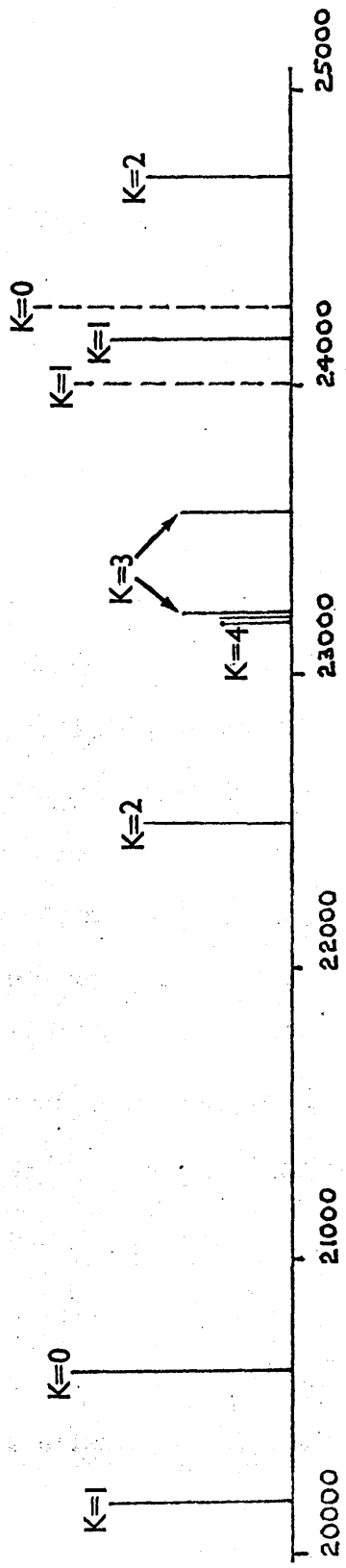
Assuming the molecule to be planar the dipole moment will be wholly along the a inertial axis. Thus the most suitable transitions to look for in an initial search of the spectrum are likely to be the μ_a R - branch transitions obeying the selection rules $\Delta K_{-1} = 0$ and $\Delta K_{+1} = +1$. The rotational constants given above predict that the J = 5 - 4 transition of γ - Pyrone will occur in the region 20 - 25 Gc/s.

Samples of γ - Pyrone were admitted to the Stark cell by first filling a section of the vacuum line with γ - Pyrone vapour and then transferring this to the cell. The pressure of vapour in the cell was then pumped down to the normal working pressure of 0.005 m.m. of mercury. It was found that the strength of the observed spectra was improved if, before commencing work, the cell was flushed out with sample vapour to remove any traces of other compounds adsorbed on the cell walls.

A search in the region predicted for the J = 5 - 4 transition with an applied Stark voltage of ~ 600 volts revealed a number of strong absorption lines. The observed pattern of these lines is shown in fig. 2.

It immediately became clear that each line in the spectrum was accompanied by at least one obvious vibrational satellite

--- J = 5-4
---- J = 6-5



Observed line pattern of γ - Pyrone in region 20 - 25 Gc/s

fig. 2.

some 30 Mc/s. to high frequency of the ground state line. Both ground state lines and vibrational satellites showed alternations in intensity characteristic of nuclear spin statistical weight effects.

The transitions were assigned on the basis of their Stark effects and by comparison of line separations expected from the model and those observed experimentally. The preliminary assignments indicated that transitions for which K_{-1} was odd were accompanied by strong vibrational satellites with intensities almost equalling those of the ground state lines while for K_{-1} even lines the ground state appeared very much stronger than the satellite. All of the strong lines ($K_{-1} = 0 - K_{-1} = 3$) of the $J = 5 - 4$ transition were assigned in this way as were some of the low frequency $J = 6 - 5$ lines.

If it is assumed that rigid rotor theory is obeyed, the frequency of an R - branch transition is given by

$$\nu = 2(J + 1) \frac{A + C}{2} + \frac{A - C}{2} \Delta E(\kappa) \quad (1)$$

where ν is the line frequency and all other terms have their usual meanings. If frequency differences between pairs of lines are taken in such a way that the J dependent term in $\frac{A + C}{2}$ is eliminated, then clearly from (1), for any given value of κ ,

$$\frac{A - C}{2} = \frac{\Delta \nu}{\Delta(\Delta E(\kappa))} \quad (2)$$

Thus since $\frac{A - C}{2}$ and κ are independent of the rotational quantum numbers, a graph of $\frac{A - C}{2}$ obtained from (2) for several pairs of lines against κ should intersect at a point giving the true values of $\frac{A - C}{2}$ and κ . Any line not intersecting at the point has either been wrongly assigned or belongs to a different vibrational state. For a non-rigid molecule there is usually some spread of the intersection points however the effect is generally quite small.

This graphical method was used to confirm the assignments of both ground state and first excited vibrational state lines for γ - Pyrone and to provide a more accurate set of rotational constants for each state. Using the improved rotational constants the study of the R - branch spectrum was extended over a range of ~ 15 Gc/s. From the line measurements thus obtained a graph similar to that described above was constructed over a smaller range of κ . Fig. 3 shows the plot for the ground state lines. From the lack of spread of the points it was concluded that at low J values γ - Pyrone may be treated as a rigid rotor.

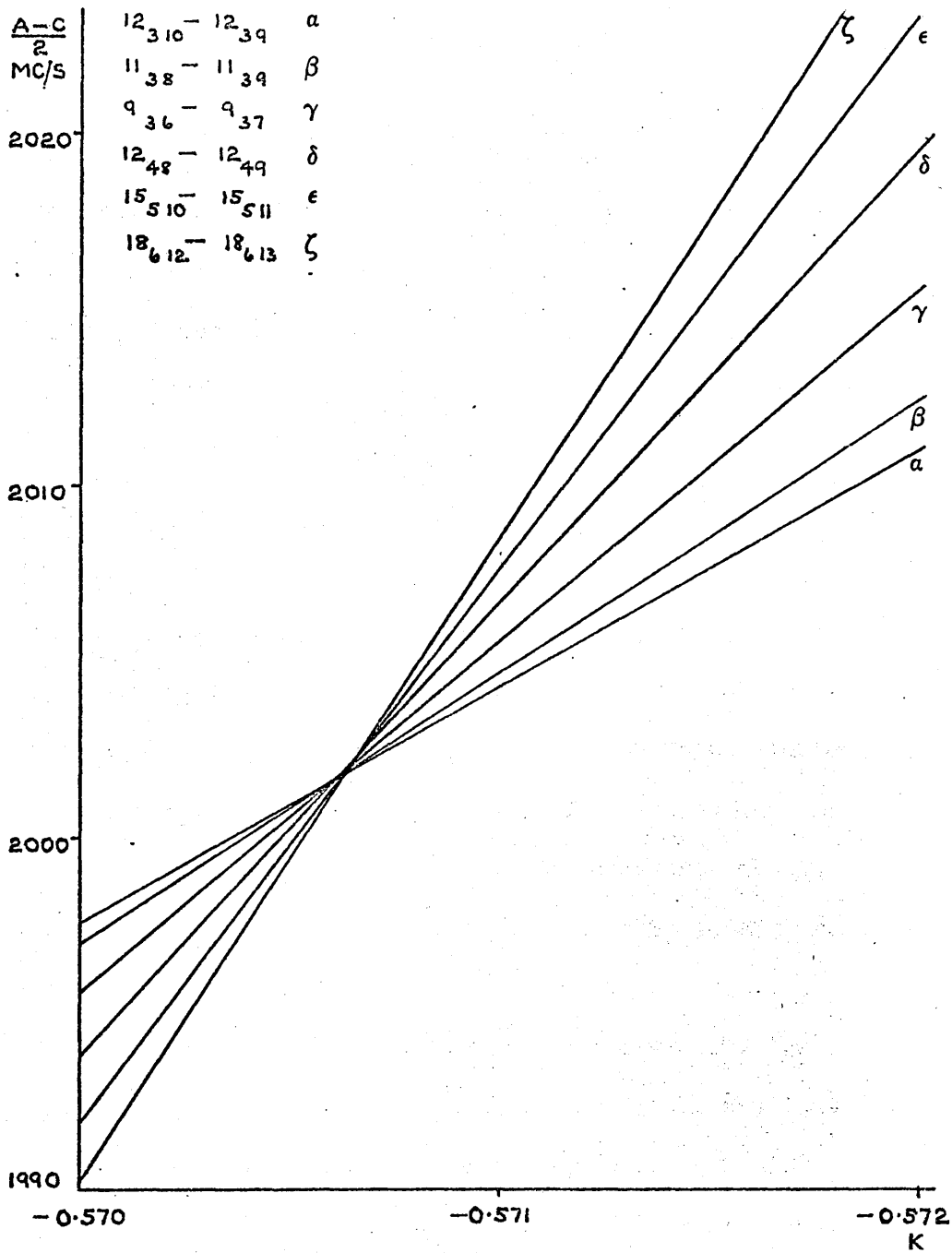
The final set of rotational constants for the normal species were obtained by fitting the observed R - branch line frequencies to equation (1) by the method of least squares, refining the parameters $\frac{A + C}{2}$, $\frac{A - C}{2}$ and κ .

These constants were used to predict the frequencies of several high J, Q - branch lines. The frequency of a Q - branch line is given by

$$\nu = \frac{A - C}{2} \Delta E(\kappa) \quad (3)$$

Hence for a number of accurately measured Q - branch lines, a plot of $\frac{A - C}{2}$ against κ obtained directly from equation (3) will have a common intersection. Such a plot is shown in fig. 4. It can be seen from fig. 4 that only in the case of transitions with $J = 15$ and $J = 18$ does the intersection deviate seriously from a point. This can be attributed to centrifugal distortion effects. The values of $\frac{A - C}{2}$ and κ obtained from these lines were in excellent agreement with those obtained from the R - branch spectrum.

Samples of 2 : 6 d₂, 3 : 5 d₂, O₁¹⁸ and O₂¹⁸ substituted γ - Pyrones were prepared by the methods outlined in Chapter 6. The observed spectra in each case showed essentially the same features as that of the normal species and analysis of the spectra proceeded along similar lines to that described above. In the cases of the two deuterated species studied the presence of nuclear spin statistical weight effects in the ground and first excited state of the molecules confirmed that the molecule had been symmetrically substituted. No spectra due to the



Q - branch plot for γ - Pyrone.

fig. 4.

mono-deuterated species were observed.

Using the available data for all the species studied the frequencies of the R - branch transitions expected from the 2 : 6 and 3 : 5 C^{13} substituted species were predicted. The error in these predictions was expected to be very small (maximum error ± 5 Mc/s.) and so an attempt was made to study the spectra in natural abundance (2%). Several lines were tentatively assigned to the ground state in the spectra of both C^{13} species. To improve the signal-to-noise ratio of the very weak lines observed they were displayed on the oscilloscope of a C.A.T. (computer of average transients). This enabled the Stark effects of the lines to be studied and in most cases they seemed consistent with the assignment. The lines were measured and rotational constants obtained from the spectra by the usual method of least squares refinement. It was found that in both cases the standard deviations on the resulting rotational constants were satisfactorily low considering the small number of lines available and that the inertial defects supported a ground state assignment. No attempt was made to assign any vibrational satellite spectra. Owing to the weakness of the spectra observed and to the large numbers of weak lines from the spectrum of the normal species in the vicinity of the observed C^{13} lines these assignments must only be regarded as tentative.

The rotational constants and observed and calculated line frequencies for the ground and first excited states of all the species studied are given in tables II - IX.

TABLE II

Observed and Calculated line frequencies for Y - Pyrone normal
Species (Mc/s.)

	V = 0		V = 1	
	observed	calculated	observed	calculated
$2_{02} - 1_{01}$	8988.01	8987.87		
$2_{11} - 1_{10}$	10000.58	10000.81		
$2_{12} - 1_{11}$	8281.80	8281.74		
$4_{13} - 3_{12}$	19637.77	19637.77	19664.18	19664.02
$4_{22} - 3_{21}$	19468.90	19468.93	19503.33	19503.52
$4_{23} - 3_{22}$	18162.36	18162.30	18190.37	18190.43
$5_{05} - 4_{04}$	20642.53	20642.55	20670.84	20670.84
$5_{15} - 4_{14}$	20188.01	20187.98	20221.40	20221.38
$5_{14} - 4_{13}$	24143.97	24144.08	24173.70	24173.62
$5_{24} - 4_{23}$	22513.40	22513.21	22547.12	22547.22
$5_{23} - 4_{22}$	24710.94	24710.87	24752.37	24752.52
$5_{33} - 4_{32}$	23223.81	23223.63	23261.61	23261.32
$5_{32} - 4_{31}$	23564.83	23565.09	23607.05	23606.97
$5_{42} - 4_{41}$	23193.52	23192.92		
$5_{41} - 4_{40}$	23205.35	23205.86		

(Cont'd.)

Table II (Cont'd.)

	V = 0		V = 1	
	observed	calculated	observed	calculated
$6_{06} - 5_{05}$	24268.36	24268.41	24303.91	24304.02
$6_{16} - 5_{15}$	24006.83	24006.85	24046.44	24046.41
$7_{34} - 6_{33}$	34055.03	34055.02		
$8_{08} - 7_{07}$	31586.32	31586.52		
$8_{36} - 7_{35}$	36934.69	36934.86		
$9_{09} - 8_{08}$	35277.21	35277.35		
$9_{19} - 8_{18}$	35246.84	35246.98		
$9_{36} - 9_{37}$	8986.72	8986.89		
$12_{48} - 12_{49}$	10223.05	10223.13		
$11_{38} - 11_{39}$	18441.72	18441.41		
$12_{3,10} - 12_{39}$	23857.83	23857.12		
$15_{5,10} - 15_{5,11}$	11129.58	11129.90		
$18_{6,12} - 18_{6,13}$	11761.81	11760.28		
$\frac{A + C}{2}$		3857.36		3849.30
$\frac{A - C}{2}$		2001.81		1990.18
κ		- 0.57062		- 0.56807

TABLE III

Observed and Calculated Line frequencies for 3 : 5 d₂ γ-Pyrone

	V = 0		V = 1	
	observed	calculated	observed	calculated
4 ₁₃ - 3 ₁₂	19258.49	19258.39	(no satellite lines were fitted for this spectrum).	
4 ₂₂ - 3 ₂₁	19386.90	19386.96		
4 ₂₃ - 3 ₂₂	17773.58	17774.01		
4 ₃₁ - 3 ₃₀	18434.87	18435.13		
4 ₃₂ - 3 ₃₁	18267.22	18267.04		
5 ₀₅ - 4 ₀₄	19806.60	19806.78		
5 ₁₅ - 4 ₁₄	19491.70	19491.64		
5 ₁₄ - 4 ₁₃	23512.29	23512.28		
5 ₂₄ - 4 ₂₃	21968.41	21968.33		
5 ₂₃ - 4 ₂₂	24551.74	24551.90		
5 ₃₃ - 4 ₃₂	22865.94	22865.77		
5 ₃₂ - 4 ₃₁	23409.78	23409.93		
5 ₄₁ - 4 ₄₀	22892.17	22892.87		
6 ₀₆ - 5 ₀₅	23298.06	23298.03		
6 ₁₆ - 5 ₁₅	23142.16	23142.18		
6 ₁₅ - 5 ₁₄	27364.53	27364.62		

(Cont'd.)

Table III (Cont'd.)

	V = 0		V = 1	
	observed	calculated	observed	calculated
$6_{25} - 5_{24}$	26017.65	26017.74		
$6_{34} - 5_{33}$	27402.74	27402.48		
$6_{43} - 5_{42}$	27555.33	27555.26		
$\frac{A + C}{2}$		3529.21		
$\frac{A - C}{2}$		1744.01		
K		- 0.47647		

TABLE IV.

Observed and Calculated Line frequencies for 2 : 6 D₂ Y - Pyrone

	V = 0		V = 1	
	observed	calculated	observed	calculated
4 ₁₃ - 3 ₁₂	18888.79	18888.98		
4 ₂₂ - 3 ₂₁	18888.79	18888.76		
4 ₃₁ - 3 ₃₀	18010.79	18010.67		
5 ₀₅ - 4 ₀₄	19597.33	19597.28	19623.40	19623.37
5 ₁₅ - 4 ₁₄	19237.54	19237.51		
5 ₁₄ - 4 ₁₃	23132.39	23132.96		
5 ₂₄ - 4 ₂₃	21587.66	21587.96		
5 ₂₃ - 4 ₂₂	23949.61	23949.53	23988.49	23988.41
5 ₃₃ - 4 ₃₂	22383.31	22383.23		
5 ₃₂ - 4 ₃₁	22822.53	22822.58		
6 ₀₆ - 5 ₀₅	23044.55	23044.54	23077.42	23077.48
6 ₁₆ - 5 ₁₅	22854.98	22854.98		
6 ₁₅ - 5 ₁₄	27018.10	27017.91		
6 ₂₅ - 5 ₂₄	25062.74	25062.70	25638.58	25638.60
6 ₂₄ - 5 ₂₃	28847.74	28847.62	28889.63	28889.70
6 ₃₄ - 5 ₃₃	26843.79	26843.57		
6 ₃₃ - 5 ₃₂	27880.37	27880.32		

(Cont'd.)

Table IV (Cont'd.)

	V = 0		V = 1	
	observed	calculated	observed	calculated
7 ₀₇ - 6 ₀₆	26518.89	26520.01	26560.67	26560.01
7 ₁₇ - 6 ₁₆	26429.71	26429.74	26471.70	26471.67
7 ₂₆ - 6 ₂₅	29486.22	29486.24	29526.26	29526.25
7 ₁₆ - 6 ₁₅	30574.14	30574.07	30602.33	30602.31
7 ₃₅ - 6 ₃₄	31214.63	31214.45		
$\frac{A + C}{2}$	3558.19		3551.83	
$\frac{A - C}{2}$	1793.87		1784.26	
K	- 0.51668		- 0.51392	

TABLE V.

Observed and Calculated Line frequencies for $O_1^{18} \gamma$ - Pyrene

	V = 0		V = 1	
	observed	calculated	observed	calculated
$4_{13} - 3_{12}$	19075.12	19075.14	19101.23	19101.19
$4_{22} - 3_{21}$	18831.34	18831.39		
$5_{05} - 4_{04}$	20196.90	20196.82		
$5_{15} - 4_{14}$	19711.69	19711.65	19744.51	19744.58
$5_{14} - 4_{13}$	23495.29	23495.16		
$5_{24} - 4_{23}$	21907.60	21907.49		
$5_{23} - 4_{22}$	23907.76	23907.67		
$5_{33} - 4_{32}$	22541.35	22541.18		
$5_{32} - 4_{31}$	22822.49	22822.97		
$6_{06} - 5_{05}$	23745.11	23744.97	23779.87	23779.82
$6_{16} - 5_{15}$	23452.73	23452.61		
$6_{25} - 5_{24}$	26052.02	26052.09		
$6_{15} - 5_{14}$	27635.34	27635.77	27667.22	27667.33
$6_{24} - 5_{23}$	28912.01	28911.94	28957.36	28957.45
$6_{34} - 5_{33}$	27063.50	27063.02	27106.89	27106.49
$6_{33} - 5_{32}$	27757.09	27757.37	27808.45	27808.61
$6_{43} - 5_{42}$	27094.35	27094.00		

(Cont'd.)

Table V (Cont'd.)

	V = 0		V = 1	
	observed	calculated	observed	calculated
$6_{42} - 5_{41}$	27137.05	27137.29		
$7_{07} - 6_{06}$	27304.77	27305.03	27347.35	27347.42
$7_{17} - 6_{16}$	27146.63	27146.76		
$7_{26} - 6_{25}$	30085.96	30085.85	30129.45	30129.43
$\frac{A + C}{2}$		3836.54		3828.40
$\frac{A - C}{2}$		2022.39		2010.75
κ		- 0.59796		- 0.59560

TABLE VI

Observed and Calculated Line frequencies for O_2^{18} γ - Pyrone

	V = 0		V = 1	
	observed	calculated	observed	calculated
$4_{13} - 3_{12}$	18714.21	18714.14	18740.31	18740.09
$4_{22} - 3_{21}$	18428.02	18427.98		
$5_{05} - 4_{04}$	19906.93	19906.87	19934.57	19934.48
$5_{15} - 4_{14}$	19403.49	19403.19	19435.95	19435.80
$5_{14} - 4_{13}$	23075.22	23075.27		
$5_{24} - 4_{23}$	21518.28	21518.23		
$5_{23} - 4_{22}$	23397.48	23396.92		
$5_{33} - 4_{32}$	22106.24	22106.24		
$5_{32} - 4_{31}$	22354.55	22354.79		
$6_{06} - 5_{05}$	23405.90	23405.77		
$6_{16} - 5_{15}$	23093.25	23093.31		
$6_{25} - 5_{24}$	25603.06	25602.93		
$6_{15} - 5_{14}$	27180.11	27180.23	27211.93	27212.06
$6_{24} - 5_{23}$	28313.36	28313.41	28358.81	28358.94
$6_{33} - 5_{32}$	27162.28	27162.51	27212.63	27212.78

(Cont'.d)

Table VI (Cont'd.)

	V = 0		V = 1	
	observed	calculated	observed	calculated
$T_{07} - {}^6_{06}$	26910.89	26911.05	26952.53	26952.70
$T_{26} - {}^6_{25}$	29583.81	29583.98	29627.25	29627.32
$T_{35} - {}^6_{34}$	30937.37	30937.25	30986.42	30986.23
$T_{34} - {}^6_{33}$	32166.67	32166.62	32227.89	32227.84
$T_{44} - {}^6_{43}$	31086.88	31086.64	31139.24	31138.95
$T_{43} - {}^6_{42}$	31203.18	31203.61	31257.94	31258.17
$\frac{A + C}{2}$	3823.22		3814.70	
$\frac{A - C}{2}$	2035.91		2023.80	
K	- 0.61484		- 0.61253	

TABLE VII

Observed and Calculated Line frequencies for C^{13} γ -Pyrone

	C_2^{13}		C_3^{13}	
	observed	calculated	observed	calculated
$5_{05} - 4_{04}$	20451.82	20451.77	20516.35	20516.67
$5_{15} - 4_{14}$	20013.13	20013.11	20086.01	20086.41
$5_{24} - 4_{23}$	22339.65	22339.02	22439.77	22438.75
$5_{23} - 4_{22}$	24558.95	24559.30	-	-
$6_{16} - 5_{15}$	23795.44	23795.47	23879.89	23879.73
$6_{25} - 5_{24}$	26533.17	26534.25	26647.27	26646.75
$7_{34} - 6_{33}$	33862.97	33863.17		
$8_{08} - 7_{07}$	31299.48	31299.62	31403.97	31403.33
$8_{36} - 7_{35}$	36656.51	36656.75	36826.11	36826.33
$8_{27} - 7_{26}$			34693.95	34693.87
$9_{09} - 8_{08}$			35074.75	35075.15
$\frac{A + C}{2}$	3803.93		3801.40	
$\frac{A - C}{2}$	1965.07		1956.31	
K	- 0.56265		- 0.55588	

As indicated above, spectra due to molecules in the first excited state of a low frequency vibration were observed for all the species except in the case of the extremely weak C^{13} spectra. For a few particularly favourable lines further vibrational satellites were detected and since there appeared to be an observable alternation in intensity it was assumed that these lines were due to molecules in higher excited states of the same vibration.

In the planar model of γ -Pyrone there are clearly two pairs of equivalent hydrogen nuclei. In such a situation the nuclear spins and statistics affect the population of molecular states and hence the transition intensities.

The total molecular wave function can be written as a product of electronic, vibrational, rotational and nuclear spin parts,

$$\psi = \psi_e \cdot \psi_v \cdot \psi_r \cdot \psi_n$$

If the ground electronic state is symmetrical then the symmetry of the overall wave function depends on the individual symmetries of the remaining parts.

A rotation of 180° around the a inertial axis of γ -Pyrone interchanges the positions of the two sets of protons and, since nuclei of odd mass always occur in antisymmetric wave functions

i.e., obey Fermi - Dirac statistics, the wave function must change sign in each case. Hence the overall wave function will remain unchanged and symmetric total spin functions must be paired with symmetric rotational functions for a symmetric vibrational state.

For a molecule with n pairs of identical nuclei the number of symmetric spin functions which can be formed is given by,

$$n_s = \frac{1}{2} \left[\prod_{i=1}^n (2I_i + 1) \right] \left[\prod_{i=1}^n (2I_i + 1) + 1 \right] \quad (4)$$

and the number of antisymmetric functions by,

$$n_a = \frac{1}{2} \left[\prod_{i=1}^n (2I_i + 1) \right] \left[\prod_{i=1}^n (2I_i + 1) - 1 \right] \quad (5)$$

where I_i is the nuclear spin of the i'th pair of nuclei.

The symmetry of the rotational wave functions is related to the parity of K_{-1} for the energy level involved. If K_{-1} is even then the wave function is symmetric and for K_{-1} odd it is antisymmetric.

From equations (4) and (5) it can be seen that for the normal species of γ - Pyrone $\frac{n_s}{n_a} = \frac{10}{6}$. Thus for transitions for which K_{-1} is even the ground state symmetric vibration will have a larger statistical weight than the first excited

antisymmetric vibrational state and will thus appear stronger. For transitions with K_{-1} odd the first excited state will have the larger statistical weight and will thus appear stronger relative to the ground state than for K_{-1} even lines.

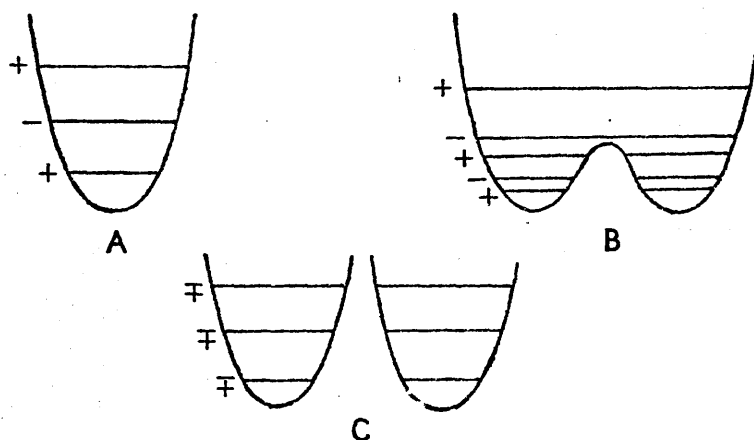
In the case of the symmetrically disubstituted deuterated γ - Pyrones the deuterium nuclei obey Bose - Einstein statistics while the protons again obey Fermi - Dirac statistics. Thus for a symmetric vibrational state symmetric total spin functions must be paired with antisymmetric rotational functions and vice-versa. From (4) and (5) in this case $\frac{n_s}{n_a} = \frac{7}{5}$ and thus K_{-1} even lines will have strong satellites while K_{-1} odd lines will have weaker satellites.

This analysis of the intensities of the vibrational satellites of γ - Pyrone is in good agreement with the qualitative intensities observed experimentally.

By analogy with similar molecules it seems likely that the vibration giving rise to the satellite pattern described above is the ring puckering mode where the ring is deformed perpendicular to the ring plane in the vicinity of O_1 .

In the case of a planar molecule the potential function for the out-of-plane deformation will be nearly parabolic in form with evenly spaced vibrational energy levels as shown in fig. 5a. The introduction of a potential barrier at the

planar configuration causes the vibrational energy levels to approach each other in pairs, fig. 5b, introducing anharmonicity into the vibration. When such a barrier is high enough to permanently bend the molecule the levels are again evenly spaced but are doubly degenerate, each level having the same statistical weight fig. 5c.



Possible potential functions for γ - Pyrone.

fig. 5.

Since statistical weight effects are observed in the spectrum of γ -Pyrone any barrier of sufficient height to permanently pucker the ring can be discounted. The higher vibrational satellites observed in the spectrum suggest that the vibration is harmonic or very nearly so and so the situation of fig. 5a would seem to fit the case of γ -Pyrone. It is possible that there may be a small potential hump at the planar

configuration bringing the ground state and first excited state closer together and only introducing slight anharmonicity into the vibration.

The conclusion that the molecule is planar in its equilibrium ground state configuration is consistent with the fact that the inertial defect for the ground state is close to zero (see table IX). The inertial defect for the first excited state is found to be large and negative supporting the assignment of the vibration to a ring bending mode. The approximate relative intensities of the ground and first excited state lines show that the 1st vibrational state is $\sim 100 \text{ cm}^{-1}$ above that of the ground state.

3. Stark Effect and Dipole Moment.

The perturbations to the rotational energy levels which arise on the interaction of a uniform electric field with the permanent electric dipole moment of an asymmetric rotor have been extensively studied by Golden and Wilson⁶.

In the presence of a static electric field the total angular momentum \underline{J} has $2J + 1$ possible orientations with respect to the field direction. These orientations are defined by the quantum number M which can take the values

$$M = |J|, |J - 1|, \dots, |-J|$$

In the absence of the field the energy levels are thus $2J + 1$ fold degenerate in M and application of the field lifts or partially lifts this degeneracy.

If the Stark effect perturbations are small compared with the spacing between the rotational energy levels then perturbation theory can be used to calculate the Stark splittings. The Stark perturbation term H is the interaction energy between the applied field E and the molecular dipole moment μ .

$$H = -\underline{\mu} \cdot \underline{E} \quad (6)$$

Expressing this scalar product in terms of the direction cosine between $\underline{\mu}$ and \underline{E} gives

$$H = -\mu E \cos \theta \quad (7)$$

In the case of an asymmetric rotor with no degenerate energy levels the Stark effect is usually second order or proportional to the square of the applied field. Application of the usual methods of perturbation theory shows that the second order correction to the energy of a given level is given by

$$\Delta E^{(2)} = \sum_{m \neq n} \frac{|\langle \psi_m | H | \psi_n \rangle|^2}{E_m - E_n} \quad (8)$$

where ψ_m and ψ_n are the two interacting states and E_m and E_n are the unperturbed energies of these states.

If for an asymmetric rotor H is expressed in terms of the

direction cosine Φ_{z_g} between the space fixed z - axis defined by the electric field and the principal axis g of the rotor and the component of μ along that principal axis then from (2)

$$H' = - E \sum_g \Phi_{z_g} \mu_g \quad (9)$$

Combining equations (8) and (9) allows the second order Stark energy correction to be written

$$\Delta E^{(2)} = \sum_g \mu_g^2 E^2 \sum_{m \neq n} \frac{|\langle \psi_m | \Phi_{z_g} | \psi_n \rangle|^2}{E_m - E_n} \quad (10)$$

The matrix elements of the asymmetric rotor direction cosines have been evaluated in an asymmetric rotor basis in ⁶. Townes and **Schawlow** express these in terms of line strengths $g_{S_{J_T J'_T}}$, as tabulated in ⁷.

$$\begin{aligned} |\Phi_{J, T, M; J-1, T', M}|^2 &= \frac{J^2 - M^2}{J(4J^2 - 1)} g_{S_{J_T J'-1 T'}} \\ |\Phi_{J, T, M; J, T', M}|^2 &= \frac{M^2}{J(J+1)(2J+1)} g_{S_{J_T J_T'}} \\ |\Phi_{J, T, M; J+1, T', M}|^2 &= \frac{(J+1)^2 - M^2}{(J+1)(2J+1)(2J+3)} g_{S_{J_T J'+1 T'}} \end{aligned} \quad (11)$$

Using (11) the entire second order Stark energy in the case of no degeneracy as given by (10) can be written

$$E^{(2)} = \sum_g \frac{\mu_g^2 E^2}{2J+1} \sum_{T'} \left[\frac{J^2 - M^2}{J(2J-1)} \frac{\xi_{S_{J_T, J-1_{T'}}}}{E_{J_T} - E_{J-1_{T'}}} + \frac{M^2}{J(J+1)} \right. \\ \left. \frac{\xi_{S_{J_T, J_{T'}}}}{E_{J_T} - E_{J_{T'}}} + \frac{(J+1)^2 - M^2}{(J+1)(2J+3)} \frac{\xi_{S_{J_T, J+1_{T'}}}}{E_{J_T} - E_{J+1_{T'}}} \right] \quad (12)$$

In the particular case of the normal species of Υ - Pyrone it was found that the $5_{05} - 4_{04}$ and the $5_{23} - 4_{23}$ transitions were most suitable for measurement of the Stark effect. In each case four Stark components were well resolved and could be followed without serious distortion of line shape to a separation of ~ 10 Mc/s from the zero field line.

Using equation (12) and the fact that Υ - Pyrone has only a μ_a component of the dipole moment, theoretical coefficients of $\mu_a^2 E^2$ were calculated for all values of M for each transition. These coefficients are given in table VIII. It can be seen from equation (12) that the frequency separation of a given Stark component from the zero-field line graphed against the square of the applied field should be a straight line with gradient equal to the appropriate coefficient $\times \mu_a^2$.

The observed Stark components of each line were measured at various values of the applied voltage. After each set of measurements the cell was calibrated using the $J = 2 - 1$ transition of OCS. Assuming a value of 0.7124D for the dipole

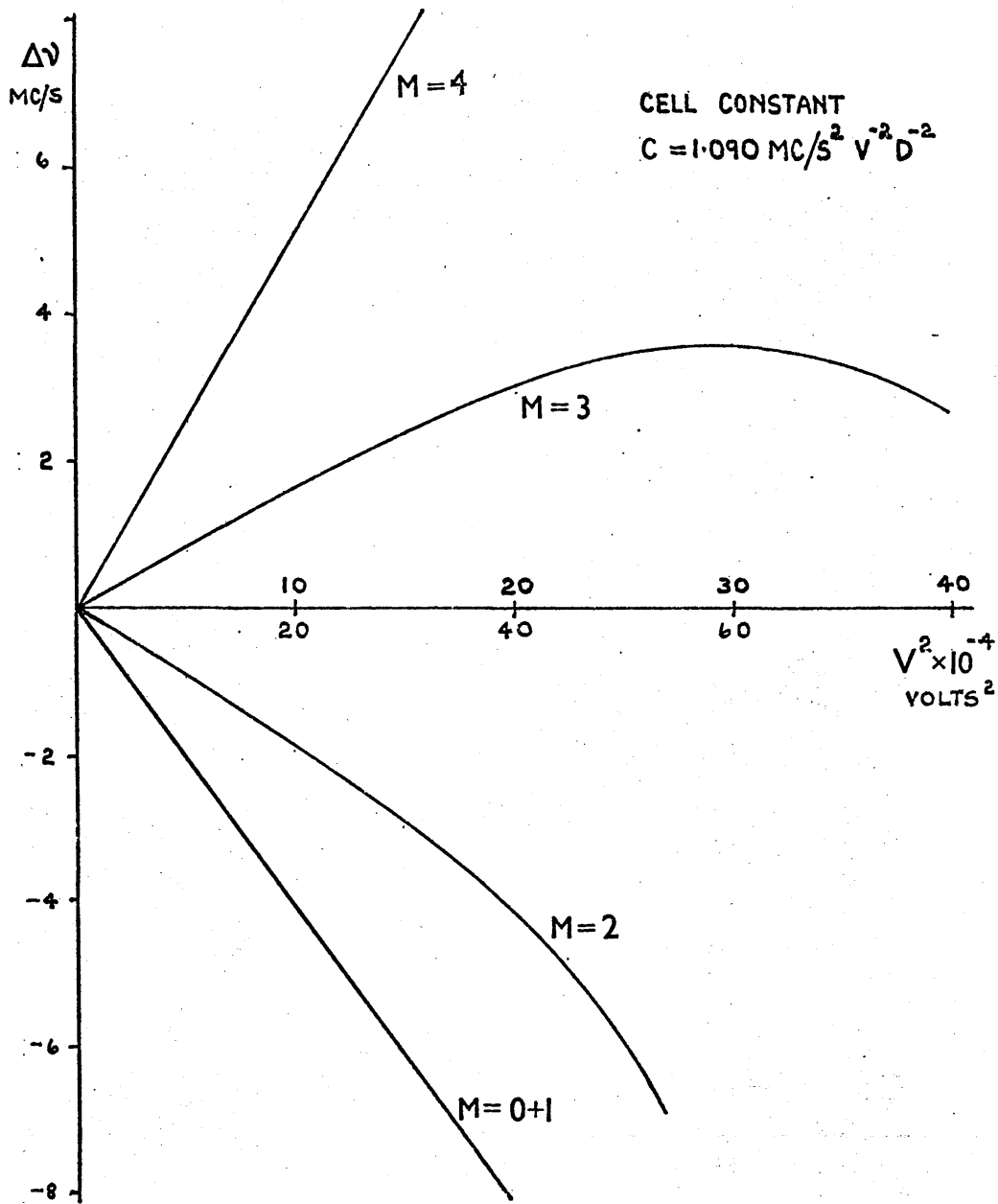
moment of OCS the calibration enables the proportionality constant between the field strength E and the applied square wave voltage V to be determined. This constant when incorporated in the slope of the experimental plot of $\Delta\nu$ against V^2 allows the experimental slopes to be directly equated with those of table VIII. The value of the μ_a dipole moment can thus be obtained for each value of M .

From the theoretical coefficients it is predicted that the Stark components will appear in order of decreasing M value for both transitions studied. On this basis the experimental graphs shown in figs. 6 and 7 were assigned an M value and the value of the μ_a dipole moment obtained for each value of M is shown in table VIII.

TABLE VIII.

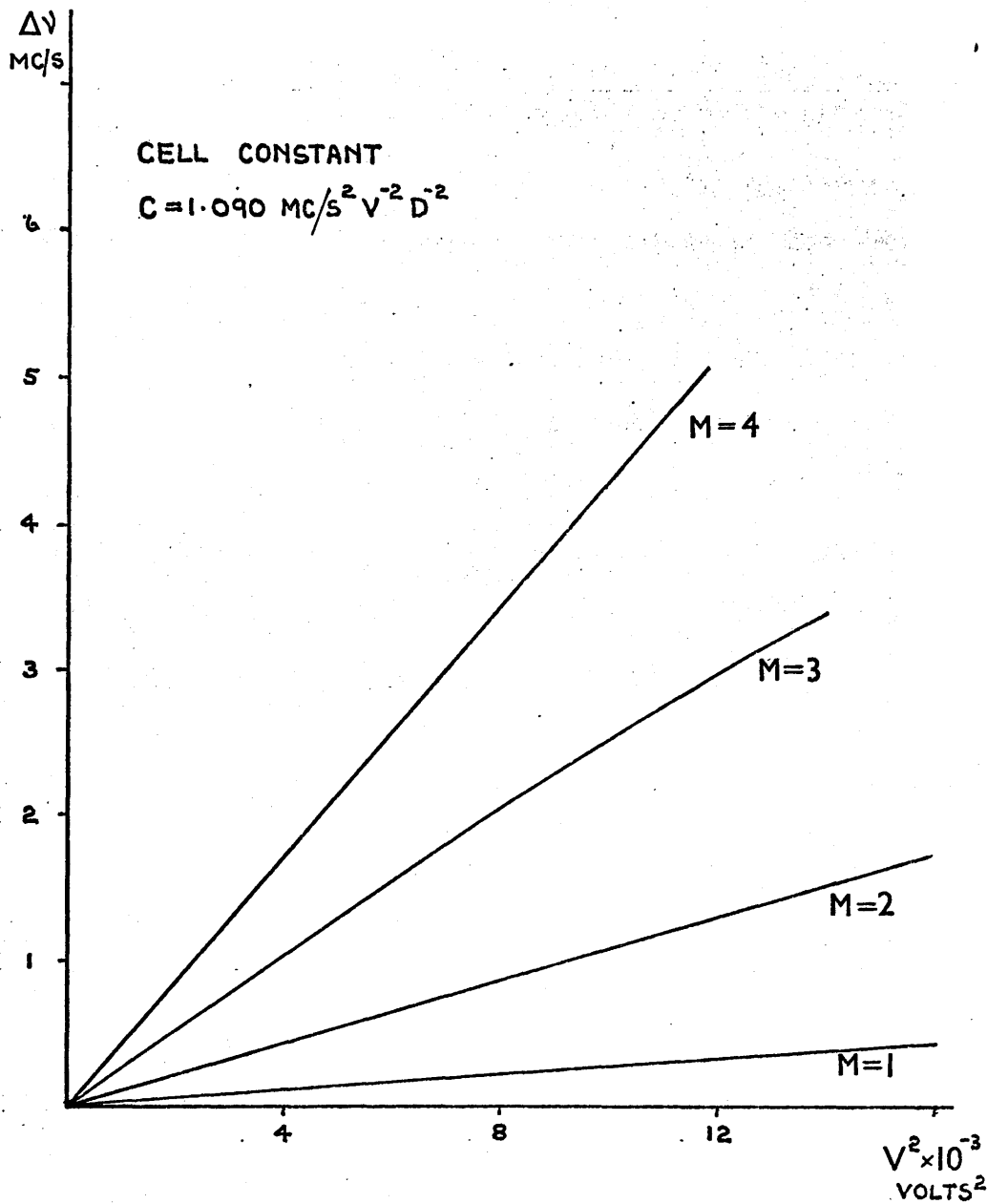
Second Order Stark coefficients of $\mu_a^2 E^2$ and experimental values
of μ_a (D) for γ - Pyrone.

M	0	1	2	3	4
$5_{05} - 4_{04}$					
Stark Coefft.	- 0.1513	-0.1201	-0.0265	0.1301	0.3491
μ_a .	-	3.74	-	-	3.70
$5_{24} - 4_{23}$					
Stark Coefft.	-0.0685	0.2949	1.3844	3.2003	5.7429
μ_a .	-	4.07	3.77	3.66	3.60



Stark effect plots for $5_{05} - 4_{04}$ transition of γ -Pyrone.

fig. 6.



Stark effect plots for $5_{24} - 4_{23}$ transition of γ - Pyrone.

fig. 7.

There are clearly several inconsistencies in the experimental results. It can be seen from fig.6 that in the case of the components assigned as $M = 2$ and $M = 3$ for the $5_{05} - 4_{04}$ transition the graphs of $\Delta\nu/V^2$ deviate seriously from the expected quadratic behaviour. Further effects of perturbation are reflected in the fact that the values for the μ_a dipole moment for each of the other measured Stark components differ by amounts well beyond the expected experimental error. It should also be noted that for each transition only four instead of five Stark components were observed. Even at applied fields of $\sim 1500V$ there was no evidence for any further component in either case. This latter fact is surprising in view of the magnitudes of the coefficients of table VIII which suggest that at high fields all five lobes should at least be visible.

Curvature of the graph of $\Delta\nu$ against V^2 such as that shown in fig.6 can often be attributed to accidental degeneracies in the energy level manifold of the molecule. If any of the energy levels connected to the particular levels on which the measurements have been made are degenerate or nearly so, then the perturbation treatment leading to equation (12) breaks down and deviations from linearity of the graph may occur.

Calculation of the rotational energy levels for γ -Pyrone showed however that the energy level separation was of the

order 2300 Mc/s. between the 4_{22} and 5_{05} levels and 1200 Mc/s. between the 3_{21} and the 4_{04} levels. These energy level spacings are not exceptionally close but it is significant that the levels $J K_{-1} = 2$ will have a strong μ_a dipole matrix element connecting them and so will move apart rapidly with increasing applied field. It seems likely therefore that at high field strengths the higher energy component of the $J K_{-1} = 2$ levels will perturb the $(J+1) K_{-1} = 0$ level and cause some deviation from second order behaviour for this level.

It was decided therefore to calculate this effect on the Stark shift of the $K_{-1} = 0$ levels from a 3×3 matrix which had rigid rotor energies for $J K_{-1} = 2$ and $(J+1) K_{-1} = 0$ on the diagonal and off-diagonal elements of the form of equation (8). The off-diagonal terms were calculated from the tabulated line strengths and equations (11). Determination of the eigenvalues of this matrix for a suitable value of the dipole moment (3.60D) enabled the effect of this particular interaction on the movement of the $K_{-1} = 0$ level to be followed for chosen values of the field strength. It was found however that the improvement on second order theory obtained by treating this interaction in this way was only slight. This is presumably

due to the fact that although the levels $J K_{-1} = 2$ and $(J+1) K_{-1} = 0$ are close in energy, the dipole matrix element connecting them is relatively weak and so the contribution to the overall Stark shift of the $K_{-1} = 0$ level from this particular connection is small.

In the case of the $5_{24} - 4_{23}$ transition none of the energy levels are obviously degenerate yet deviations in the value of μ_a for each Stark component occur.

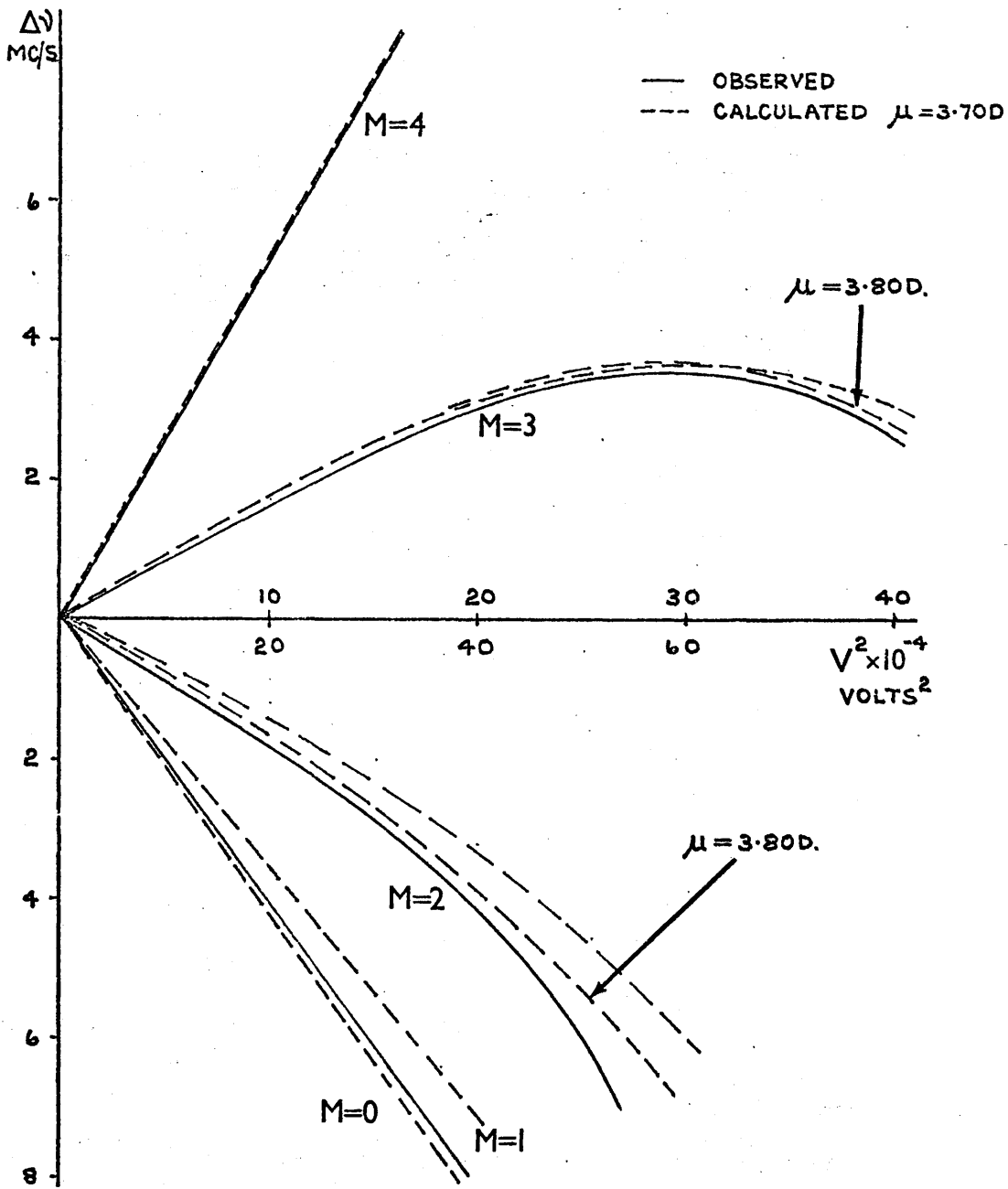
A possible, although in this case unlikely, explanation for the observed variation in the measured dipole moments could be failure to include a further component of the dipole moment in the calculations. A μ_b component seemed completely unlikely and it would be extremely difficult to justify the inclusion of a μ_c contribution in view of the evidence for planarity of the molecule given in the previous section.

It was therefore decided to extend the 3×3 matrix in the calculation described above to include all the energy levels from $J = 2$ to $J = 6$ and all the appropriate Stark connection terms. In this way it could be shown whether the observed perturbations were caused by a build up of effects operating throughout the energy level scheme, as opposed to effects operating in the local region of the levels being studied.

A computer programme designed to run on the English Electric KDF9 computer was written which sets up and diagonalises the energy matrix for given values of M , μ_a and the field strength E . From the eigenvalues of the matrix the separation of any energy level from the zero-field line for a given applied field could be obtained and thus a series of theoretical plots for the Stark effect of a given transition could be constructed. When this was carried out for the transitions studied in this case, it was found that for a dipole moment of 3.70 - 3.80 D the correspondence between theoretical and experimental graphs was fairly satisfactory, figs. 8, 9.

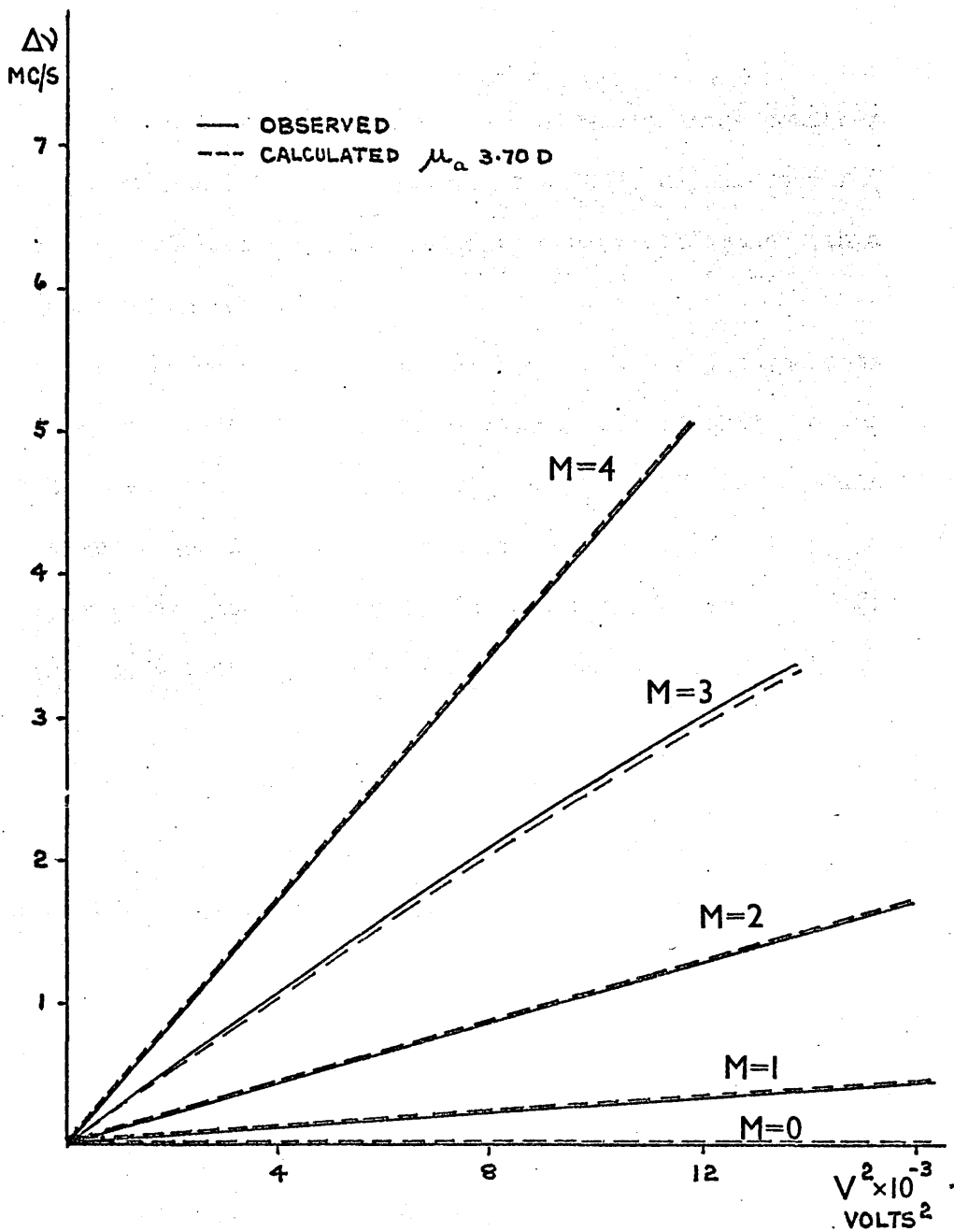
The straight line graphs obtained for the $5_{24} - 4_{23}$ transition are fitted to within experimental error by $\mu_a = 3.70$ D. It can also be seen from fig. 9 that the $M = 0$ component has negligible slope for $\mu_a = 3.70$ D. The calculations show that this component will only be 0.7 Mc/s. separated from the zero-field line at 1200V, i.e. within a line-width. This explains its absence from the experimental observations.

For the $5_{05} - 4_{04}$ transition the theoretical $M = 4$ plot fits well with the experimental result, again for $\mu_a = 3.70$ D. The observed component giving the other straight line plot for



Experimental and Calculated Stark plots for $5_{05} - 4_{04}$

fig. 8.



Experimental and Calculated Stark plots for $5_{24} - 4_{23}$

fig. 9.

this transition almost certainly contains both the $M = 0$ and $M = 1$ components. At low field strength these components are less than 1 Mc/s. apart and at $\sim 800V$ they are separated by only 1.5 Mc/s. The slope is consistent again with a dipole moment of 3.70 D.

In the cases of the curved $M = 2$ and $M = 3$ components the calculated and observed curves do not fit quite so well. Indeed a better fit is obtained with $\mu_a = 3.80$ D. Using this higher value of μ_a discrepancies are small, deviations from the experimental curves being of the order of 0.2 Mc/s. For $\mu_a = 3.70$ D the error between the experimental and observed curves is however considerably greater as shown in fig. 8.

Deviations of the calculated graphs from the experimental ones may be expected to arise from two main factors. Firstly the definition of the experimental plots themselves is in some doubt owing to the experimental error on each measurement taken. This is of the order ± 0.1 Mc/s. on a well defined Stark component. A more serious source of error is inherent in the method of calculation itself. The calculation carried out here is an extended perturbation calculation on the rigid rotor energy levels. Such a treatment can only be completely satisfactory if at all times the shifts in the energy levels in

the presence of the Stark field are small compared to the asymmetry splittings of the levels. This however is apparently not true for γ -Pyrene.

In the absence of the electric field the asymmetric rotor energy matrix factorises into the four Wang submatrices E^+ and O^+ for each value of J . The Stark effect however introduces terms into this matrix which in the case of the μ_a connections alone connect the E^+ and E^- submatrices and the O^+ and O^- submatrices. This therefore destroys the complete factoring of the energy matrix and it becomes necessary to diagonalise it as E and O matrices only to obtain the energy levels for a given applied Stark field. In the calculation described above the diagonal elements of the matrix are rigid rotor energies. It has therefore been assumed that the asymmetric rotor energy matrix is diagonal in the presence of a Stark field.

This latter source of error is almost certainly responsible for a large part of the deviations shown in figs. 8, 9.

At this stage therefore it can be concluded that the dipole moment of γ -Pyrene is 3.70 ± 0.1 D. This rather large error can hopefully be reduced by use of the more exact treatment of the Stark energies outlined above.

4. Structure of γ -Pyrone.

In microwave spectroscopy the location of an atom in the principal axis system of a molecule is best carried out in most cases by the method of isotopic substitution.

Expressions have been developed by Kraitchman⁸ relating the co-ordinates of an atom to the changes in the equilibrium moments of inertia (I^e) which occur on isotopically substituting that atom.

The moments of inertia obtained from a microwave spectrum are not however equilibrium moments but are averaged over the particular vibrational state of the molecule. They are usually termed effective moments of inertia (I^o) and in general $I^o \neq I^e$.

In the determination of effective geometric parameters (r^o) which result from the I^o it must be assumed that the r^o are the same for each isotopic species. This assumption is clearly invalid for a vibrating molecule.

Costain⁹ has dealt at length with the errors introduced into a structure by carrying out the calculations using each type of moment of inertia. He concludes that the structure which is closest to the equilibrium structure of the molecule is the r^s structure obtained by isotopically substituting each

atom in turn in the molecule. Except for extremely simple cases the r^s parameters have no simple relation with either r^e or r^o parameters.

For a planar asymmetric top molecule like γ -Pyrone, Kraitchman's equations take the form

$$\begin{aligned} x^2 &= \frac{\Delta I_y}{\mu} \left[\frac{I'_x - I_y}{I_x - I_y} \right] \\ y^2 &= \frac{\Delta I_x}{\mu} \left[\frac{I'_y - I_x}{I_y - I_x} \right] \end{aligned} \quad (13)$$

where $\mu = \frac{M\Delta M}{M+\Delta M}$ is the reduced mass for the isotopic substitution and the primes refer to the substituted molecule.

The coordinates obtained for an atom by using I^o values rather than I^e values in equations (13) are substitution coordinates related to r^s parameters. For γ -Pyrone all the atoms except the ring carbon atoms have been located by isotopic substitution. The moments of inertia and inertial defects (Δ) for both the ground states and first excited states of each species studied are given in table IX. Included in table IX are data obtained for the ring C^{13} species in natural abundance, however considering the rather large standard deviations on the rotational constants of these species and the

TABLE IX

Moments of inertia and inertial defects for ground and first excited states of γ -Pyryone

		Ia	Ib	Ic'	Δ
		(a.m.u. \AA^2)	(a.m.u. \AA^2)	(a.m.u. \AA^2)	(a.m.u. \AA^2)
γ -Pyryone	V = 0	86.2803	186.1931	272.4427	- 0.0307
	V = 1	86.5712	185.9431	271.9195	- 0.5948
$\dot{\gamma}$ -Pyryone 3:5d ₂	V = 0	95.8676	187.3558	283.1789	- 0.0445
	V = 1	-	-	-	-
γ -Pyryone 2:6d ₂	V = 0	94.4554	192.1199	286.5302	- 0.0451
	V = 1	94.7381	191.8626	286.0034	- 0.5973
γ -Pyryone 0 ₁ ¹⁸	V = 0	86.2838	192.4198	278.6600	- 0.0436
	V = 1	86.5761	192.1594	278.1234	- 0.6121

(Cont'd.)

Table IX (Cont'd.)

	Ia	Ib	Ic'	Δ
	(a.m.u. $\cdot\text{\AA}^2$)	(a.m.u. $\cdot\text{\AA}^2$)	(a.m.u. $\cdot\text{\AA}^2$)	(a.m.u. $\cdot\text{\AA}^2$)
γ - Pyrone O_2^{18}	V = 0 86.2809	196.5938	282.8446	- 0.0301
	V = 1 86.5838	196.3235	282.2981	- 0.6092
γ - Pyrone C_2^{13}	V = 0 87.6288	187.3518	274.9147	- 0.0659
γ - Pyrone C_3^{13}	V = 0 87.8006	186.2734	273.9872	- 0.0862

uncertainty in the assignments themselves resulting from the small number of lines measured it was felt that it would be unwise to include such data in a calculation of the molecular structure.

The coordinates obtained from equations (13) for the atoms of γ -Pyrone are listed in table X. It is estimated that the error on a typical coordinate calculated from Kraitchman's equations is of the order $\pm 0.008 \text{ \AA}$ for an error of $\pm 0.1 \text{ Mc/s.}$ on each rotational constant.

The location of the ring carbon atoms were carried out using the first and second moment conditions. From the second moment conditions it can readily be seen that,

$$x_{c_2}^2 + x_{c_3}^2 = \frac{I_b - \sum_{n \neq c_2, c_3} m x_n^2}{2m_c} \quad (14)$$

and

$$y_{c_2}^2 + y_{c_3}^2 = \frac{I_x - 2m_H(y_{H_1}^2 + y_{H_2}^2)}{2m_c} \quad (15)$$

application of the first moment condition yields,

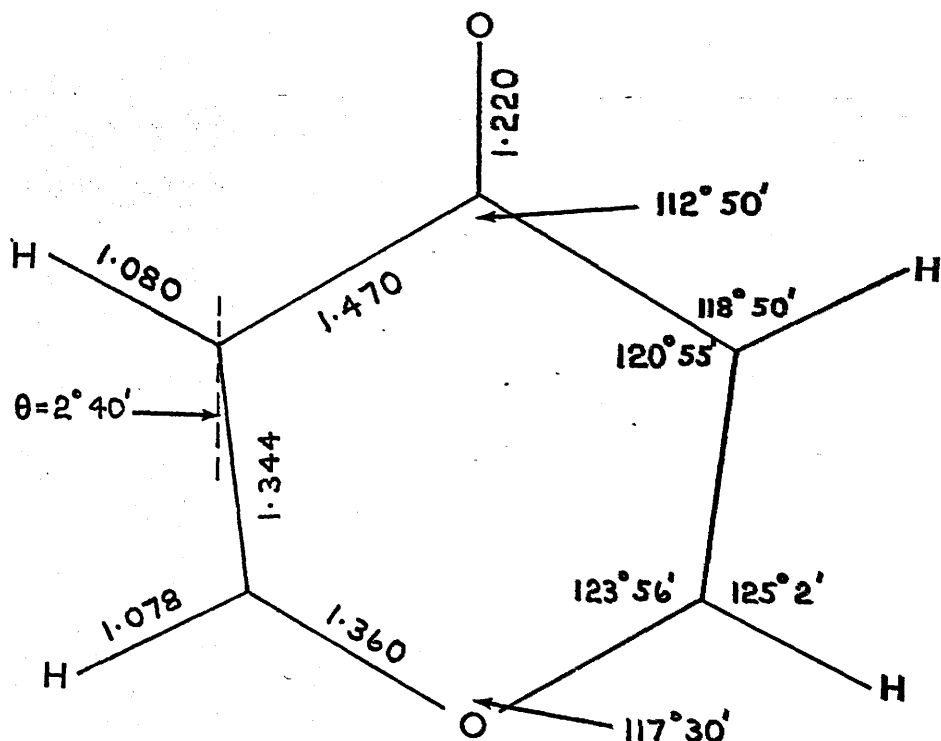
$$x_{c_3} - x_{c_2} = \frac{\sum_{n \neq c_2, c_3} m x_n}{2m_c} \quad (16)$$

TABLE X

Coordinates of the atoms of γ -Pyrone relative to the Principal axes of the molecule (\AA)

	<u>a</u>	<u>b</u>
C ₂	- 1.0746	1.1627
C ₃	0.2679	1.2251
C ₄	1.0813	0
C ₅	0.2679	- 1.2251
C ₆	- 1.0746	- 1.1627
O ₁	- 1.7805	0
O ₂	2.3013	0
H ₁	- 1.7337	2.0152
H ₂	0.7679	2.1823
H ₃	0.7679	- 2.1823
H ₄	- 1.7337	- 2.0152

In order to use equations (14) - (16) to determine the coordinates of C_2 and C_3 it is necessary to assume two parameters. Using the r^s structure obtained for acrolein¹⁰ as a guide, the coordinate of C_4 was fixed by assuming the length of the $C_4 - O_2$ bond to be 1.220 Å. If the apparently reasonable assumption is now made that the $C_2 - C_3$ bond is parallel to the x or a axis of the molecule and the coordinates of the ring carbon atoms are calculated, the resulting structure has totally unreasonable bond lengths for both the $C_3 - H_2$ and $C_2 - H_1$ bonds. In a saturated hydrocarbon the C - H bond length is of the order 1.10 Å while that to a pure ethylene carbon atom is about 1.07 Å. The bonds in γ -Pyrone are therefore expected to be somewhere between these two extremes and probably closer to the value of 1.084 Å found in benzene. It is also expected by comparison with similar molecules that $C_3 - H_2$ and $C_2 - H_1$ bond lengths will be similar. With these criteria the most satisfactory structure for γ -Pyrone was that with a $C_3 - H_2$ bond length of 1.080 Å. The structure is shown in fig.10 and the coordinates of the atoms with respect to the principal axis system of the normal species are given in table X.



The Structure of γ - Pyrone (A).

fig.10

The use of the ground state moment of inertia conditions and the first moment condition to determine atomic coordinates generally gives results which are greater than the true r^s coordinates of the atom⁹. The magnitude of this error is inversely proportional to the mass of the atom involved and is consequently largest for hydrogen atoms for which it can be $\sim 0.01 \text{ \AA}$. For the carbon atoms located in this manner in this work the error is not expected to be any larger than experimental error on a given r^s coordinate.

It can be seen from fig.10 that the $C_2 - C_3$ bond is not parallel to the a axis of the molecule. The angle θ is thought to be too large to be simply attributed to any error in the carbon atom coordinates. It seems more likely that it is a genuine indication of angular distortion of the ring to accommodate the oxygen hetero-atom in a planar structure.

5. The Spectrum and Structure of Thiapyrone.

On the assumption that thiapyrone, like γ -Pyrone, is planar, the model given in table XI was used to predict line frequencies for the molecule. The molecular geometry of that part of the ring around the carbonyl group was assumed to be identical with that of γ -Pyrone while the parameters for the lower portion of the ring were based on the microwave structure of thiophene¹¹.

TABLE XI.

Preliminary Model for Thiapyrone (Å).

$C_2 - S$	1.71	$C_2 SC_6$	102°
$C_3 - C_2$	1.36	$C_3 C_2 S$	122°
$C_3 - C_4$	1.42	$C_4 C_3 C_2$	122°
$C_4 - O$	1.21	$S C_2 H_1$	119°
$C - H$	1.08	$C_2 C_3 H_2$	119°
		$C_3 C_4 C_5$	112°

From this structure the following set of rotational constants was predicted for thiapyrone.

$$\frac{A + C}{2} = 3311.77 \text{ Mc/s.}; \quad \frac{A - C}{2} = 1909.15 \text{ Mc/s.}; \quad \kappa = -0.730.$$

The dipole moment, measured in benzene solution as $3.96 \text{ D}^{2,3}$ was assumed to be directed wholly along the a inertial axis of

the molecule. The most outstanding lines in the spectrum were therefore expected to be the μ_a R - branch transitions for which $\Delta K_{-1} = 0$, $\Delta K_{+1} = +1$. For this molecule it was expected that the $J = 7 - 6$ transition would fall in the region 21 - 24 Gc/s.

Thiapyrone was found to have no detectable vapour pressure at room temperature. In order to admit a sample to the absorption cell it was necessary that both the sample and the cell be maintained at a temperature of at least 50°C. This was done simply by circulating water thermostated at the required temperature through a water jacket around the sample tube which was attached directly to the cell. The hot water was then passed through a length of copper tubing laid on top of the cell itself. The heating effect obtained in this way was found to be quite adequate and provided care was taken that the cell temperature was sufficiently high to prevent trapping out of the sample, a steady stream of vapour could be drawn through the absorption cell.

Even at this elevated temperature however, the spectrum was never very strong and most of the preliminary line assignments for this molecule were made from recordings. A number of lines, each accompanied by a vibrational satellite some 30 Mc/s to high frequency of the ground state lines, were detected in

the region 21 - 24 Gc/s. It was clear therefore that the low frequency ring deformation mode responsible for the satellite spectrum of γ - Pyrone was again present in thiapyrone. Since the nuclear spin statistical weights are identical with those of the normal species of γ - Pyrone this proved a useful aid in the assignment of the spectrum. Those lines which were accompanied by a strong vibrational satellite could be immediately assigned to a transition for which K_{-1} was odd while those with a weak satellite have even values of K_{-1} .

The lines observed in the 21 - 24 Gc/s region were assigned to the $J = 7 - 6$ transition, the analysis of the spectrum following almost identical lines to that described in section 2 for γ - Pyrone. Once located on the recordings, most of the lines were just strong enough to be displayed on the oscilloscope and measured by the usual method. Having improved the rotational constants by the graphical method (section 2) the study of the spectrum was extended to cover the range 18 - 25 Gc/s, most of the lines belonging to the $J = 6 - 5, 7 - 6$ transitions being assigned.

The final set of rotational constants for the molecule was again obtained by fitting the observed line frequencies to equation (1) by the method of least squares. The resulting

rotational constants and observed and calculated line frequencies for the ground and first excited states are given in table XII.

The moments of inertia and inertial defects for both states are given in table XIII.

It can be seen from table XIII that the inertial defect (Δ) for the ground state is again close to zero and slightly negative. This suggests that this molecule also has a planar equilibrium configuration and that, like γ -Pyrone, the principal contribution to the inertial defect is from the low frequency ring deformation mode. This has the effect of making Δ for the first excited state large and negative.

It is interesting to compare the magnitudes of the inertial defects for both these states with those for the corresponding states in γ -Pyrone (table IX). In the case of thiapyrone the Δ 's are even more negative than those for γ -Pyrone, an effect which might be expected if the deformation involved the ring hetero atom. Sulphur being a heavier atom than oxygen would contribute more to Δ in a vibration perpendicular to the ring plane which involves that atom. This seems to be consistent with the assignment of the vibration given in the last section.

Owing to the involatility of the compound no isotopic work has been done on thiapyrone and the lines of the normal species

TABLE XII

Observed and Calculated Line frequencies for thiapyrone (Mc/s.)

	V = 0		V = 1	
	observed	calculated	observed	calculated
$6_{06} - 5_{05}$	18124.90	18124.90		
$6_{15} - 5_{14}$	20658.32	20658.32	20686.10	20686.12
$6_{25} - 5_{24}$	19427.34	19427.25		
$6_{24} - 5_{23}$	20990.50	20990.42		
$6_{34} - 5_{33}$	19921.78	19921.73	19954.57	19954.48
$6_{33} - 5_{32}$	20154.18	20154.19	20189.19	20189.25
$6_{43} - 5_{42}$	19901.21	19900.75		
$6_{42} - 5_{41}$	19909.69	19910.24		
$6_{52} - 5_{51}$	19850.06	19850.00		
$6_{51} - 5_{50}$	19850.06			
$7_{07} - 6_{06}$	20832.46	20832.53		
$7_{17} - 6_{16}$	20584.96	20584.92	20621.14	20621.09
$7_{35} - 6_{34}$	23250.88	23250.95	23288.82	23288.82
$7_{34} - 6_{33}$	23742.24	23742.27	23784.66	28784.71
$7_{44} - 6_{43}$	23270.93	23270.68		
$7_{43} - 6_{42}$	23301.47	23301.75		
$7_{62} - 6_{61}$	23151.42	23151.29		

(Cont'd.)

Table XII (Cont'd.)

	V = 0		V = 1	
	observed	calculated	observed	calculated
$\delta_{08} - \tau_{07}$	23544.19	23544.24		
$\delta_{18} - \tau_{17}$	23392.74	23392.68	23433.86	23433.91
$\frac{A+C}{2}$		3196.89		3189.75
$\frac{A-C}{2}$		1817.10		1807.19
κ		- 0.71199		- 0.71051

TABLE XIII

Moments of inertia and inertial defects for ground and first
excited states of thiapyrone

		Ia	Ib	Ic	Δ
		(a.m.u. \AA^2)	(a.m.u. \AA^2)	(a.m.u. \AA^2)	(a.m.u. \AA^2)
thiapyrone	V=0	100.8241	265.6314	366.3825	-0.0730
	V=1	101.1681	265.2703	365.6485	-0.7899

Fig. 11

spectrum were too weak to permit any Stark effect measurements to determine the dipole moment.

Using the experimental moments of inertia for the ground state of the normal species an approximate structure has been calculated for thiapyrone with the following assumptions. The bond lengths of that part of the molecule around the carbonyl group were taken to be the same as those for γ -Pyrone. The C - S bond length was initially taken as 1.71 Å as found for thiophene¹¹ and the two C - H bond lengths were assumed equal at 1.080 Å. The $C_4C_3H_2$ angle and the SC_2H_1 angle were both taken as 119°.

Expressing the y coordinates of C_3 and H_2 in terms of the angle ζ (fig.11).,

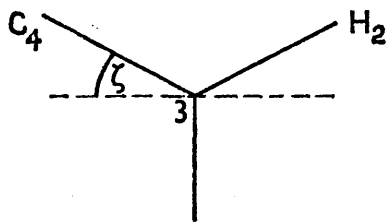
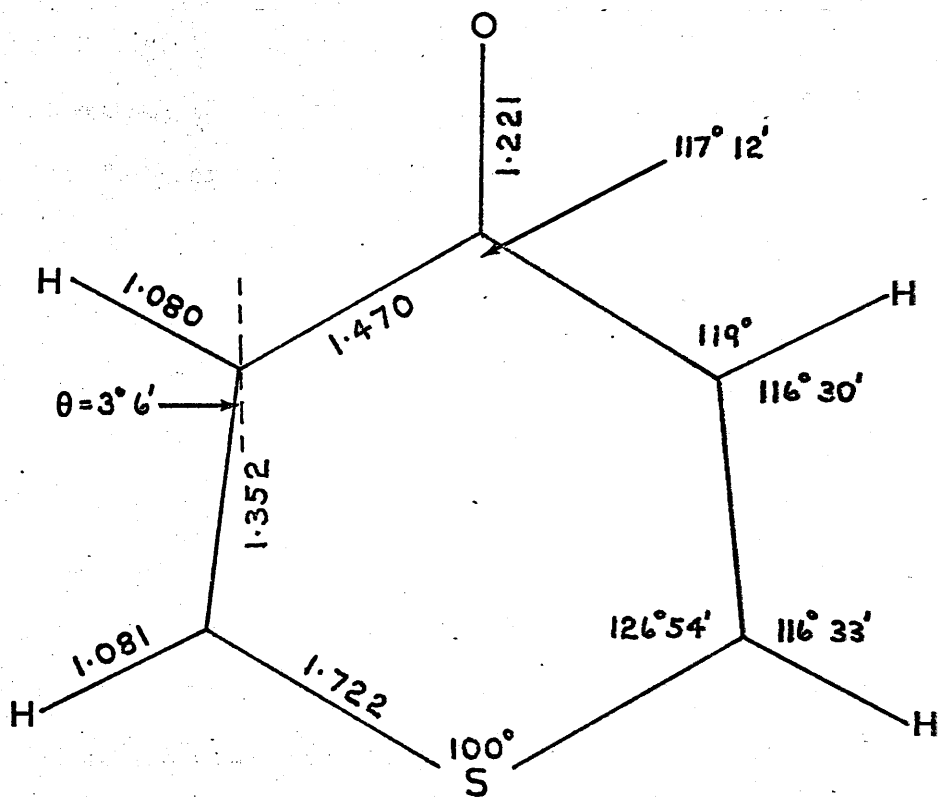


fig.11.

the values of ζ consistent with the experimental value of I_a was determined from the second moment condition

$$I_a = \sum my^2 \quad (17)$$

as $\zeta = 31^{\circ}24'$. Thus the y coordinates of C_3 , C_2 , H_2 , H_1 which



The Structure of Thiapyrone (Å)

fig.12.

satisfy equation (17) were calculated. The x - coordinates of C₄ and O were then determined.

Assuming the C₃ - C₂ bond length to be ~ 1.35 Å and keeping the geometry of the remainder of the molecule fixed, the x - coordinates of the sulphur atom which satisfied the appropriate first and second moment conditions was calculated. A value of 1.722 Å was obtained for the C₂ - S bond length which, in the accuracy of the calculation, is sufficiently close to an acceptable C - S bond length.

The final structure of thiapyrone is shown in fig.12. Although this structure is highly approximate it does indicate that similar trends in bond lengths reflecting the electronegativities of the hetero atoms may exist for the 4-pyrone series as for the series of five membered heterocyclic rings including furan and thiophene. A detailed discussion of the structure of thiapyrone would however require the further structural evidence provided by isotopic substitution.

6. Discussion.

The experimental results obtained for γ -Pyrone and thiapyrone are good evidence for the planarity of these molecules. In view of this it seems reasonable to assume that the remaining two members of the 4-pyrone series are also planar and indeed

recent experimental evidence confirms that the assumption is correct for thiopyrone¹².

Having established the planarity of the ring systems the most important remaining factor affecting the aromaticity of the molecules is the availability of the lone-pair electrons of the ring hetero atom for interaction with the π electron system of the remaining part of the molecule. It would be expected that the effects of such delocalisation would be reflected in the measured bond lengths of the molecule. At the present time only the structure of γ -Pyrone has been determined with sufficient accuracy to provide any reliable evidence of this nature.

The length of the $C_2 - O_1$ bond in γ -Pyrone (1.360 Å) shows considerable shortening from the "normal" C - O bond length of 1.426 Å as found in diethyl ether¹³. There is a striking similarity between the 1.360 Å for γ -Pyrone and the 1.362 Å obtained for the C - O bond length in the planar five membered heterocycle furan. While some of this bond shortening will be due to the hybridisation states of the atoms involved in the C - O bond there seems to be some evidence for some double bond character in the bond due to conjugation effects.

The $C_2 - C_3$ bond (1.344 \AA) is somewhat longer than the pure ethylenic double bond of 1.337 \AA . The value obtained in this work is very similar to the $C = C$ bond length in acrolein for which the r^S bond length has been determined as 1.345 \AA ¹⁰. It has been suggested by Lide¹⁴ that even when conjugation is assumed to affect other molecular properties in an important way, the effect on the lengths of multiple bonds will be extremely small being of the order $\pm 0.005 \text{ \AA}$ or less. While such a small variation is within the experimental error for the γ -Pyrone structure and can thus not be detected with certainty, the length of the $C_2 - C_3$ bond seems quite consistent with such a postulate.

One of the most interesting features of the γ -Pyrone structure is the length of the $C_3 - C_4$ bond which is situated between two double bonds. The value of 1.470 \AA obtained for γ -Pyrone is comparable with the values of 1.476 \AA and 1.470 \AA for the corresponding $C - C$ bonds in butadiene¹⁵ and acrolein¹⁰ respectively. The bond is 0.05 \AA longer than that originally estimated (1.42 \AA) from the x-ray work cited in section 2. It might appear that there is no real basis for comparison of the x-ray bond length with that of γ -Pyrone since the former work was carried out on a derivative of thiopyrone the exocyclic sulphur analogue of γ -Pyrone. The molecular orbital L.C.A.O. calculations⁴ discussed in the following paragraph show however

that the calculated bond orders of this bond in both molecules are very close and correspond to a variation of only 0.003^o in the bond length from one molecule to the other.

The molecular orbital calculations have been carried out using the Huckel approximation. There are two separate sets of calculations^{3,4}. The more recent calculations of Zarahdnik et al cover the whole of the 4- pyrone series while the earlier calculations of Brown are on γ - Pyrone only. The bond orders obtained in each of these calculations are given in table XIV for γ - Pyrone.

TABLE XIV

Bond orders for γ - Pyrone from M.O. Calculations

	Brown	Zarahdnik	Calculated	
			Empirical	M. O.
C ₂ - O ₁	0.565	0.575	0.278	0.383
C ₂ - C ₃	0.711	0.707	0.961	0.870
C ₃ - C ₄	0.570	0.576	0.261	0.360
C = O	0.488	0.484	-	0.800

From these bond orders, using either the bond order/length curve of Coulson¹⁶ or the empirical relationship¹⁷,

$$r_{c-c} = 1.517 - 0.18 p_y \quad (18)$$

where r_{c-c} is the C - C bond length and p_y the bond order, the bond length of $C_3 - C_4$ is predicted as 1.420\AA and $C_3 - C_2$ as 1.390\AA . Equation (18) has been shown to reproduce bond lengths to $+ 0.01\text{\AA}$ from bond orders and so the agreement of the calculated bond orders with experimental results is rather poor for γ -Pyrone. Using equation (18) and the corresponding equation for C - O bonds

$$r_{c-o} = 1.410 - 0.18 p_y \quad (19)$$

bond orders were calculated from the experimental bond lengths of γ -Pyrone and are shown in table XIV for comparison. Also included in table XIV are preliminary results of a Pariser-Par-Pople molecular orbital calculation on γ -Pyrone¹⁷, using the structure derived in this work. It can be seen that there is a considerable difference between the bond orders given in the last column and those of the first two columns of table XIV.

From table IX it can be seen that the inertial defects for the ground states of the various isotopically substituted species of γ -Pyrone are in general very similar in magnitude to that of the normal species. Such behaviour is entirely in accord with the evidence presented earlier for planarity of the system.

The measured value of 3.70 ± 0.10 for the dipole moment of γ -Pyrone agrees very well with the solution value of $3.72D$.

In valence bond language, a large contribution from structures e^* ($\sim 20D$) would be expected to produce an extremely polar structure, much more so than is implied by the measured value.

REFERENCES

1. H.C. Smitherman and L.N. Ferguson, *Tetrahedron*, 24(2), 932 (1968).
2. Rolla, Travers and Saneoi, *Ann. Chem. Rome*, 42, 507 (1925)
3. R.D. Brown, *J. Chem. Soc.*, (1951), 2670.
4. R. Zahrandink, C. Parkanji and J. Kontecky, *Coll. Czech. Chem. Comm.*, 27, 1242 (1962)
5. J. Toussaint, *Acta. Cryst.*, 7, 648 (1954)
6. S. Golden and E.B. Wilson, *J. Chem. Phys.*, 16, 669 (1948)
7. Tables of Line Strengths, P.F. Wacker and M.R. Pratto, National Bureau of Standards, Monograph 70 - vol. II, (1964)
8. J. Kraitchman, *Am. J. Phys.*, 21, 17 (1953)
9. C. C. Costain, *J. Chem. Phys.*, 29, 864 (1958)
10. E. Cherniak, C.C. Costain, *J. Chem. Phys.*, 45, 104 (1966)
11. B. Bak, D. Christensen, L. Hansen - Nygaard, J. Rastrup - Andersen, *J. Mol. Spec.*, 1 (1961)
12. S. A. Manley, B.Sc., Thesis, University of Glasgow (1968)
13. J. E. Boggs, J. E. Whiteford and C. M. Thompson, *J. Phys., Chem.*, 62, 713 (1959)
14. D. R. Lide Jr., *Tetrahedron*, 17, 125 (1962)

(Cont'd.)

References (Cont'd.)

15. D. J. Marais, N. Sheppard and B. P. Stoicheff,
Tetrahedron, 17, 163 (1962)
16. C. A. Coulson, "Valence", Oxford University Press
(1961)
17. P. Carrington, Private communication.

CHAPTER 3.

^{14}N - Quadrupole Coupling in the Microwave Spectra of Cyanamide and Nitramide.

1. Introduction.

As a result of the intensive studies carried out in recent years on the microwave spectra of cyanamide and nitramide the molecular geometries of these molecules in the gas phase are now well established ¹⁻⁶ and are given in tables I and II.

Both molecules have C_s symmetry and in the tables the angle ϕ denotes the out of plane angle of the amino hydrogen atoms.

TABLE I.

Structure of Cyanamide (\AA)

$\text{N}_1 - \text{N}_2$	2.506	\pm	0.002
$\text{N}_1 - \text{C}$	1.346	\pm	0.005
$\text{C} - \text{N}_2$	1.160	\pm	0.005
$\text{N}_1 - \text{H}$	1.001	\pm	0.015
HNH	$113^{\circ}31'$	\pm	2°
ϕ	$37^{\circ}58'$	\pm	1°

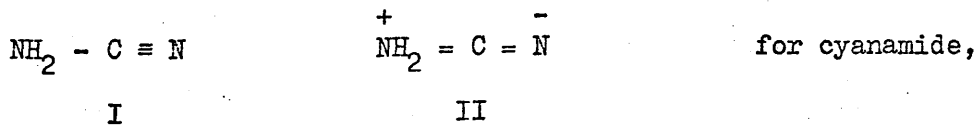
TABLE II.

Structure of Nitramide (\AA)

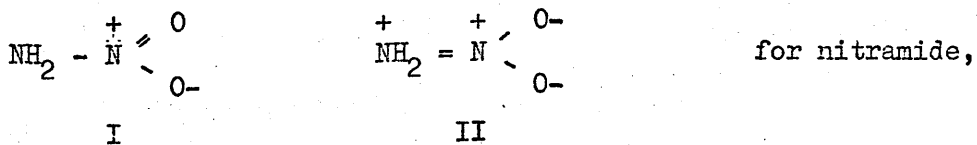
$N_2 - O$	1.206 (assumed)
$N_1 - N_2$	1.427 \pm 0.002
$N_1 - H$	1.005 \pm 0.010
HNH	115 $^{\circ}$ 11' \pm 2 $^{\circ}$
ONO	130 $^{\circ}$ 8' \pm 15'
ϕ	51 $^{\circ}$ 47' \pm 1 $^{\circ}$

In the case of cyanamide ϕ is the angle between the HN_1H bisector and the linear spine of the molecule extended and for nitramide it is the angle between the HN_1H bisector and the NNO_2 plane. In each case N_1 is the amino nitrogen atom.

It is usual to consider the electronic structure of each of these molecules as a resonance hybrid of two canonical forms,



and



The weights of these structures in the overall molecular wave functions for the molecules are unknown. It is to be expected, however, that if the contributions from structures II are significant and the amino nitrogen atom tends towards the sp^2 hybridised state implied by II then this atom will lose some of the pyramidal configuration associated with the nitrogen atom in ammonia. This effect is reflected to some extent in the measured values for the out-of-plane angles ϕ in tables I and II. Because of the adjacent like charges in structure II for nitramide this form is unlikely to be favoured. A small contribution from this form is indicated by the large value of ϕ obtained for the molecule.

Contributions from II are also indicated by the lengths of the $N_1 - N_2$ bond in nitramide and the $N_1 - C$ bond in cyanamide. These bonds show a shortening from the expected single bond lengths⁷ which may be attributed to delocalisation of the lone pair electrons of the amino nitrogen atom or to changes in hybridisation of the atoms forming the bond.

In an attempt to obtain further information about the electron distribution in cyanamide ^{14}N - quadrupole hyperfine structures for the species NH_2CN ¹⁵ and $^{15}NH_2CN$ were studied by Tyler⁸ and

and the following approximate values for the coupling constants obtained;

$$N_1 : \chi_{aa} \sim + 3.0 \text{ Mc/s} ; \quad \chi_{bb} \sim + 2.0 \text{ Mc/s} .$$

$$N_2 : \chi_{aa} \sim - 3.4 \text{ Mc/s} ; \quad \chi_{bb} \sim + 2.8 \text{ Mc/s} .$$

It was pointed out that the accuracy of the measured splittings obtained in this work was degraded by the fact that the signal-to-noise ratio of the lines was poor due to the lack of sample. The results do however show clearly the signs of the coupling constants and serve as a good starting point for a further investigation.

In order to refine the values given above and to see whether accurate experimental coupling constants can be interpreted in terms of the postulated structures, it was decided to investigate the hyperfine pattern of some lines in the spectrum of normal cyanamide $^{14}\text{NH}_2\text{CN}^{14}$. The treatment of this molecule is complicated by the presence of two non-equivalent nitrogen atoms which have coupling constants of similar magnitude.

Good resolution was obtained for several lines and while the results show the expected effects attributable to a contribution from structure II, the presence of other effects

influencing the electron distribution is indicated.

No previous investigation of the quadrupole hyperfine structure in the spectrum of nitramide has been made. Earlier work carried out on the quadrupole coupling of nitrogen atoms in nitro groups^{9,10,22}, has shown that in all cases the coupling constant of the nitrogen atom is very small and in many cases less than 1 Mc/s.

Owing presumably to the small coupling constants of N_2 in nitramide, the hyperfine structure resolved on the lines investigated could be accounted for by assuming that it was due to N_1 coupling alone. In no case was any finer structure due to N_2 coupling resolved.

2. Quadrupole Coupling in Molecules containing two Nitrogen Nuclei.

In this section a brief account is given of the theory of Bardeen and Townes¹¹ for the hyperfine structure due to two nitrogen nuclei in the same molecule. This is the treatment followed in the analysis of the spectra of cyanamide and nitramide described in the next section.

The spin angular momentum \underline{I} of a nucleus is represented by an integral or half-integral quantum number I .

$$\underline{I} = \sqrt{I(I + 1)} \hbar$$

There exist $2I + 1$ possible spin states for the nucleus.

Nuclei with spin angular momentum quantum no. $I > \frac{1}{2}$ have a non-vanishing nuclear quadrupole moment and for these nuclei the spin angular momentum can couple with the rotational angular momentum to produce a hyperfine structure in the rotational spectrum. The mechanism of this coupling is through the interaction of the nuclear quadrupole moment eQ and the electric field gradient of the molecule at the quadrupolar nucleus. When more than one quadrupolar nucleus is present in a molecule the individual quadrupole moments can couple via the molecular rotation.

In the absence of external fields the spin angular momentum \underline{I} couples with the rotational angular momentum \underline{J} to produce a resultant total angular momentum \underline{F} .

$$\underline{F} = \underline{J} + \underline{I} \quad (1)$$

$$F = |J + I|, |J + I - 1| \dots |J - I| \quad (2)$$

In a representation in which the quadrupole moments are not coupled to each other, the Hamiltonian is the sum of the two individual quadrupole terms

$$H = H_1 (I_1 J) + H_2 (I_2 J) \quad (3)$$

The method used to treat the problem in which the quadrupole moments are coupled depends on the degree of coupling in a particular case. If one nucleus couples much more strongly than the other then the major contribution to the hyperfine splitting is from that nucleus and the effect of the weakly coupled nucleus can be treated as a perturbation on these splittings. This treatment would almost certainly suffice for nitramide in which the amino nitrogen atom clearly couples to a much greater extent than the nitrogen atom of the nitro group.

When the coupling for both nuclei is comparable in magnitude as in the case of cyanamide, the treatment is more involved. If, for example, I_1 is strongly coupled and I_2 weakly coupled, then

$$\begin{aligned} F_1 &= J + I_1 \\ \text{and } F &= F_1 + I_2 \end{aligned} \quad (4)$$

Let $\psi_1 (F_1, F)$ be the wave functions for the states defined by F_1 and F . These wave functions are eigenfunctions of H_1 and the energy due to H_1 can be readily evaluated for wave functions of this type.

Reversing the situation and combining J with I_2 generates a similar set of wave functions represented by $\psi_2 (F_2, F)$ which are eigenfunctions of H_2 .

$$\begin{aligned} F_2 &= J + I_2 \\ F &= F_2 + I_1 \end{aligned} \tag{5}$$

For the particular case of nitrogen $I = 1$ and hence for cyanamide and nitramide $I_1 = I_2 = 1$. It is readily seen from (4) and (5) that

$$\begin{aligned} F_1 = F_2 &= |J + 1| \text{ --- } |J - 1| \\ \text{and } F &= |J + 2| \text{ --- } |J - 2| \end{aligned} \tag{6}$$

It is to be noted from (6) that there are a number of wave functions which have the same value of F but different values of F_1 and F_2 . These states will in general have different energies.

The two sets of different wave functions with the same F are linearly related, i.e.,

$$\psi_1 (F_1, F) = \sum_{F_2} C(F_1, F_2) \psi_2 (F_2, F) \quad (7)$$

$$\text{and } \psi_2 (F_2, F) = \sum_{F_1} C(F_1, F_2) \psi_1 (F_1, F)$$

The transformation coefficients $C(F_1, F_2)$ for $I_1 = I$, $I_2 = 1$ have been evaluated by Bardeen and Townes¹¹ and table III gives these coefficients in terms of J for the special case $I_1 = I_2 = 1$.

The two sets of eigenfunctions (7) have been derived on the basis that one or other of the two nuclei involved is weakly coupled relative to the other. In the case where the couplings are of similar magnitude the eigenfunctions will be given by a linear combination of either set, i.e.,

$$\psi (F) = \sum_{F_1} a(F_1) \psi_1 (F_1, F) \quad (8)$$

The equation $H\psi = E\psi$ will now be satisfied by the functions of equation (8). Using this and making use of equation (3) and the fact that ψ_1 is an eigenfunction of H_1 and ψ_2 of H_2 , and also that the wave functions $\psi_1 (F_1, F)$ are orthogonal then

it can be shown that

$$\left[A(F_1, F_1) + E(F_1) - E \right] a(F_1) + \sum_{F_1 \neq F_1'} A(F_1, F_1') a(F_1') = 0 \quad (9)$$

where
$$A(F_1, F_1') = \sum_{F_2} C(F_1, F_2) C(F_1', F_2) E_2(F_2)$$

for each value of F_1 and F_2 associated with the same F .

For equation (9) to have a non-trivial solution the determinant of the coefficients of the $a(F_j)$'s must be zero.

From (6) it can be seen that for the particular case under consideration there will be five sets of equations (9) each with different F values. Since the form of the secular determinants for the case of two atoms for which $I_1 = I_2 = 1$ will always be the same, the complete determinants are given in appendix A.

Each of the elements of the determinants is made up from quantities of the form $E_i(F_j)$. These can be readily evaluated as they are the energies for the case of a single nucleus coupling in an asymmetric top molecule and are given by the expression first derived by Golden and Bragg¹².

it can be shown that

$$[A(F_1, F_1) + E(F_1) - E] a(F_1) + \sum_{F_1 \neq F_1'} A(F_1, F_1') a(F_1') = 0 \quad (9)$$

$$\text{where } A(F_1, F_1') = \sum_{F_2} C(F_1, F_2) C(F_1', F_2) E_2(F_2)$$

for each value of F_1 and F_2 associated with the same F .

For equation (9) to have a non-trivial solution the determinant of the coefficients of the $a(F_j)$'s must be zero.

From (6) it can be seen that for the particular case under consideration there will be five sets of equations (9) each with different F values. Since the form of the secular determinants for the case of two atoms for which $I_1 = I_2 = 1$ will always be the same, the complete determinants are given in appendix A.

Each of the elements of the determinants is made up from quantities of the form $E_i(F_j)$. These can be readily evaluated as they are the energies for the case of a single nucleus coupling in an asymmetric top molecule and are given by the expression first derived by Golden and Bragg¹².

$$E_i(F_j) = eQ \left\{ \frac{\partial^2 V}{\partial a^2} [J(J+1) + E(\kappa) - (\kappa+1) \cdot \frac{\partial E(\kappa)}{\partial \kappa}] + 2 \frac{\partial^2 V}{\partial b^2} \cdot \frac{\partial E(\kappa)}{\partial \kappa} \right. \\ \left. + \frac{\partial^2 V}{\partial c^2} [J(J+1) - E(\kappa) + (\kappa-1) \cdot \frac{\partial E(\kappa)}{\partial \kappa}] \right\} \frac{Y(F_j)}{J(J+1)} \quad (10)$$

where

$$Y(F_j) = \frac{\frac{3}{2} C(C+1) - I(I+1) J(J+1)}{2I(2I-1)(2J-1)(2J+3)} \quad (\text{Casimir's function})$$

$$\text{and} \quad C = F(F+1) - I(I+1) - J(J+1)$$

In (10) Q is the nuclear quadrupole moment, e the electronic charge; a , b and c are the principal axes of the top and all other terms have their usual meanings. Casimir's function is tabulated for various values of F , I and J in¹³.

Since only charges outside the nucleus are considered as contributing to the potential V Laplace's equation $\nabla^2 V = 0$ will hold. Applying this to (10) and writing $\chi_{aa} = eQ \frac{\partial^2 V}{\partial a^2}$ etc., then

$$E_i(F_j) = \left\{ 2 \chi_{aa} \left[E(\kappa) - \kappa \frac{\partial E(\kappa)}{\partial \kappa} \right] + \chi_{bb} \left[E(\kappa) - J(J+1) - (\kappa-3) \frac{\partial E(\kappa)}{\partial \kappa} \right] \right\} \\ \times \frac{Y(F_j)}{J(J+1)} \quad (11)$$

The $E_i(F_j)$ can now be calculated from (11) and the elements of the secular determinant of (9) obtained. The solutions of this determinant then give the values of the coupling energies E for a given F value.

The interpretation of observed hyperfine patterns is simplified if the relative intensities of the individual components of the line are known. Evaluation of exact intensities in the case of two nuclei coupling to similar degree is an involved process. It would necessitate the solving of (9) for the $a(F_j)$'s. The intensity of a given component of a transition could then be calculated exactly using the matrix elements of the electric dipole between the states given by Condon and Shortley¹⁴.

There is however, a more rapid although approximate method for determining intensities in the intermediate coupling case. This involves interpolation between the component intensities calculated for the two extreme cases of one nucleus coupling much more strongly than the second. These latter intensities can be obtained from the tabulations in ¹³. This simple method of intensity calculation has been favoured in the analysis described in the next section.

TABLE III

Transformation Coefficients $C(F_1, F_2)$ for $I_1 = I_2 = 1$

<u>F</u>	<u>$C(F_1, F_2)$</u>
$J + 2$	$C(J+1, J+1) = 1$
$J + 1$	$C(J+1, J+1) = -C(J, J) = -\frac{1}{J+1}$
	$C(J+1, J) = C(J, J+1) = \frac{1}{J+1} \sqrt{J(J+2)}$
J	$C(J+1, J+1) = \frac{1}{(2J+1)(J+1)}$
	$C(J, J) = \frac{J(J+1)-1}{J(J+1)}$
	$C(J-1, J-1) = \frac{1}{J(2J+1)}$
	$C(J+1, J) = C(J, J+1) = -\frac{1}{J+1} \sqrt{\frac{2J+3}{2J+1}}$
	$C(J+1, J-1) = C(J-1, J+1) = \frac{1}{2J+1} \sqrt{(2J-1)(2J+3)}$
	$C(J, J-1) = C(J-1, J) = \frac{1}{J} \sqrt{\frac{2J-1}{2J+1}}$
$J - 1$	$C(J, J) = -C(J-1, J-1) = -\frac{1}{J}$
	$C(J, J-1) = C(J-1, J) = \frac{1}{J} \sqrt{(J-1)(J+1)}$
$J - 2$	$C(J-1, J-1) = 1$

3. Analysis of the Spectra.

Since both cyanamide and nitramide decompose readily if left in the absorption cell for any length of time, the spectra were studied by drawing a continuous stream of sample through the cell. This technique minimises decomposition on the cell walls and at the same time constantly removes any decomposition products which may be formed. In the case of cyanamide, vapour from the just molten sample was used and for nitramide observations were made with both sample and cell at 0°C.

3.1 Cyanamide.

A rough estimate of the magnitude and sign of the coupling constants for N_1 and N_2 can be obtained by applying the theory of Townes and Dailey¹⁵. They have shown that if the bond axis is taken as the z axis then for p electrons $q_x = q_y = \frac{1}{2}q_z$. If n_x , n_y , and n_z are the occupation numbers of the p_x , p_y and p_z orbitals respectively then there exists an unbalance of p electrons in the z direction given by

$$Up_z = \frac{N_x + N_y}{2} - N_z \quad (12)$$

The choice of a suitable value (10 Mc/s) for the coupling of one unbalanced p electron at the ^{14}N quadrupolar nucleus enables the coupling constant in the z direction to be obtained from (12).

If for cyanamide it is assumed that the structures I and II each contribute 50% to the overall wave function for the molecule and that N_1 is sp^2 hybridised and N_2 is sp hybridised then the coupling constants will be the mean of these calculated for the limiting canonical forms. Due account must be taken in this calculation of the negative charge on N_2 in structure II. It has been estimated from atomic fine structure measurements that in such a case the unbalance of p electrons at the nucleus in question should be multiplied by 1/1.25. This leads to the following set of approximate coupling constants,

$$\begin{array}{ll} \chi_{aa}(1) = + 2.5 \text{ Mc/s} & \chi_{bb}(1) = + 2.5 \text{ Mc/s.} \\ \chi_{aa}(2) = - 2.5 \text{ Mc/s} & \chi_{bb}(2) = + 4.25 \text{ Mc/s.} \end{array}$$

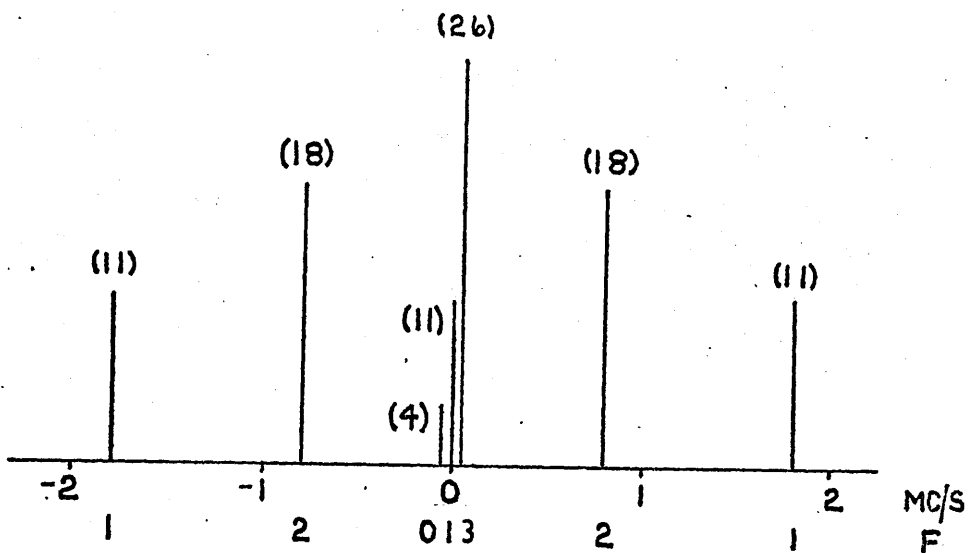
It can be seen that the signs and approximate magnitudes of these constants are consistent with the results obtained by Tyler for cyanamides containing ^{15}N given in the introduction.

In the study of normal cyanamide good resolution and measurements of fine structure were obtained for the ground state lines of the following transitions, $1_{01} - 0_{00}$, $8_{17} - 8_{18}$, $12_{1,11} - 12_{1,12}$, and $13_{1,12} - 13_{1,13}$.

Analysis of the fine structure of the $1_{01} - 0_{00}$ R - branch transition requires the use of the full secular determinants for the 1_{01} energy level. However considerable simplification of the determinants is possible in this case. Taking the asymmetry parameter κ to be -1 then from (11) it can be seen that for the 1_{01} level the coupling energies depend only on χ_{aa} for each nucleus

$$E_i(F_j) = -\chi_{aa}(i) \gamma(F_j) \quad (13)$$

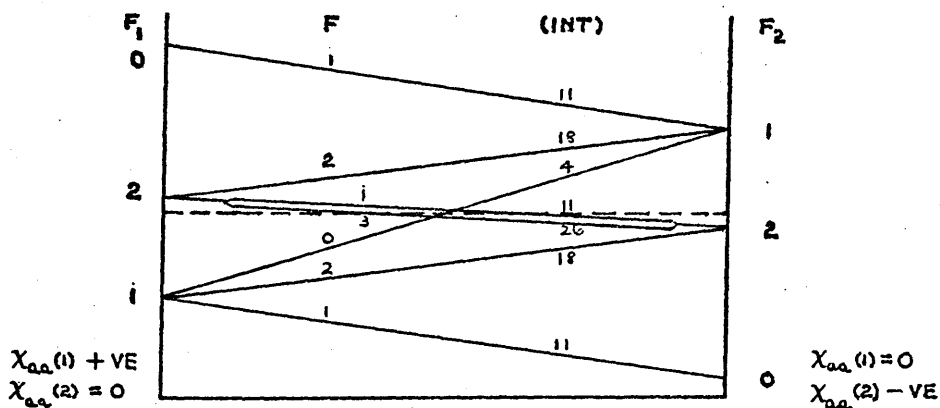
From (13) and table III the determinants for the 1_{01} level can be readily set up. Solution of these determinants for reasonable values of $\chi_{aa}(i)$ shows a seven line pattern of the form shown in fig. 1. is to be expected. The relative intensities of the components shown in brackets were calculated by the method described in the last section.



Predicted Hyperfine Pattern of $1_{01} - 0_{00}$ Transition of NH_2CN .

fig. 1.

If the coupling energy of the two nuclei is assumed to vary linearly as the ratio $\alpha = \frac{\chi_{aa}(1)}{\chi_{aa}(2)}$ varies between the two extreme cases of a single nucleus coupling then a qualitative correlation diagram such as fig. 2 may be constructed for the 1_{01} level.



Qualitative Correlation Diagram for the Hyperfine Components of 1_{01} energy level of NH_2CN .

fig. 2.

The deviation of a component from the line origin is plotted for the extreme cases of a single nucleus coupling on the left hand and right hand ordinates of fig. 2. The quantity a is plotted on the abscissa. In the intermediate coupling case the energy levels are labelled by the appropriate value of F .

A line diagram of the experimentally observed hyperfine pattern for the $1_{01} - 0_{00}$ transition is shown in fig. 3, while fig. 4A shows a photograph of the oscilloscope trace of the transition.

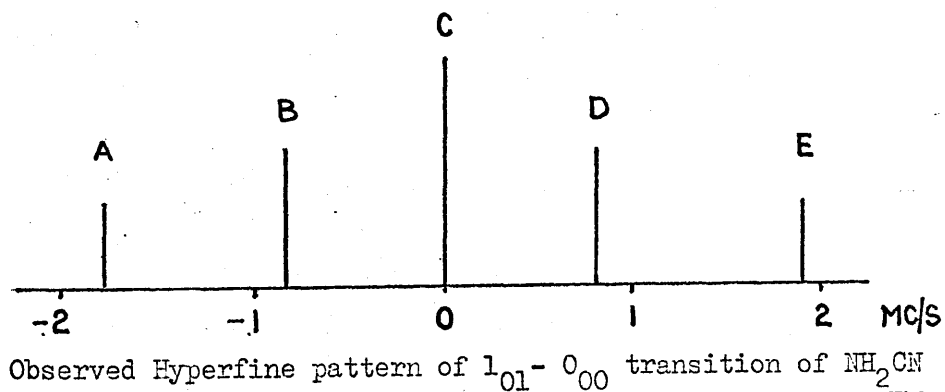


fig. 3.

The pattern is that of a nearly symmetrical quintet and comparison with figs. 1 and 2 show that peak C is likely to be a composite peak comprising the three central components of fig. 1.

A



B

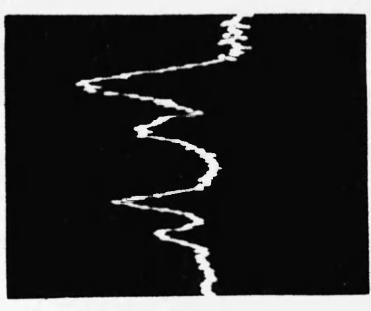


FIG 4

The peak maximum in this case is assumed to be the weighted mean of the three components.

An iterative fitting procedure initially carried out on the accurately measured components B and D ($F = 2$) and finally on all the components of the transition gave the following accurate values for $\chi_{aa}(i)$,

$$\chi_{aa}(1) = + 3.05 \pm 0.02 \text{ Mc/s} \quad \chi_{aa}(2) = - 3.30 \pm 0.02 \text{ Mc/s}$$

To determine values for $\chi_{bb}(i)$ the three Q - branch transitions mentioned above were studied. From table III it can be seen that the off-diagonal elements in the secular determinants depend on terms of the form $\frac{1}{J}$. For high J values these become very small compared with the diagonal elements and for $J \geq 8$ can be neglected. In this case the coupling energies reduce simply to the sum of the energies for each individual nucleus coupling,

$$\Delta E_Q(F) = \Delta E_1(F_1) + \Delta E_2(F_2) \quad (14)$$

Using the fact that for $\kappa = -1$ the energy levels with $K_{-1} = 1$ are degenerate and that $\frac{\partial E(\kappa)}{\partial \kappa} = \frac{1}{2} J(J+1)$, it can be shown from (11) that the splittings between the strongest

components, $\Delta F = 0$, $\Delta F_1 = 0$, $\Delta F_2 = 0$, of a $K_{-1} = 1$ high J Q-branch transition can be expressed in terms of $\chi_{aa} + 2\chi_{bb}$.

$$\Delta E_i(F_j) = (\chi_{aa} + 2\chi_{bb}) \gamma(F_j) \quad (15)$$

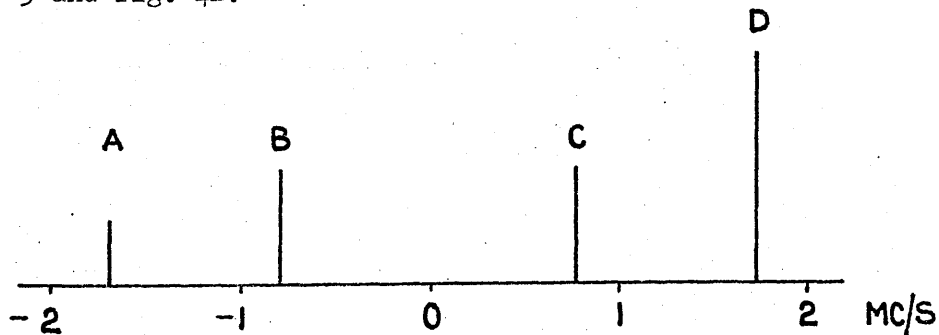
now writing $\alpha = \chi_{aa}(1) + 2\chi_{bb}(1)$ and $\beta = \chi_{aa}(2) + 2\chi_{bb}(2)$

(14) becomes

$$\Delta E_Q(F) = \alpha \gamma(F_1) + \beta \gamma(F_2) \quad (16)$$

The nine component lines all have similar intensities and divide into four groups as shown in table IV.

The observed pattern of each of the Q-branch lines studied was the very characteristic quartet structure shown in fig. 5 and fig. 4B.



Observed Hyperfine pattern of the μ_a , $K_{-1}=1$, Q-branch transitions
of NH_2CN

fig. 5.

For the $8_{17} - 8_{18}$ transition there was evidence of finer structure on peaks C and D but no measurements were made.

TABLE IV.

Frequency deviations ΔE of components for high J
 $K_{-1} = 1$ Q - branch transitions of $^{14}\text{NH}_2\text{CN}^{14}$.

A	J	$\alpha \gamma(J) + \beta \gamma(J)$
B	{ J + 1	$\alpha \gamma(J) + \beta \gamma(J + 1)$
	{ J - 1	$\alpha \gamma(J) + \beta \gamma(J - 1)$
C	{ J + 1	$\alpha \gamma(J + 1) + \beta \gamma(J)$
	{ J - 1	$\alpha \gamma(J - 1) + \beta \gamma(J)$
D	{ J + 2	$\alpha \gamma(J + 1) + \beta \gamma(J + 1)$
	{ J	$\alpha \gamma(J + 1) + \beta \gamma(J - 1)$
	{ J	$\alpha \gamma(J - 1) + \beta \gamma(J + 1)$
	{ J - 2	$\alpha \gamma(J - 1) + \beta \gamma(J - 1)$

Taking the peak maxima of fig. 5 to correspond to the mean frequency of each group in table IV then it is seen that,

$$\begin{aligned}
 AB = CD &= \beta \left\{ \frac{1}{2}(\gamma(J+1) + \gamma(J-1)) - \gamma(J) \right\} \\
 AC = BD &= \alpha \left\{ \frac{1}{2}(\gamma(J+1) + \gamma(J-1)) - \gamma(J) \right\}
 \end{aligned}
 \tag{17}$$

Accurate measurements of the fine structure in the three Q - branch lines and the use of the $\alpha_{aa}(i)$ values obtained from R - branch data enabled the values of $\alpha_{bb}(i)$ to be obtained from (17).

The final results for the coupling constants are :

$$N_1 : \chi_{aa}(1) = +3.05 \pm 0.02 \text{ Mc/s} \quad \chi_{bb}(1) = +1.85 \pm 0.02 \text{ Mc/s}$$

$$N_2 : \chi_{aa}(2) = -3.30 \pm 0.02 \text{ Mc/s} \quad \chi_{bb}(2) = +2.86 \pm 0.02 \text{ Mc/s}$$

As a final check on these values the splittings for the case of a single nucleus coupling in ^{15}N substituted cyanamides were recalculated. The agreement obtained between observed and calculated splittings for all the species studied is shown in table V.

TABLE V.

Observed and Calculated ^{14}N - Quadrupole splittings
for NH_2CN (Mc/s).

$F'-F$	$\Delta\nu$ (obs.)	$\Delta\nu$ (calc.)
<u>$^{14}\text{NH}_2\text{CN}^{15}$</u>		
$^2_{02} - ^1_{01}$	(1-0, 2-2) (3-2, 2-1) 1-1	0.84 - -
$^2_{12} - ^1_{11}$	2-2 2-1 (3-2, 1-0) 1-1	0.40 1.05 1.03 1.44
$^2_{11} - ^1_{10}$	1-1 2-1 3-2 2-2 1-0	0.94 0.91 0.70 1.14 0.59 1.28

(Cont'd.)

TABLE V (Cont'd.)

	F' - F	$\Delta\nu$ (obs.)	$\Delta\nu$ (Calc.)
<u>$^{15}\text{NH}_2\text{CN}^{14}$</u>			
$^2_{02} - ^1_{01}$	1-1 (3-2,2-1) (2-2,1-0)	- 0.87	- 0.94
$^2_{12} - ^1_{11}$	1-0 (3-2,2-2) (2-1,1-1)	1.42 0.96	1.39 0.92
$^2_{11} - ^1_{10}$	1-0 1-1 3-2 (2-1,2-2)	- - 1.00	- - 1.00
<u>$^{14}\text{NH}_2\text{CN}^{14}$</u>			
	<u>PEAK</u>		
$^8_{17} - ^8_{18}$	D C B A	0.93 1.61 0.93	0.91 1.64 0.91
$^{12}_1 11 - ^{12}_1 12$	D C B A	0.91 1.62 0.91	0.91 1.62 0.91
$^{13}_1 12 - ^{13}_1 13$	D C B A	0.91 1.62 0.91	0.91 1.63 0.91
$^1_{01} - ^0_{00}$	E D C B A	1.10 0.80 0.85 1.02	1.08 0.80 0.85 0.96

3.2 Nitramide.

Assuming N_1 and N_2 to be sp^2 hybridised and structures I and II to contribute equally to the nitramide wave function, application of the Townes and Dailey theory predicts the coupling constants for both nitrogen atoms as :

$$N_1 : \chi_{aa}(1) = + 2.5 \text{ Mc/s} \quad ; \quad \chi_{bb}(1) = + 2.5 \text{ Mc/s.}$$

$$N_2 : \chi_{aa}(2) = 0 \quad ; \quad \chi_{bb}(2) = 0$$

Again a coupling of 10 Mc/s for one unbalanced p electron at the ^{14}N nuclei is assumed.

In the secular determinants of equation (9) the off-diagonal elements are due entirely to coupling from N_2 . Clearly in this case it is sufficient to consider these elements to be negligible compared with the diagonal elements and thus treat the observed hyperfine structure as due mainly to N_1 coupling with only slight perturbations caused by the interaction of nucleus N_2 .

Experimental observations made on the ground state lines of the $3_{13} - 3_{12}$, $4_{13} - 4_{12}$, and $1_{11} - 2_{12}$ transitions showed each line to be a well defined doublet. Since it proved impossible to obtain any further resolution on any of the lines it was assumed that the observed splittings were due to the coupling of the amino nitrogen nucleus only. The analysis was therefore carried out with $\chi_{aa}(2) = 0$ and $\chi_{bb}(2) = 0$.

With this assumption it can be shown from (11) that the coupling energies of the components of the transitions are given by the following expressions :

$$\begin{aligned}
 3_{13} - 3_{12} \quad \Delta E_Q &= (1.1287 \chi_{aa}(1) + 1.3962 \chi_{bb}(1)) Y(F) \\
 4_{13} - 4_{32} \quad \Delta E_Q &= (0.8130 \chi_{aa}(1) + 0.6735 \chi_{bb}(1)) Y(F) \quad (18). \\
 1_{11} - 2_{12} \quad \Delta E_Q &= \chi_{bb}(1) (Y(F)) - (\chi_{aa}(1) + \chi_{bb}(1)) Y(F)'
 \end{aligned}$$

where ΔE_Q is the coupling energy and the prime refers to the upper state of a transition.

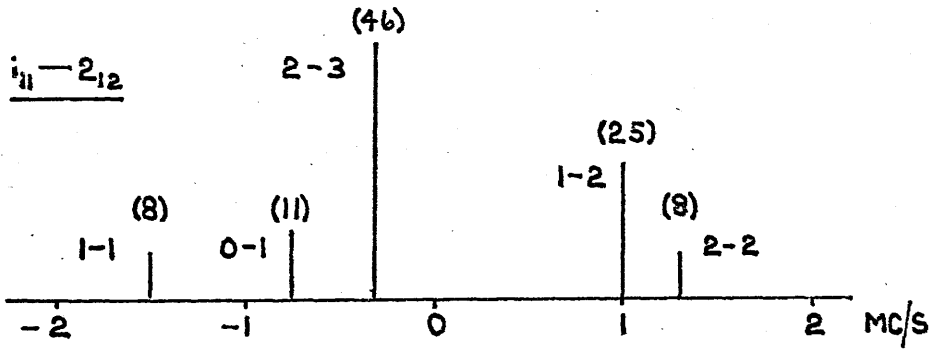
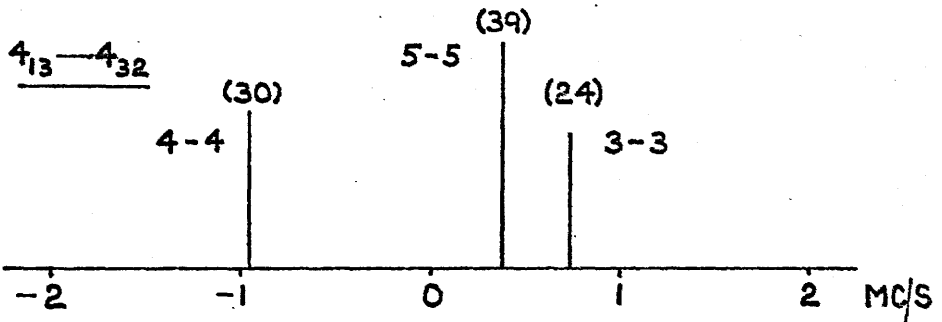
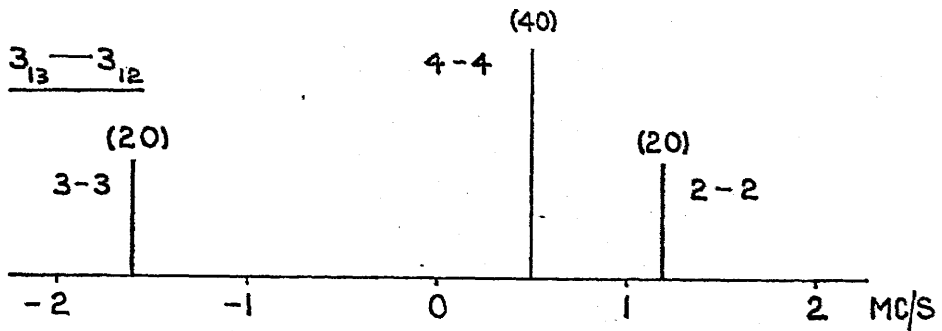
For each transition studied the components form two distinct groups for any reasonable values of the coupling constants.

Fig. 6 shows typical hyperfine patterns calculated for $\chi_{aa}(1) = 4$ Mc/s, $\chi_{bb}(1) = 1$ Mc/s.

In fig. 6 the figures in parenthesis are the component intensities and the components are labelled alongside.

If it is assumed that the peak maxima in the experimentally observed hyperfine patterns correspond to the weighted mean of the component lines of the groups in fig. 6, then it can be shown that the doublet splitting (Δ) can be expressed as a function of $\chi_{aa}(1)$ and $\chi_{bb}(1)$. The expressions are given in table VI.

The best fit to the observed splittings was obtained with $\chi_{aa}(1) = + 3.00$ Mc/s and $\chi_{bb}(1) = + 2.35$ Mc/s.



Calculated Hyperfine patterns for NH_2NO_2 with $X_{aa}(1) = 4 \text{ Mc/s}$.
 and $X_{bb}(1) = 1 \text{ Mc/s}$.

fig. 6.

The doublet separations (Δ) calculated using these values of the coupling constants are shown in table VI and can be seen to be in good agreement with the observed splittings.

It must be emphasised that these results for the coupling constants take no account of the contribution to the hyperfine structure from N_2 . The position of an observed peak maximum will depend to some extent on the coupling of the nitrogen of the nitro group, however this is expected to be very small and may possibly be zero.

TABLE VI.

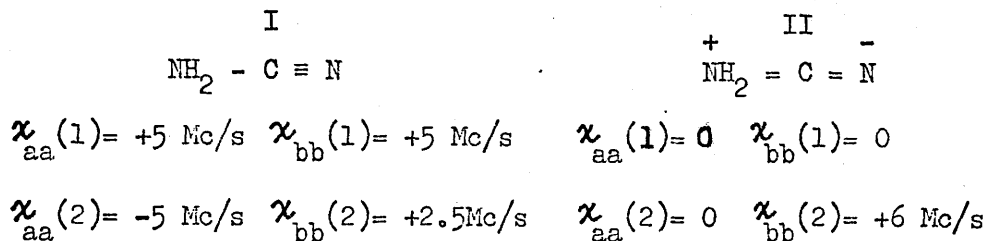
Observed and Calculated Hyperfine Splittings for NH_2NO_2 (Mc/s)			
	Δ	observed	calculated
$3_{13} - 3_{12}$	$0.4156\chi_{aa}(1) + 0.5197\chi_{bb}(1)$	2.41	2.46
$4_{13} - 4_{32}$	$0.3043\chi_{aa}(1) + 0.2521\chi_{bb}(1)$	1.58	1.51
$1_{11} - 2_{12}$	$0.3831\chi_{aa}(1) + 0.1094\chi_{bb}(1)$	1.34	1.41

4. Discussion of Results.

Quadrupole coupling constants are related to the field gradient round the quadrupolar nucleus and may be interpreted in terms of the bonding present in the molecule.

If cyanamide is considered to be planar and the amino

nitrogen sp^2 hybridised, application of the theory of Townes and Dailey to the limiting canonical forms I and II indicates that the field gradient in the a-b molecular plane is symmetrical about the N_1 nitrogen nucleus.



If, as implied in table I, N_1 has a pyramidal configuration, the field gradient in the a direction will be slightly reduced relative to the pure sp^2 case while that in the b direction will remain unchanged. It is expected therefore that $\chi_{aa}(1)$ will be smaller than $\chi_{bb}(1)$ their magnitudes depending on the contribution from structure II. The experimental results for the amino nitrogen atom show that $\chi_{aa}(1)$ and $\chi_{bb}(1)$ have their expected signs however their relative magnitudes conflict with those expected from the Townes and Dailey approach. A similar situation has been found in formamide¹⁶ where χ_{aa} is greater than χ_{bb} , and also in carbamyl fluoride¹⁷. An explanation is therefore required which provides for a considerable increase in the field gradient along the a ($N_1 - C$ bond) axis of the molecule. Such an electron distribution could result if the electrons of the $N_1 - C$ σ -bond

were polarised towards the carbon atom.

The effect of the expected delocalisation of the lone pair electrons of N_1 is clearly shown up in the coupling constants for the cyanide nitrogen atom. In the simple case where N_1 is sp^2 hybridised the lone pair electrons occupy a p_y orbital. Interaction of these electrons with the π -electron system of the nitrile group will therefore take place through the corresponding p_y orbitals on the carbon and nitrile nitrogen atoms. This approach provides for an electron drift in the a-c plane of the molecule towards N_2 . An asymmetric field gradient round the C - N_2 bond is to be expected therefore with $\kappa_{aa}(2)$ consequently reduced in magnitude compared to the usual value for a nitrile group¹⁸. The observed figure of - 3.30 Mc/s for $\kappa_{aa}(2)$ is entirely in accord with this view and the experimental coupling constants indicate the expected asymmetry of the field gradient around the bond.

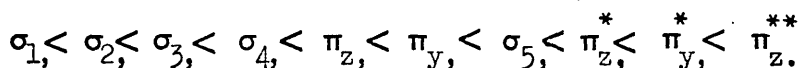
The observed coupling constants suggest that the contribution from structure II is certainly less than the value of 50% previously assumed and show that it is in fact probably closer to 35 - 40%. This estimate however is based entirely on the valence bond description of the molecule and thus takes no account of the effect of any polarisation of the σ -electrons of the

N_1 - C bond on the coupling constants of the amino nitrogen atom. It seems likely that if allowance could be made for this the contribution of structure II may well be closer to 40%.

These results are in fair agreement with the estimate of 36% for the weight of structure II obtained using the empirical formula due to Pauling¹⁹ for the double bond character of the N_1 - C bond. This last result may however be in error since it is difficult to say to what extent the shortening of the bond is due to the hybridisation states of the amino nitrogen atom and carbon atom in cyanamide rather than the delocalisation of the lone pair electrons of N_1 into the π - electron system of the molecule. A better measure of the contribution of structure II might come from a consideration of the degree of non-planarity of the molecule. If it is assumed that ϕ varies linearly between the values 0° for the pure sp^2 case and 60° for ammonia then taking $\phi = 38^\circ$ for cyanamide leads to an estimate of 38% of structure II in the overall wave function of the molecule.

The ideas outlined above attempt to describe the electron distribution and bonding in cyanamide in terms of the contributing valence bond structures. A more realistic description can be obtained from the molecular orbital approach²⁰. Of the sixteen available electrons eight go into four low lying σ - orbitals. The π - electron system consists of two sets

of orbitals. The p_y orbitals on N_1 , carbon and N_2 form a three-centre π - system comprising one bonding, one non-bonding and an antibonding orbital. The p_x orbitals on carbon and N_2 form the usual two-centre system. The highest filled molecular orbital is the non-bonding π_y^* orbital of the three-centre system, which contains the lone pair electrons of the amino nitrogen atom. The order of the molecular orbitals found for $\phi = 25^\circ$ is



The σ_5 orbital contains the lone pair electrons of the nitrile nitrogen atom. Two sets of molecular orbitals are tabulated in ²⁰ for the non-planar form of cyanamide. These were obtained by different approaches to the extended Huckel calculation carried out by the authors. The form of the orbitals they obtain indicates that the N_1 - C bond has between 31% and 43% double bond character in non-planar cyanamide.

On the whole the available evidence is in fair agreement that, in valence bond language, structure II contributes quite significantly to the cyanamide wave equation. It seems consistent with the experimental results to consider this contribution to be of the order of 40%.

As for cyanamide, the Townes and Dailey approach for

nitramide predicts that in the non-planar case $\chi_{aa}(1)$ will be smaller than $\chi_{bb}(1)$. However once again the experimental results show the situation to be reversed. Thus a similar electron distribution and polarisation effect of the σ - electrons seems to exist around the amino nitrogen nucleus in nitramide as exists in cyanamide although the relative magnitudes of the coupling constants indicate that in this case the effect may not be so pronounced for nitramide.

In the simple valence bond approach the magnitude of $\chi_{aa}(1)$ suggests again about a 40% contribution from structure II and consideration of polarisation effects of σ - electrons would tend to increase this estimate rather than decrease it. This is rather surprising since, as explained earlier in this chapter, form II would not normally be expected to be as important for nitramide as for cyanamide. Indeed the large value of ϕ (51°) for nitramide suggests that structure II may contribute only about 20% to the wave function.

Nitramide, cyanamide, formamide and carbamyl fluoride all belong to the general class $\text{NH}_2 - \text{X}$ where X is an electron withdrawing group. For this type of molecule it might be expected that the measured field gradient of the N_1 atom in the

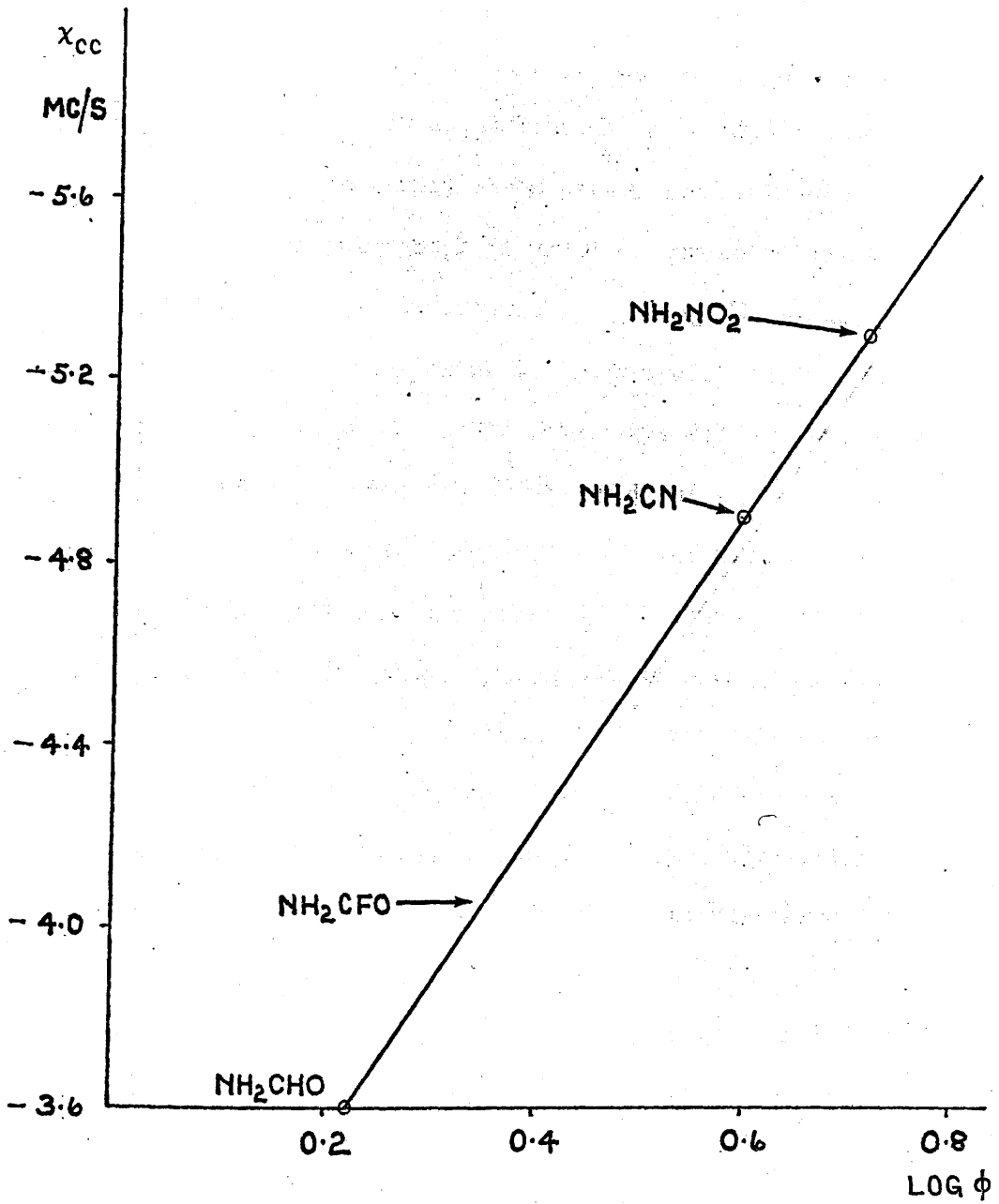
a - c inertial plane will systematically reflect any change in the out of plane angle ϕ . This value of $\chi_{cc}(1)$ will presumably reflect the degree of interaction of the lone pair electrons of N_1 with the π - electron system of the molecule. The assumption that the extent to which such an interaction takes place is a function of ϕ is to some extent supported by the molecular orbital calculations for cyanamide. It can be seen by comparing the coefficients of the individual atomic orbitals contributing to the molecular orbitals that the two three - centre π - orbitals are affected to the greatest extent by a change in ϕ .

Table VII shows that for the three molecules for which ϕ has been measured there does indeed appear to be a correlation between the experimental out of plane angle and $\chi_{cc}(1)$.

TABLE VII

Experimental Quadrupole Data (Mc/s) and ϕ ($^\circ$) for NH_2-X

	NH_2CHO	NH_2CFO	NH_2CN	NH_2NO_2
$\chi_{aa}(1)$	+ 1.9	+ 2.36	+ 3.05	+ 3.00
$\chi_{bb}(1)$	+ 1.7	+ 1.69	+ 1.85	+ 2.35
$\chi_{cc}(1)$	- 3.6	- 4.05	- 4.90	- 5.35
ϕ	17	-	38	51



Graph of $\log \phi$ against x_{cc} for NH_2X .

fig. 7.

Fig. 7 shows that the graph of $\log \phi$ against $\chi_{cc}(1)$ for these molecules is a straight line although it should be emphasised that since only three points are available at the present time for this graph it would be unwise to place too much credence on the fit obtained.

On the basis of experimental quadrupole coupling data¹⁷ carbamyl fluoride seems to fit into table VII between formamide and cyanamide. From fig. 7 it would therefore be expected to be non-planar with $\phi \sim 20 - 25^\circ$. The microwave study of this molecule by Rigden and Jackson¹⁷ does not give any estimate of ϕ since only the normal species spectrum was studied although the inertial defect ($+ 0.06 \text{ a.m.u. \AA}^2$) strongly suggests a near planar structure. It is worth noting however that similar results obtained for formamide in an early study of that molecule¹⁶ were erroneously interpreted with regard to the planarity of the molecule²¹. It should prove interesting if further isotopic work is carried out on carbamyl fluoride to see whether it indeed fits into the expected position on fig. 7.

REFERENCES

1. J.K. Tyler, L.F. Thomas and J. Sheridan, Proc. Chem. Soc., 1959, 155.
2. D.J. Millen, G. Topping and D.R. Lide Jr., J. Mol. Spectry., 8, 153 (1962)
3. D.R. Lide Jr., J. Mol. Spectry., 8, 142 (1962)
4. G.P. Shipulo, Opt. Spectry., (U.S.S.R.)(English Transl.) 10, 288 (1961)
5. J.K. Tyler, J. Sheridan and C.C. Costain, unpublished results.
6. J.K. Tyler, J. Mol. Spectry., 11, 39 (1963)
7. Cox and Jeffrey, Proc. Roy. Soc., A207, 110 (1951)
8. J.K. Tyler, private communication.
9. Smith and Magnuson, Phys. Rev., 87, 226(A) (1952)
10. Millen and Morton, J. Chem. Soc., 1523, (1960)
11. J. Bardeen and C.H. Townes, Phys. Rev., 73, 97 (1948)
12. S. Golden and J.K. Bragg, Phys. Rev., 75, 735 (1949)
13. C.H. Townes and A.J. Shawlow, "Microwave Spectroscopy", McGraw - Hill Book Co. Inc., (1955)
14. Condon and Shortley, "Theory of Atomic Spectra" McGraw Hill, New York, 1935.
15. C.H. Townes and B.P. Dailey, J.Chem.Phys., 17, 782 (1949)
16. R.J. Kurland and E.B. Wilson Jr., J. Chem. Phys., 27, 585 (1951)
17. J.S. Rigden and R.H. Jackson; J. Chem. Phys., 45, 3646 (1966)
18. R. Trambarulo and W. Gordy, Phys., Rev., 79 224A (1950)

19. L. Pauling, "The Nature of the Chemical Bond",
Cornell Univ. Press, (1939)
20. H.F. Henneike and R.S. Drago, J.A.C.S., 90 5112 (1968)
21. C.C. Costain and J.M. Dowling, J. Chem. Phys., 32,
158 (1960)
22. Hess - Bander and Gunthard, J.Mol. Spectry., 22, 208
(1967)

CHAPTER 4.

Vibration - Rotation Interactions in Dideuterocyanamide

1. Introduction

In the microwave spectrum of a near symmetric rotor such as dideuterocyanamide the three components of the $J = 2 - 1$ μ_2 R - branch transition are expected to give rise to near symmetric triplets for both ground and excited states. The central component of each triplet has $K_{-1} = 0$ and the two outer components have $K_{-1} = 1$.

In the previous investigations of the cyanamide spectrum^{1,2,3} this was shown to be the case for the ground and first excited states of the inversion mode of the normal species (HC_2CN). However, for ND_2CN it was found that while the lines for the ground state of the $J = 2 - 1$ transition gave the expected near - symmetric triplet those of the first excited state did not, the mean of the $K_{-1} = 1$ lines being displaced by $\sim + 13$ Mc/s. from the $K_{-1} = 0$ line.

Lide² has shown that this perturbation can be attributed to a vibration - rotation interaction between the rotational energy levels of the ground state and these of the first excited state. The derivation of the Hamiltonian including terms taking account of the vibration - rotation interactions has been thoroughly discussed by Lide. The Hamiltonian has the

following form:

$$H = H_{sr} + H_{as} + H_1 + Gp_{\phi}^2 + V(\phi) + 2Fp_{\phi} P_i \quad (1)$$

where H_{sr} is the symmetric rotor Hamiltonian and H_{as} the asymmetry correction term. H_1 is a vibration - rotation interaction term containing cross-products between components of the rotational angular momentum. This term can be removed from the Hamiltonian by choosing the axis system for the development of H in such a way that it coincides with the principal axes of the instantaneous inertial tensor⁴. The fourth and fifth terms are the kinetic and potential energies for the inversion vibration, and the last term couples this vibration with the i 'th component of the total angular momentum.

In a symmetric rotor basis the energy matrix of (1) factors into two sub-matrices of order $2J + 1$ whose diagonal elements contain alternately terms in E_i and E_j , where E_n is the energy of the n 'th vibrational energy level. Application of a Van Vleck transformation to these matrices removes the off-diagonal elements of H_{as} , H_1 and term six to second order and reduces the problem to a series of smaller matrices, one for each set of levels which were degenerate in the symmetric top limit.

In ND_2CN the rotational energy levels mainly involved in

the vibration - rotation interactions belong to the $v = 0$ and $v = 1$ states and have $K_{-1} = 2$ and $K_{-1} = 1$ respectively. Lide has shown the matrix elements for $K_{-1} \geq 2$ for the ground state to have the form

$$\begin{aligned}
 v = 0 \quad H_{+K+K} &= E_0 + E_{+K}'^{(2)} - G \\
 H_{-K-K} &= E_0 + E_{-K}'^{(2)} - G
 \end{aligned} \tag{2}$$

$$\begin{aligned}
 \text{where } G &= \frac{[d_{01}^2 + (2K+1)^2 e_{01}^2] (J-K)(J+K+1)}{E_1 - E_0 + (2K+1) [A - \frac{1}{2}(B+C)]} \\
 &+ \frac{[d_{01}^2 + (2K-1)e_{01}^2] (J+K)(J-K+1)}{E_1 - E_0 - (2K-1) [A - \frac{1}{2}(B+C)]}
 \end{aligned}$$

$$\begin{aligned}
 \text{and } H_{+K-K} = H_{-K+K} &= \frac{-2d_{01}e_{01}(2K+1)(J-K)(J+1K+1)}{E_1 - E_0 + (2K+1) [A - \frac{1}{2}(B+C)]} \\
 &- \frac{2d_{01}e_{01}(2K-1)(J+K)(J-K+1)}{E_1 - E_0 - (2K-1) [A - \frac{1}{2}(B+C)]}
 \end{aligned} \tag{3}$$

and for $K_{-1} = 1$ the matrix elements are:

$$\begin{aligned}
 H_{+1+1} = E_0 + E_{+1}'^{(2)} &- \frac{2d_{01}^2 J(J+1)}{E_1 - E_0 - [A - \frac{1}{2}(B+C)]} \\
 &- \frac{(d_{01}^2 + 9e_{01}^2)(J-1)(J+2)}{E_1 - E_0 + 3 [A - \frac{1}{2}(B+C)]}
 \end{aligned} \tag{4}$$

$$\begin{aligned}
H_{-1 \ -1} = E_0 + E_{-1}'^{(2)} - \frac{2e_{01}^2 J(J+1)}{E_1 - E_0 - [A - \frac{1}{2}(B+C)]} \\
- \frac{(d_{01}^2 + 9e_{01}^2)(J-1)(J+2)}{E_1 - E_0 + 3[A - \frac{1}{2}(B+C)]}
\end{aligned} \tag{4}$$

$$\begin{aligned}
H_{+1 \ -1} = H_{-1 \ +1} = - \frac{2d_{01}e_{01} J(J+1)}{E_1 - E_0 - [A - \frac{1}{2}(B+C)]} \\
- \frac{6d_{01}e_{01} (J+2)(J-1)}{E_1 - E_0 + 3[A - \frac{1}{2}(B+C)]}
\end{aligned} \tag{5}$$

To obtain the matrix elements for the $v = 1$ state the terms E_i are interchanged in (2) - (5). In these expressions E_i is the energy of the i 'th vibrational state and $E_K'^{(2)}$ are the rigid asymmetric rotor energies correct to second order. In the notation $H_{+K \ +K}$ the signed K subscripts have the same significance as the King, Hainer and Cross asymmetric rotor notation E^{\pm} and O^{\pm} .

The effects of the vibration - rotation interaction terms on the energy levels can be seen from equations (2) - (5). The term $H_{+K \ -K}$ modifies the asymmetry splittings of the levels while the G term produces a shift in the mean position of these levels. From (3) it can be seen that when $E_1 - E_0$ (hereafter referred to as Δ' the inversion splitting) is comparable with

$(2K - 1) [A - \frac{1}{2} (B+C)]$ the two levels $J, K, v = 0$ and $J, K - 1, v = 1$ can strongly perturb each other.

On the basis of the theory outlined above, Millen, Topping and Lide¹ postulated that the near degeneracy in ND_2CN giving rise to the observed perturbation of the $v = 1, J = 2, K_{-1} = 1$ energy levels must be between the $v = 0, J = 2, K_{-1} = 2$ and $v = 1, J = 2, K_{-1} = 1$ energy levels. They were thus able to estimate Δ' as $\sim 15 \text{ cm}^{-1}$.

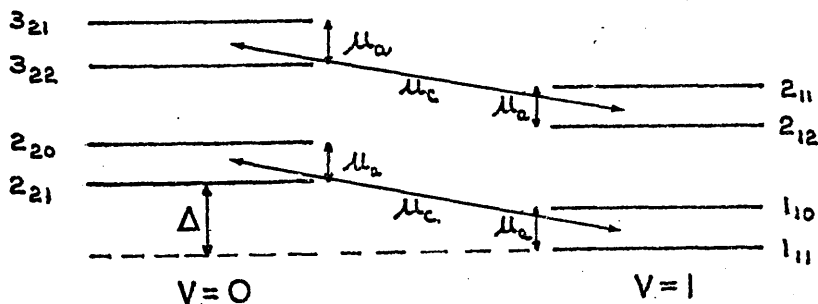
In this work experimental evidence has been obtained which provides a direct link between the rotational energy levels of the $v = 0$ and $v = 1$ states. This has enabled the predicted near degeneracies to be verified and some qualitative conclusions to be drawn regarding Lide's approximate second order solution of the energy matrix.

Measurement of the Stark effect of the $J = 2 - 1, v = 1, \mu_a$ R - branch transition has provided a direct relation between μ_c and Δ (Δ is defined as the separation between the $v = 0, 2_{21}$ and $v = 1, 1_{11}$ energy levels). Measurements have also been made of the Stark effects of the two μ_c R - branch transitions in the 8 - 40 Gc/s region, $v = 0, 4_{23} - v = 1, 3_{13}$ and $v = 0, 4_{22} - v = 1, 3_{12}$. Thus μ_c has been obtained as 0.86D and Δ as $\sim 11010 \text{ Mc/s}$.

Lines belonging to the series of $v = 1, K_{-1} = 1, \mu_a$ Q - branch lines have been observed and assigned. The transitions are strongly perturbed by the vibration - rotation interactions and the measurements have provided experimental evidence on the $J, K_{-1} = 1$ energy level splitting in the $v = 1$ state. A number of the μ_c Q - branch inversion transitions of the type $v = 1, J_{1J} - v = 0, J_{2,J-2}$ have also been assigned.

2. Stark effects in the $J = 2 - 1$ transition.

On the evidence of the vibration - rotation interactions discussed earlier it has been suggested that the $v = 0, J = 2, K_{-1} = 2$ and $v = 1, J = 2, K_{-1} = 1$ energy levels are closely degenerate. The orientation of the rotational energy levels in the $v = 1$ state relative to those of the $v = 0$ state will therefore be approximately that shown in fig. 1.



Approximate orientation of $v = 0$ and $v = 1$ Rotational energy levels in ND_2OH

fig. 1.

In a molecule of the type $\text{NH}_2 - \text{X}$, transitions between energy levels connected by a μ_c dipole matrix element also involve a change in vibrational quantum number. The μ_c connections in the energy level manifold are therefore between $v = 0, J + 1, K_{-1} = 2$ and $v = 1, J, K_{-1} = 1$ levels as shown in fig. 1. Thus if the energy level displacement parameter Δ as defined in fig. 1 is relatively small, there should be a detectable contribution from μ_c to the Stark effect of the $J = 2 - 1, K_{-1} = 1$ transition components.

In an attempt to detect this contribution, the Stark effects of the $2_{02} - 1_{01}, 2_{12} - 1_{11}, 2_{11} - 1_{10}$ transitions have been measured for both ground and first excited states. In each case measurements were made on both the $M = 0$ and $M = 1$ Stark components. The absorption cell was calibrated in the usual way using OCS and assuming its dipole moment to be 0.7124D.

It is clear from fig. 1 that in any case where the μ_a Q - branch interactions contribute to the Stark effect the dominant factor affecting the observed frequency shift will be repulsion between the closely degenerate $v = 0, J, K_{-1} = 2$ levels and to a lesser extent between the $v = 1, J, K_{-1} = 1$ levels. This large contribution from μ_a to the Stark effect will render any small μ_c contribution experimentally undetectable. The Q - branch contribution is present in

all cases except for $M = 0$ components for which it is zero.

It is therefore to be expected that only in the case of the $M = 0$ components will the effects of μ_c on the Stark effect be comparable with the effects of μ_a .

It was assumed in the first instance that the μ_a contributions dominated the Stark effects of all the measured components and values of μ_a were calculated for each component. From the argument outlined above, the μ_a value obtained from the $M = 0$ components was expected to deviate seriously from the values obtained from the other cases.

The coefficients of $\mu_a^2 E^2$ in the expression for the Stark energies of each line were calculated using the usual second order expression as given by Townes and Schawlow⁵. The expression is given in chapter 2 section 3 and will not be repeated here.

Where it was suspected that energy levels may be closely degenerate their contributions to the Stark effect were calculated from the more exact expression

$$E = \frac{E_1 + E_2}{2} \pm \sqrt{(E_1 - E_2)^2 + \frac{4\mu^2 \cdot E^2 \cdot K^2 \cdot M^2}{J^2 (J + 1)^2}} \quad (6)$$

where all terms have their usual meaning.

The resulting coefficients ^{WERE} corrected for the cell constant

(see chapter 2 section 3); the slopes $\frac{\Delta\nu}{V^2}$ of the corresponding graphs and the resulting values of μ_a are given in table. I.

TABLE I.

μ_a values obtained from Stark effect of J = 2 - 1 transition.

		M	$\frac{\Delta\nu}{V^2} \times 10^{-5}$	μ_a (D)
$K_{-1} = 0$	V = 0	0	17.10	4.23
		1	14.20	4.28
	V = 1	0	17.30	4.26
		1	14.00	4.25
$K_{-1} = 1$ (lower)	V = 0	0	14.50	4.30
		1	13.00	(4.53)
	V = 1	0	11.20	3.78
		1	12.50	(4.44)
$K_{-1} = 1$ (upper)	V = 0	0	14.75	4.39
		1	13.00	(4.57)
	V = 1	0	10.75	3.75
		1	12.00	(4.39)

The figures in brackets in table I are the μ_a values obtained from the $M = 1$ Stark components. The graphs of $\frac{\Delta\nu}{V^2}$ for these components show curvature at high values of the applied voltage due to the μ_c contribution to these components. This contribution increases as the levels connected by μ_c are forced closer together by the larger μ_a contribution to these components. The μ_a values in the table were derived from the limiting slopes of these graphs.

The $M = 1$ components excepted, the graphs of $\frac{\Delta\nu}{V^2}$ for all the other Stark components were, to within experimental error, straight lines. From table I it can be seen that, neglecting the results for the $v = 1, K_{-1} = 1, M = 0$ components, the mean value of μ_a is 4.33 D for both ground and first excited states. The measured values of μ_a for NH_2CN are 4.34 D and 4.26 D for $v = 0$ and $v = 1$ states respectively³.

As expected, the values of μ_a obtained from the $M = 0$ components of the $v = 1, K_{-1} = 1$ transitions are very different from the other results in table I, strongly suggesting an appreciable μ_c contribution to the Stark effect in these cases. It is interesting to note that the $M = 0$ components of the other transitions show no effects due to a μ_c contribution. This provides immediate confirmation of the fact that neither the $v = 0,$

$K_{-1} = 0$ or 1 or $v = 1$, $K_{-1} = 0$ levels are perturbed by the vibration - rotation interactions since the absence of a μ_c contribution to the Stark effect suggests that the levels are well separated in energy.

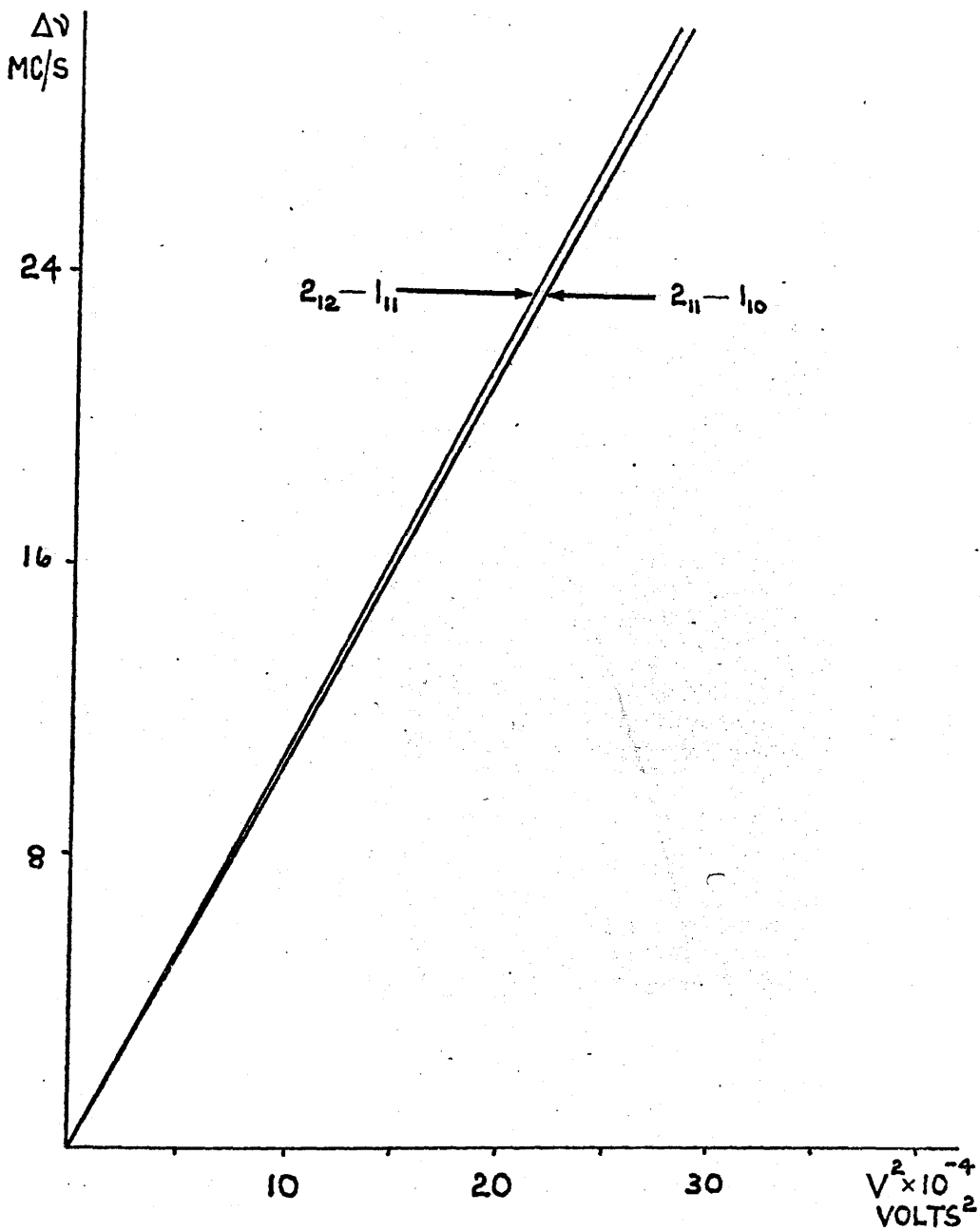
The slopes $\frac{\Delta\nu}{V^2}$ for the $M = 0$ components of each transition can be seen from fig. 2 to be very similar as are the theoretical coefficients of $\mu_x^2 E^2$ in the expression for the Stark effect. There is little gain therefore in considering these measurements as separate pieces of information and so only the Stark effect of the $v = 1$, $2_{12} - 1_{11}$, $M = 0$ component is treated here.

The Stark effect of this transition can be written as,

$$\frac{\Delta\nu}{V^2} = C f(J,M) \mu_a^2 + C f'(J,M) \mu_c^2 \quad (8)$$

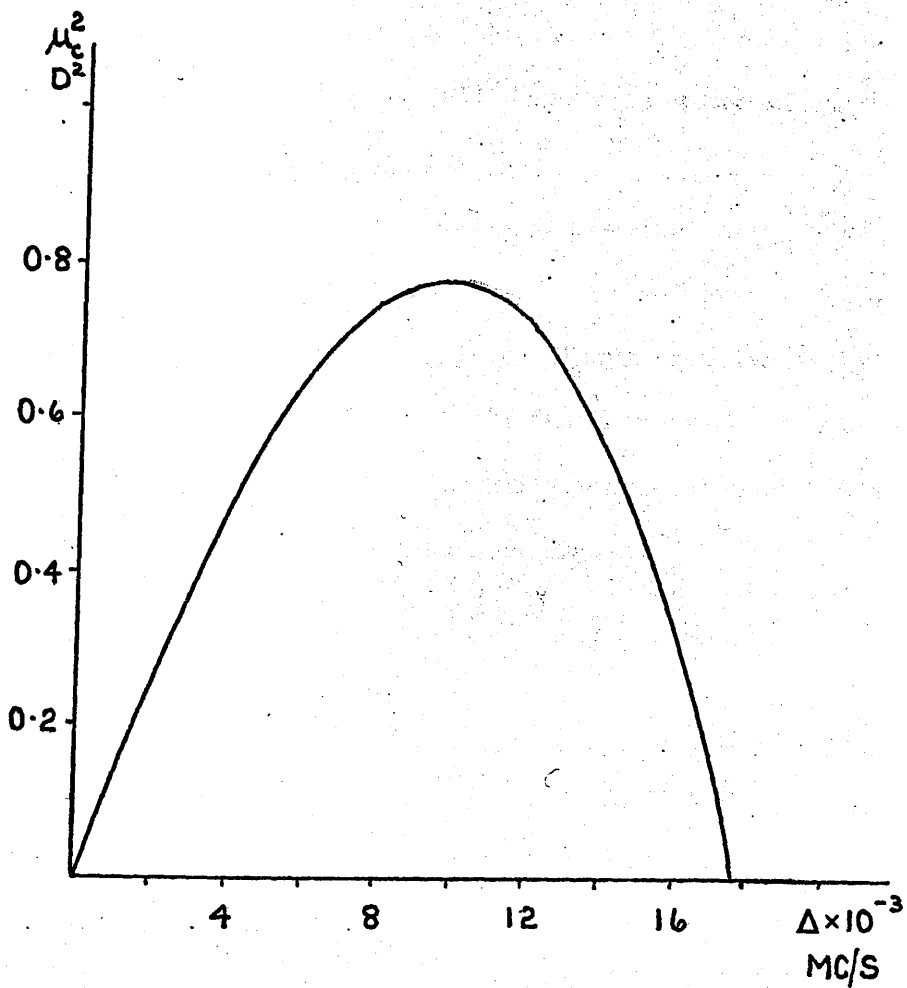
where C is the cell constant and $f(J,M)$ and $f'(J,M)$ are the theoretical second order Stark coefficients. All other terms have their usual meanings.

Making the approximations that the separation between the levels J, K and $J + 1, K$ is given by $(J + 1)(B + C)$ for each vibrational state, that the $v = 0$, $K_{-1} = 2$ levels are degenerate and determining the $v = 1$, $K_{-1} = 1$ splitting from the previous. μ_a R - branch measurements³ then (8) becomes,



Stark effect of $K_{-1} = 1, M = 0$ components of $J = 2 - 1$ transition
of ND_2CN

fig. 2.



Graph of μ_c^2 / Δ for ND_2CN .

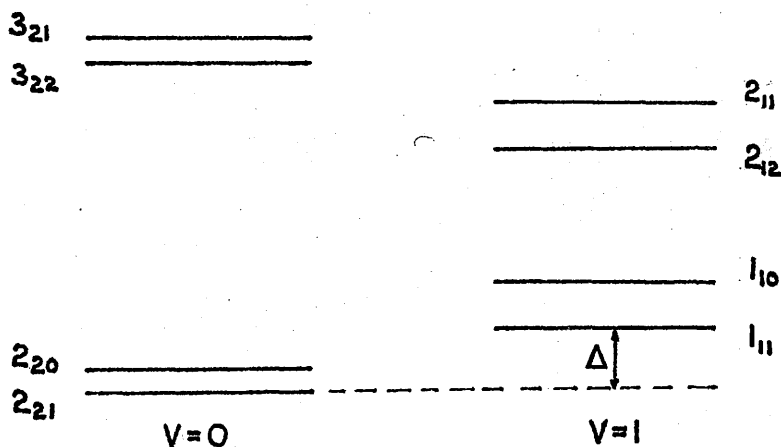
fig. 3.

$$11.20 = 0.7829 \mu_a^2 + \left[\frac{6398.90\Delta + 4009.43 \times 10^5}{17899.27\Delta + \Delta^2} \right] \mu_c^2 \quad (9)$$

where Δ is as defined in fig. 1.

Taking a value of 4.33 D for μ_a a graph of μ_c^2 against Δ has the form shown in fig. 3.

Fig. 3 shows that the maximum value for μ_c^2 is of the order 0.78 D and thus $\mu_c \leq 0.86$ D. For reasonable values of μ_c^2 the values of Δ satisfying (9) are always negative implying that the $v = 1, 1_{11}$ energy level is in fact higher in energy than the $v = 0, 2_{21}$ level. Thus the orientation of the energy levels has now been shown to be as in fig. 4.



Corrected energy level configuration for $\text{ND}_2 \text{CN}$.

fig. 4.

It is also clear from fig. 3 that, for a finite μ_c , Δ is less than ~ 18000 Mc/s.

3. The $v = 1, K_{-1} = 1, \mu_a$ Q - branch Lines.

The $v = 0, J, K_{-1} = 1$ energy levels of ND_2CN are unaffected by vibration - rotation interactions. The frequencies of the $K_{-1} = 1, \mu_a$ Q - branch transitions for the ground state of the molecule can therefore be readily predicted.

Polo⁶ has shown that for a slightly asymmetric top molecule like ND_2CN the rotational energy levels are given by a power series of the form

$$E(J_{KK_c}) = \frac{1}{2} (B+C)J(J+1) + [A - \frac{1}{2}(B+C)] K^2 + [A - \frac{1}{2}(B+C)] \left\{ K^2 \sum_{n=2}^{\infty} C_{on} \epsilon^n + J(J+1) \sum_{n=1}^{\infty} C_{1n} \epsilon^n + J^2(J+1)^2 \sum_{n=2}^{\infty} C_{2n} \epsilon^n + \dots \right\} \quad (10)$$

where K is the prolate K value and K_c the oblate value. The coefficients C_{mn} have been tabulated up to $K_{-1} = 5$ and ϵ^6 by Polo. ϵ , the asymmetry parameter used in this treatment is defined as

$$\epsilon = \frac{B - C}{2(2A - B - C)} = -\frac{1}{2} b$$

where b is the Wang asymmetry parameter.

Polo also includes the appropriate first order centrifugal distortion corrections to be added to the rigid rotor energy levels as calculated from (10). These corrections are given in terms of the six centrifugal distortion constants $D_J, D_{JK}, D_K, \delta_J, R_5, R_6$ first introduced by Nielsen⁸.

In terms of Polo's expressions the frequencies of the μ_a $K_{-1} = 1$ Q - branch lines can be readily shown to be³.

$$\frac{\nu}{J(J+1)} = \frac{B-C}{2} + 4R_5 - (J-2)(J+2)(J-1)(J+3) \left[\frac{B-C}{128} \epsilon^2 + \frac{1}{2} R_6 \epsilon \right] - 2J(J+1) \delta_J \quad (11)$$

The $\nu = 0$, $K_{-1} = 1$ μ_a Q - branch series has been previously located and assigned³, and from equation (11) has been shown to be consistent with a value of $B - C + 8R_5$ of 412.37 Mc/s. Owing to N^{14} - nuclear quadrupole coupling effects of the type discussed in detail in chapter 3, each of these lines exhibits a quartet hyperfine structure (see chapter 3 figs. 4B and 5).

Since the $\nu = 1$, $K_{-1} = 1$ energy levels are perturbed by vibration - rotation interaction with the $\nu = 0$, $K_{-1} = 2$ energy levels the frequencies of the $K_{-1} = 1$ μ_a Q - branch lines for the first excited state will deviate considerably from the frequencies predicted from equation (11).

As described earlier the effect of the vibration - rotation interaction terms on two J , $K_{-1} = 1$ energy levels is to modify the asymmetry splitting of the levels. This effect can be simply represented in the form of a 2 x 2 matrix;

$$\begin{vmatrix} W_1 & F \\ F & W_2 \end{vmatrix} \quad (12)$$

where W_1 and W_2 are the energies of the $K_{-1} = 1$ levels and F corresponds to the term $H_{+K -K}$ in Lide's theory. Clearly since Lide's G term only produces a shift in the mean positions of the levels it can be omitted from matrix (12) altogether provided the absolute energies are not required. The difference ΔE between the eigenvalues E_1 and E_2 of (12) is the frequency of the required $K_{-1} = 1$ Q - branch transition and is given by

$$\Delta E = \sqrt{(W_1 - W_2)^2 + 4F^2} \quad (13)$$

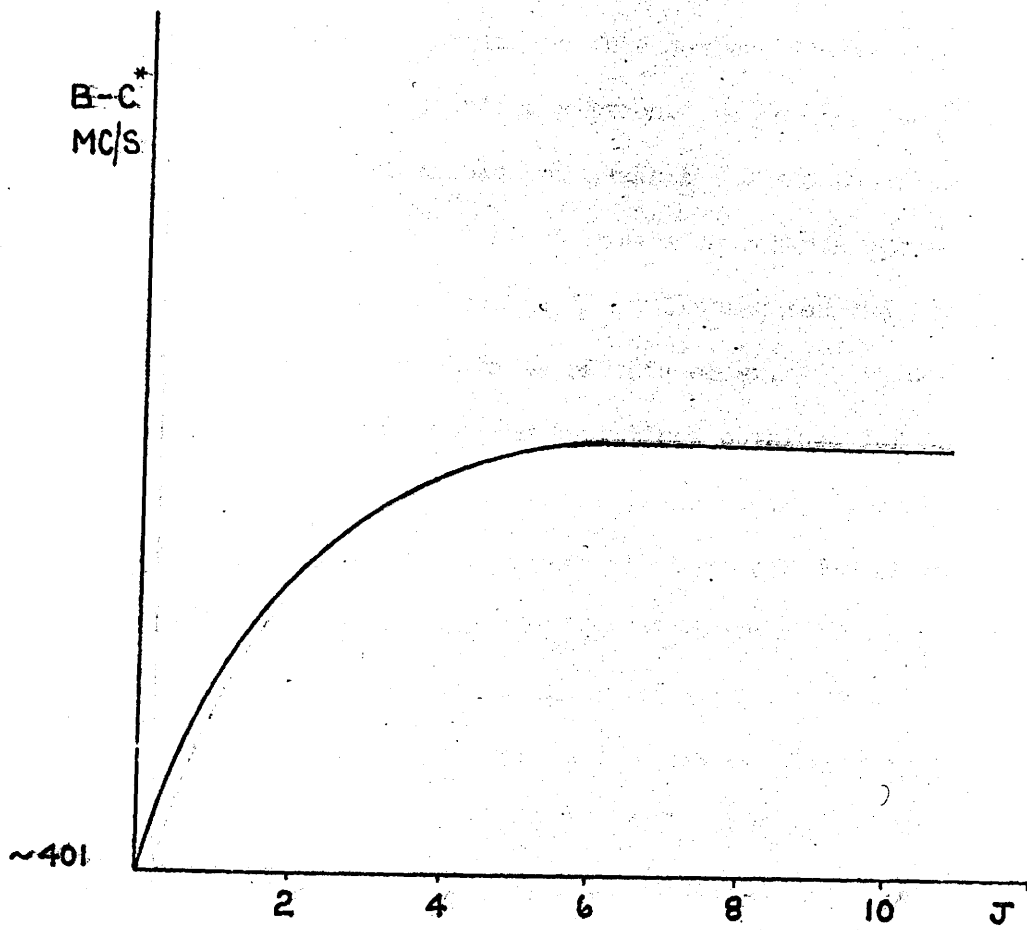
Now for $K_{-1} = 1$ energy levels in ND_2CN

$$W_1 - W_2 \sim \frac{J(J+1)}{2} (B - C) \quad (13a)$$

Hence (13) becomes

$$\Delta E = \nu = \frac{J(J+1)}{2} \sqrt{(B-C)^2 + 16 \left[\frac{(J-1)(J+1)}{J(J+1)} \right] F'^2} \quad (14)$$

The term under the square root sign in (14) is now an effective parameter $(B - C)^*$ which may differ for each transition. It is clear from (14) that, as J increases the coefficient $f(J)$ of F'^2 approaches unity rapidly and is almost constant at J values greater than 6. Thus a graph of $(B - C)^*$ against J for the Q - branch series would be expected to take the form shown in fig. 5.



Graph of effective (B - C) against J for $v = 1$ $K_{-1} = 1$ μ_a

Q-branch lines of ND₂CN

fig. 5.

An extremely useful aid to the identification of the Q - branch lines belonging to this series lies in the ^{14}N nuclear quadrupole coupling pattern. In the case of the ground state lines the separation of peaks A - C and B - D is ~ 2.4 Mc/s (the labelling of the fine structure components corresponds to that used in chapter 3), and the splitting for the first excited state is also expected to be of this order. This value is slightly different from the splittings obtained for NH_2CN (2.54 Mc/s). Such a change is to be expected since the principal axes of the molecule will have rotated slightly on deuteration and thus the diagonal elements of the nuclear electric quadrupole tensor on which the splittings depend will have changed.

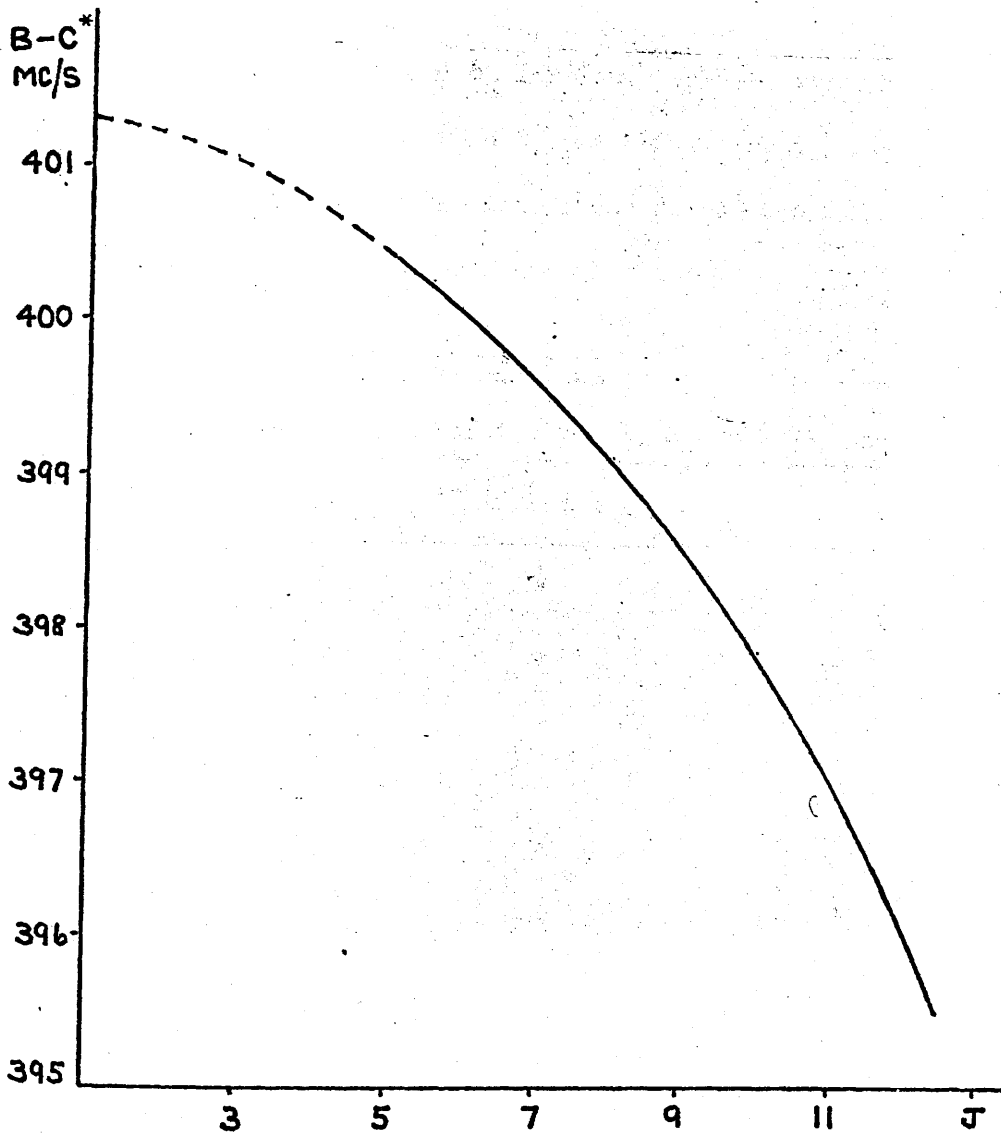
In order to locate the lines a search of the spectrum from 38 - 20 Gc/s was carried out. All lines exhibiting the required quartet structure and having a Stark effect consistent with a Q - branch line were noted. Lines belonging to the $v = 0$ and $v = 1$ states of NHDCN and to the $v = 0$ state of ND_2CN were observed at their predicted frequencies and could thus immediately be eliminated from the list of candidates for the $v = 1, K_{-1} = 1$ series. No lines from the normal species were observed suggesting there was very little of this species present in the sample. There remained a number of unidentified lines at

wavemeter frequencies (Mc/s) 35951, 30892, 26210, and 21890. Measurement of the A - C, B - D splittings of these lines showed them to be consistently ~ 2.4 Mc/s as predicted for the $v = 1$ series of lines. The lines were therefore tentatively assigned to the required series.

The lines were accurately measured and the line frequencies corrected to take account of the quadrupole splitting using the coupling constants for the normal species. From the R - branch spectrum it is known that (B - C) for the first excited state is ~ 401 Mc/s. Using (14) the observed lines were each assigned a J value such that $(B - C)^*$ was close to 401 Mc/s at low J values. The line frequencies and values of $(B - C)^*$ obtained from each line are shown in table II. The search was extended into X - band and the J = 6 and J = 7 lines were assigned. A graph of $(B - C)^*$ against J has the form shown in fig. 6. There is no direct experimental evidence from the Q - branch series for values of $(B - C)^*$ below J = 6 therefore the points on the graph connected by the broken line were obtained from data available from the R - branch transitions.

From Polo's expressions the difference in frequency between two $K_{-1} = 1$ R - branch lines can be written³

$$\frac{\Delta\nu}{J+1} = B - C + 8R_5 - 8(J+1)^2 \delta_J$$



Observed behaviour of graph of effective (B - C) against J for
 $v = 1 \ K_{-1} = 1$ Q-branch of ND_2CN

fig. 6.

Now δ_J has been estimated at $\sim 10^{-4}$ Mc/s, therefore, neglecting terms in R_5 and δ_J for low J values, the separation Δ_1 in fig. 7 is given by (B - C). Thus, knowing the experimental values, for the line frequencies ν_1 and ν_2 the J = 2, $K_{-1} = 1$ separation can be calculated.

TABLE II

Measured Line frequencies of the $\nu = 1$, $K_{-1} = 1$ μ_a Q - branch series (Mc/s).

J	ν	(B - C)*
1	-	(401.30)
2	-	(401.15)
3	-	(400.96)
6	8401.17	400.06
7	11189.51	399.63
9	17934.32	398.54
10	21882.49	397.86
11	26208.21	397.09
12	30902.76	396.19
13	35956.12	395.12

$$\Delta_3 \begin{array}{|l} \hline \hline \hline \end{array} \left. \vphantom{\Delta_3} \right\} K_{-1}=1 \quad J=3$$

$$\Delta_2 \begin{array}{|l} \hline \hline \hline \end{array} \left. \vphantom{\Delta_2} \right\} K_{-1}=1 \quad J=2$$

$$\Delta_1 \begin{array}{|l} \hline \hline \hline \end{array} \left. \vphantom{\Delta_1} \right\} K_{-1}=1 \quad J=1$$

Estimation of effective (B-C) from R - branch data for ND_2CN .

fig. 7.

Using the observed line frequencies⁷ of the $K_{-1} = 1$ transitions for $J = 3 - 2$ the separation Δ_3 for $J = 3$ can be obtained in a similar way. These results are included in table II in brackets.

From fig. 6 it can be seen that the value of $(B - C)^*$ decreases very rapidly with increasing J from an origin of 401.30 Mc/s. This behaviour is in sharp contrast to that expected from fig. 5. The most likely reason for this discrepancy is the breakdown of the perturbation treatment which led to the relationship shown graphically in fig. 5.

Fig. 6 implies that the splitting between the $K_{-1} = 1$ energy levels in fact decreases with increasing J . This suggests that the observable effect of the perturbing term F , which would normally cause an increase in the splitting as J increased, is being eliminated by a stronger perturbing force.

Such a perturbing effect can arise from the levels connected by matrix elements of the form

$$\langle J K v \mid H_2 \mid J K + 1 v' \rangle$$

$$\langle J K v \mid H_3 \mid J K + 1 v' \rangle$$

It is clear that the energy difference between the upper level $J, K, v = 0$ and the lower level $J, K - 1, v = 1$ is smaller than that between the lower and upper K_{-1} components of these energy

levels. The vibration - rotation effects will have a larger effect on the levels closer in energy. As J increases so the asymmetry splitting of the $v = 1, K_{-1} = 1$ levels increases as does the splitting of the $v = 0, K_{-1} = 2$ levels. Thus since the nett effect of the vibration - rotation interaction terms is to produce a repulsion between the connected levels, the lower $K_{-1} = 1, v = 1$, level will be pushed more to higher energy than the upper level, the effect increasing as J increases. Thus if this effect is sufficiently large the observable effect of the F term will be lost and the $K_{-1} = 1$ energy levels splitting will get smaller as J increases.

Thus it is concluded that, in the case of ND_2CN , the approximate treatment of the energy levels given in the latter stages of Lide's paper is insufficient and in order to calculate the rotational energy levels for the $v = 0$ and $v = 1$ states, a truncated form of the full energy matrix will have to be set up and diagonalised.

4. The μ_c inversion transitions in ND_2CN

Owing to the difficulties outlined in the previous section the rotational energy levels of the $v = 1$ state cannot be

located exactly relative to the levels of the ground state. It is therefore desirable to measure experimentally transitions which directly connect the two sets of rotational energy levels. Such transitions necessarily involve the μ_c component of the dipole moment and, since $\Delta < 18000$ Mc/s, the transitions most likely to fall in the region 8 - 40 Gc/s are those of the Q - branch series $v = 0, J, K_{-1} = 2$ - $v = 1, J, K_{-1} = 1$, and possibly a few μ_c R - branch lines of the type $v = 1, J, K_{-1} = 1 - v = 0, J + 1, K_{-1} = 2$.

Considering first the Q - branch series. From Polo's expressions, ignoring centrifugal distortion corrections, the energy of the $K_{-1} = 1$ energy levels is given by

$$E(K_{-1} = 1) \sim \frac{B+C}{2} J(J+1) \pm \frac{B-C}{4} J(J+1) + \frac{B-C}{4\epsilon} \quad (16)$$

similarly, assuming the $K_{-1} = 2$ levels to be degenerate at low J values, the energy of these levels can be written

$$E(K_{-1} = 2) \sim \frac{B+C}{2} J(J+1) + \frac{B-C}{\epsilon} \quad (17)$$

for this Q - branch series the $K_{-1} = 1$ levels belong to the first excited states and thus the inversion frequency Δ' must be added to the energy as given by (16). The frequencies of the μ_c Q - branch transitions are therefore given by

$$\nu \sim \Delta'' + \frac{J(J+1)}{2} \left[(B+C)' - (B+C) \right] \pm \frac{(B-C)'}{4} J(J+1) \quad (18)$$

where the single primes refer to the upper vibrational state in the transition and Δ'' now includes all constant terms involving the rotational constants. From (18) it can be seen that the separation between consecutive Q - branch lines is given by

$$\Delta \nu \sim \frac{(B-C)^{*'}}{2} (J+1) \quad (19)$$

where $(B-C)^{*'}$ is again an "effective" parameter for the excited state.

Equations (18) and (19) show that the Q - branch series will consist of two sets of lines spreading out to high and low frequency of an origin, each line separated from its neighbours by a J dependent function of $(B-C)^{*'}$. The lines to low frequency of the Q - branch origin are the transitions $v = 1, J_{1,J} - v = 0, J_{2,J-2}$ while those to high frequency are $v = 1, J_{1,J-1} - v = 0, J_{2,J-1}$. It is expected that the Stark effect of the low frequency series will be to low frequency and that of the high frequency series to high frequency.

Considering now only the low frequency series. The energies of the levels involved in the transitions can be rewritten as,

$$\begin{aligned} E_{1,J} &= R + (J-1)(J+2) G' \\ E_{2,J-2} &= R' - (J-1)(J+2) G' \end{aligned} \quad (20)$$

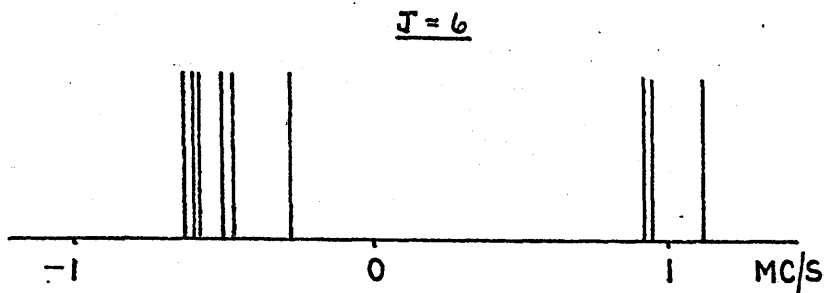
where R and R' are rigid rotor energies and G' is a composite perturbation term, having the same J dependence as Lide's G term. Thus from (20), including in R higher terms in the asymmetry than were used in (16), it is readily shown that for this Q - branch series

$$\frac{\Delta\nu}{J+1} = 2\left[\alpha - \beta + 2G'\right] + \left[\frac{(B-C)'}{2}\epsilon - \frac{3}{2}\frac{(B-C)'}{2}\epsilon\right] - \left[\frac{(B-C)'}{8}\epsilon + \frac{5}{3}\frac{(B-C)'}{4}\epsilon\right] (J+1)^2 \quad (21)$$

where $\alpha = \left[\frac{(B+C)'}{2} - \frac{(B+C)}{2}\right]$ and $\beta = \frac{(B-C)'}{4}$. Thus a graph of $\frac{\Delta\nu}{J+1}$ against $(J+1)^2$ is expected to be linear.

Estimating $G' = 3.2$ Mc/s from the perturbation to the $J = 1 - 2$ R - branch spectrum this graph is expected to have an intercept of ~ 180 Mc/s.

As an aid to the assignment of the lines the ^{14}N quadrupole hyperfine pattern was calculated. In this calculation it was assumed that the ^{14}N quadrupole coupling constants for ND_2CN are identical to those of NH_2CN . The calculations were carried out for $J = 5 - 10$ using the computer program described in chapter 3. The pattern for each of the transitions calculated was a doublet (fig. 8).



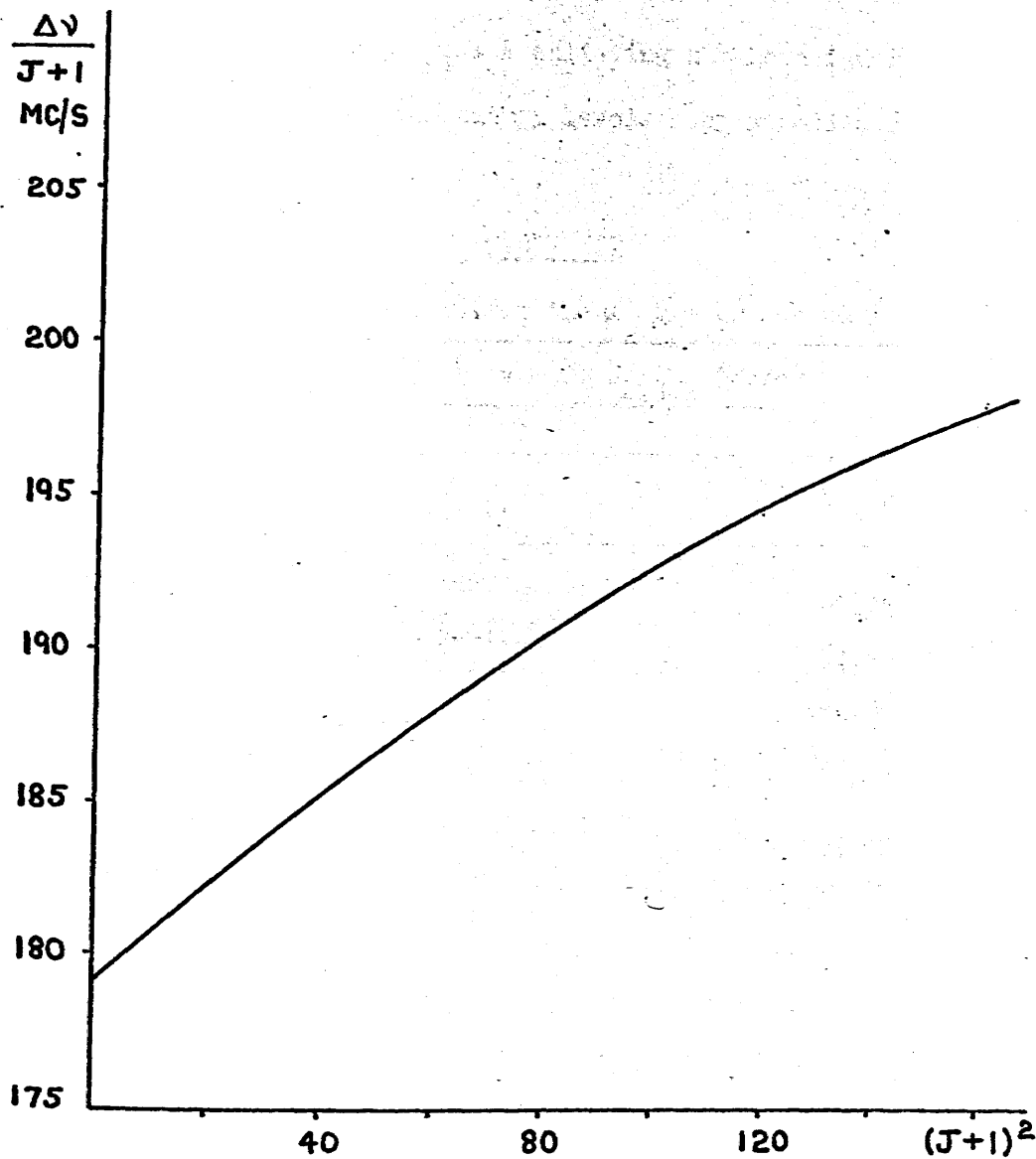
Theoretical quadrupole hyperfine pattern for μ_c Q-branch
transitions of ND_2CN

fig. 8.

The low frequency component was expected to be twice as intense as the other component, the separation being ~ 1.5 Mc/s. This pattern coupled with the fast low frequency Q - branch type Stark effect made the μ_c Q - branch lines very characteristic.

A search of the spectrum in the range 38 - 20 Gc/s revealed a number of strong lines with exactly the characteristics predicted above. The lines were measured and were found to have a splitting consistently ~ 1.3 Mc/s. The lines were assigned a J value such that the value of $\frac{(B-C)^{*1}}{2}$ as determined from (19) converged on ~ 180 Mc/s with decreasing J. The resulting assignments with the corresponding values of $\frac{(B-C)^{*1}}{2}$ are given in table III.

The graph of $\frac{\Delta\nu}{J+1}$ against $(J+1)^2$ drawn from the results in table III is shown in fig. 9. Since no experimental points were available for J less than nine the lower section of fig. 9 is poorly defined. Extrapolation did however show that the intercept was ~ 180 Mc/s as required. The slight curvature



Graph of $\frac{\Delta\nu}{J+1}$ against $(J+1)^2$ for μ_c Q - branch transitions of

ND₂CN.

fig. 9.

of the graph reflects the approximations used in the derivation of equation (21) e.g., $K_{-1} = 2$ splitting has been ignored and it has been assumed that the energy levels obey second order perturbation theory.

TABLE III

Measured Line frequencies for the μ_c Q - branch series

$v = 1, J_{1,J-1} - v = 0, J_{2,J-2}$ (Mc/s)

J	ν	$\frac{(B-C)^{*1}}{2}$
9	38607.06	
10	36679.56	192.75
11	34535.36	194.93
12	32171.33	197.00
13	29585.92	198.88
15	23765.27	-
16	20554.37	200.68
> 20	(18917.10)	
	(23813.11)	
	(29456.30)	

On consideration of the $v = 1, K_{-1} = 1$ and $v = 0, K_{-1} = 2$ energy level manifolds it is clear that as J increases the $v = 1, J_{1J}$ level approaches the $v = 0, J_{2,J-2}$ level in energy. From fig. 8 and equation (19) it is easily shown that these levels are closest in energy (~ 830 Mc/s) at $J = 20$. At

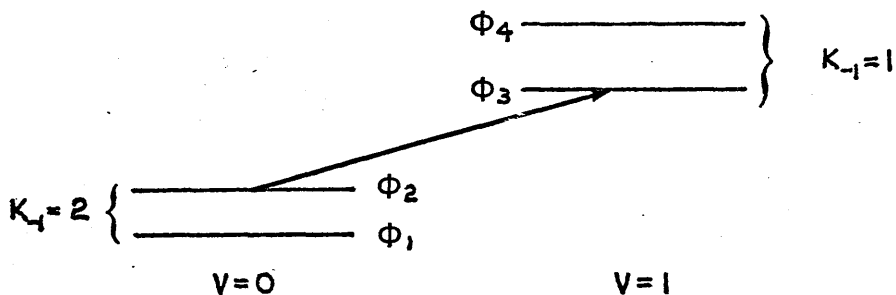
higher J values the $K_{-1} = 1$ level drops below the $K_{-1} = 2$ level in energy and thus the μ_c Q - branch series turns back and frequency increases with increasing J . After the turning point the quadrupole pattern therefore becomes reversed and the Stark effect changes to a high frequency one. Thus lines with J greater than twenty are mirror images of those with J less than or equal to twenty. Several such lines have been observed and measured. The frequencies are included in table III although no assignment has been attempted.

The observed intensities of this series of lines is interesting. It is found that for the lines with J less than twenty the intensity drops steadily with increasing J . However the lines for which J is greater than twenty are exceptionally strong, the intensity apparently decreasing with increasing J . This anomalous pattern may result from a change in the transition probabilities between the levels, resulting from mixing of the energy levels through the vibration - rotation matrix elements. This type of effect might be expected to build up to a maximum as the $v = 1, J_{1J}$ level gets closer to the $v = 0, K_{-1} = 2$ levels and then to diminish as the J value increases further.

It is well known that modifications of molecular wave

functions occur on the application of an electric field thus modifying transition probabilities between rotational states. While this is perhaps a contributing factor in this case when the levels are very close together, it cannot be a major effect in the case of ND_2CN , since variations in intensity are observed when the levels are $\sim 20 - 30$ Gc/s apart. It was therefore concluded that the interactions were mainly due to vibration - rotation connections between the levels.

For the purposes of this treatment the energy levels are labelled as shown in fig. 10.



Labelling of energy levels used for ND_2CN .

fig.10.

The transition $\Phi_2 - \Phi_3$ is the observed μ_c Q - branch transition. If $\Phi_n(V)$ are the modified wave functions in the presence of a finite vibration - rotation matrix element then they may be expanded in the form

$$\Phi_n(V) = \Phi_n + \sum_m C_{nm} \Phi_m \quad (22)$$

where
$$C_{nm} = \frac{\langle \Phi_n | H_2 + H_3 | \Phi_m \rangle}{W_n - W_m} = \frac{V_{nm}}{W_n - W_m}$$

Φ_n and Φ_m being the unperturbed wave functions. Thus the transition probability between two states α and β must be written

$$\mu_{\alpha\beta} = \int \Phi_\alpha(V) \mu \Phi_\beta(V) d\tau \quad (23)$$

From (22) and (23), ignoring the second order terms in C_{nm} , it can be shown that

$$\begin{aligned} \mu_{23}(V) &= \mu_{23} + \frac{V_{31} \mu_{21}}{W_3 - W_1} - \frac{V_{24} \mu_{43}}{W_2 - W_4} \\ \mu_{12}(V) &= \mu_{12} - \frac{V_{13} \mu_{23}}{W_1 - W_3} - \frac{V_{24} \mu_{14}}{W_2 - W_4} \\ \mu_{34}(V) &= \mu_{34} + \frac{V_{42} \mu_{32}}{W_4 - W_2} + \frac{V_{31} \mu_{14}}{W_3 - W_1} \end{aligned} \quad (24)$$

where the upper signs are the normal algebraic signs resulting from the assignment of a positive sign to all the coefficients C_{nm} of (22), and the lower signs are the signs of the energy denominators. The denominator $|W_3 - W_1|$ will reduce in magnitude as J approaches twenty while $|W_2 - W_4|$ will tend to increase.

It is clear from equations (24) that, depending on the signs

of the matrix elements V_{nm} , the transition probability for $\Phi_2 - \Phi_3$ will either increase or decrease at the expense of the transition probabilities of the $v = 0, K_{-1} = 2$ and $v = 1, K_{-1} = 1 \mu_a$ Q - branch transitions. Since experimentally it is known that $\mu_{23}(V)$ is reduced as J increases it seems likely that V_{31} is a negative quantity. If it is assumed that V_{24} is a positive quantity then it is clear that the μ_a Q - branch transitions both gain intensity at the expense of the μ_c transition.

While this discussion is purely speculative it does fit reasonably with the experimental observations. Any more detailed analysis must await evaluation of the integrals e_{vv} and d_{vv} , which appear in the matrix elements V_{nm} .

As mentioned earlier there was the possibility of a few μ_c R - branch transitions falling in the region 8 - 40 Gc/s. The experimental evidence which was available at this stage of the analysis enabled the frequencies of such transitions to be estimated quite accurately. The energy separations between the $v = 1, J, K_{-1} = 1$ levels were estimated from fig. 5 and equation (13A) while the separations $v, J, K = 1 - v, J+1, K_{-1} = 1$ readily calculated for low J values from the μ_a R - branch data. Assuming degeneracy at low J of the $v = 0, K = 2$ levels, the

separations between the levels $J = 1, J_{1J} - V = 0 J_{2,J-2}$ were obtained from the relationship shown graphically in fig. 9.

Having thus established the relative positions of the energy levels it was easily shown that the only μ_c R - branch transitions of the type $v = 1, J, K_{-1} = 1 - v = 0, J + 1, K_{-1} = 2$ with suitable frequencies were

$v = 1$	2_{12}	$- v = 0$	3_{22}	7219 Mc/s.	$2_{11} - 3_{21}$	6016 Mc/s.
	3_{13}		4_{23}	25664 Mc/s.	$3_{12} - 4_{22}$	23258 Mc/s.
	4_{14}		5_{24}	44296 Mc/s.	$4_{13} - 5_{23}$	42291 Mc/s.

Thus it was decided to carry out a search in K - band for the μ_c 4 - 3 R - branch transitions.

Consideration of the relative positions of the $v = 0, 4, K_{-1} = 2$ and $v = 1, 3, K_{-1} = 1$ energy levels showed that both transitions would have very characteristic Stark effects. There are four Stark components for each line and, owing to the very strong μ_a Q - branch connection between the nearly degenerate $v = 0, K_{-1} = 2$ levels the components $M = 1 - 3$ will all move to low frequency for the $v = 0 4_{23} - v = 1 3_{13}$, and to high frequency for the $v = 0 4_{22} - v = 1 3_{12}$. For the $M = 0$ components the Q - branch connections are zero and thus these components will be higher field and will probably move in the same direction for both transitions.

A search was made using the recorder in the predicted regions and the lines located. Both lines displayed the expected Stark effects with the $M = 0$ components moving to low frequency in both cases. The N^{14} - quadrupole coupling pattern was a doublet in each case the low frequency component being approximately half the intensity of the high frequency component. Fig. 10A is a reproduction of a recording of the $v = 0, 4_{23} - v = 1, 3_{13}$. The line frequencies were measured and corrected for quadrupole coupling effects. The corrected frequencies are given in table IV.

TABLE IV.

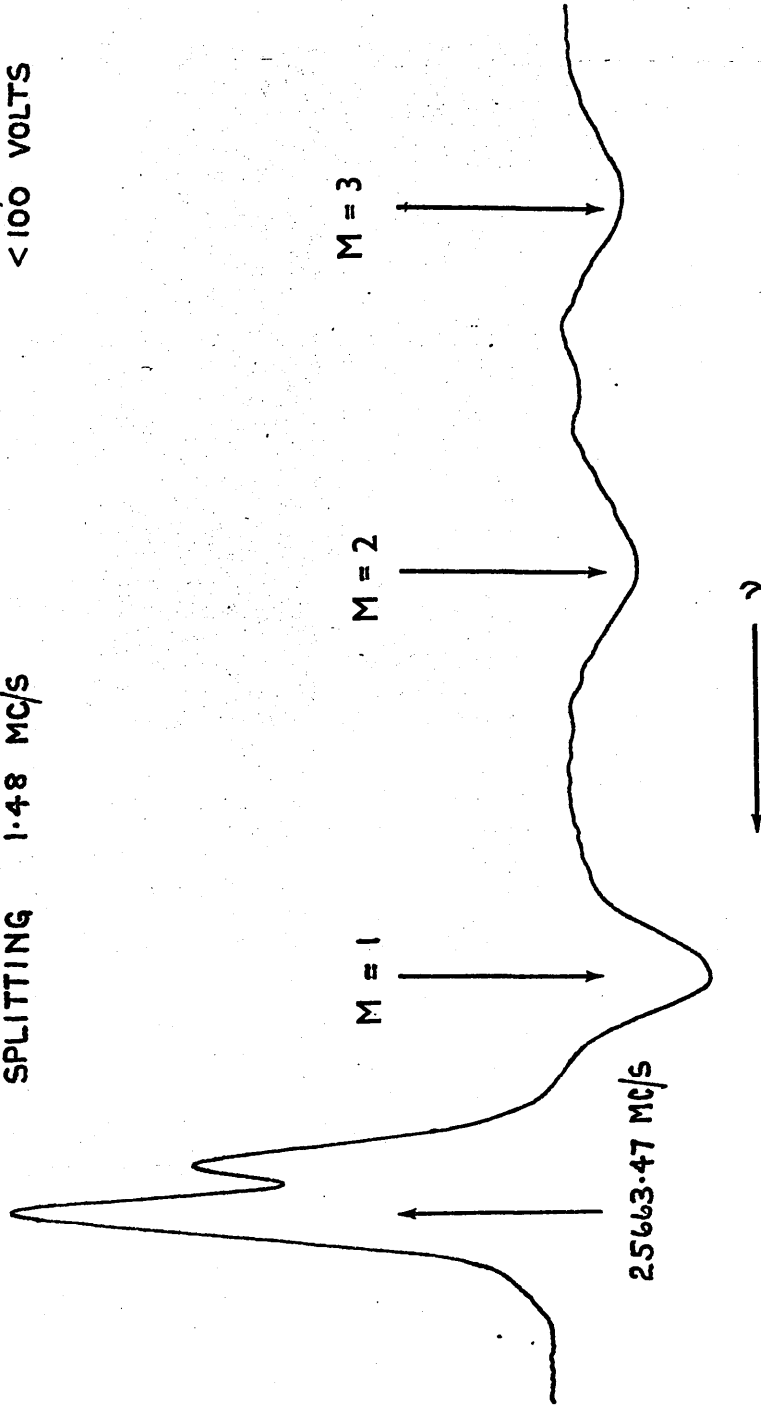
Measured Line frequencies of μ_o R - branch transitions (Mc/s.)

	ν	doublet séparation
$v = 0, 4_{23} - v = 1, 3_{13}$	25662.98	1.48
$v = 0, 4_{22} - v = 1, 3_{12}$	23275.68	0.79

It is interesting to note from table IV that the splittings of the lines differ considerably. From equation (11) of chapter 3 it can readily be shown that the magnitudes of the quadrupole splittings of the $v = 1, 3_{13}$ and 3_{12} levels are quite

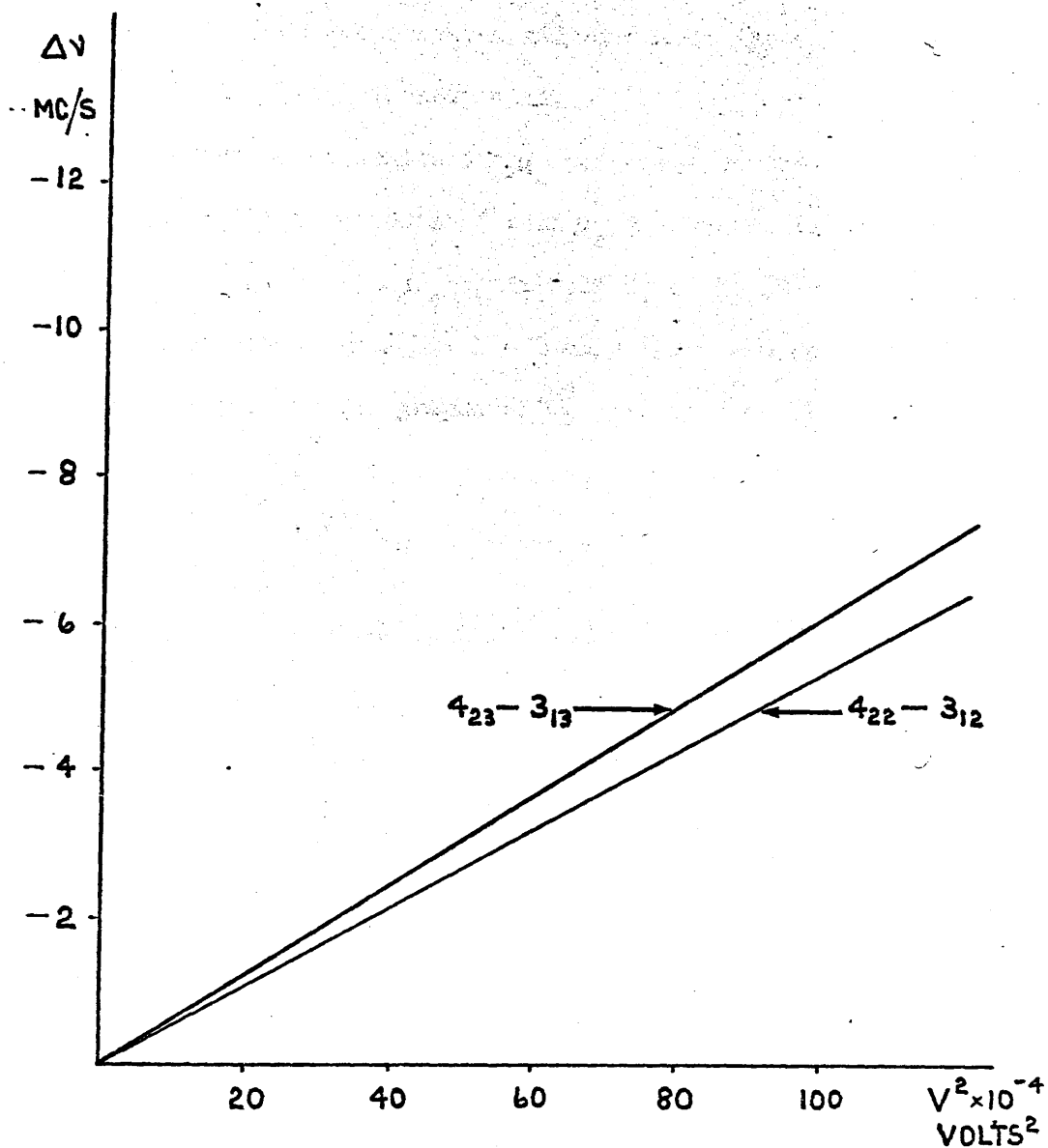
SPLITTING 1.48 MC/S

< 100 VOLTS



The $\nu = 0, 4_{23} - \nu = 1, 3_{13} \mu_{\text{O}}$ R - branch transition for ND_2CN .

fig. 10A.



The Stark effect of the $M = 0$ components of the μ_c R - branch
 transitions of ND_2OH

fig. 11.

different while those of the $v = 0, 4_{22}$ and 4_{23} levels are very similar. Thus the observed difference in the splittings of the transitions is not unexpected.

In order to determine the μ_c component of the dipole moment of ND_2CN the Stark effects of both μ_c R - branch lines were measured. Since the μ_a contribution to the Stark effect will dominate for components $M = 1 - 3$ only the $M = 0$ components have been measured. The graphs of $\frac{\Delta\nu}{V^2}$ are in fig. 11. The expressions for the Stark shifts of these components are,

$$v = 1 \ 3_{13} - v = 0 \ 4_{23} \ \Delta\nu = 0.8907 \ \mu_c^2 E^2 - 0.0651 \ \mu_a^2 E^2 \quad (25)$$

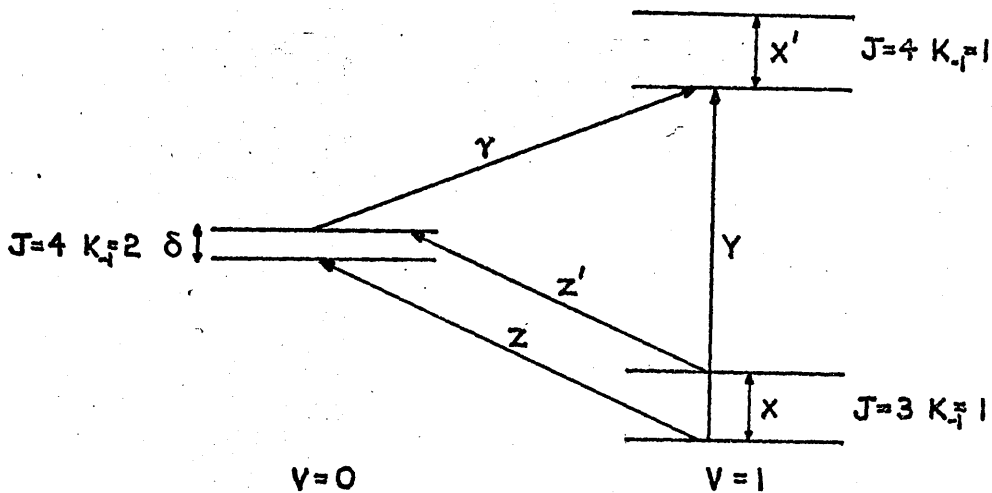
$$v = 1 \ 3_{12} - v = 0 \ 4_{22} \ \Delta\nu = 0.9401 \ \mu_c^2 E^2 - 0.0630 \ \mu_a^2 E^2$$

Calibration of the absorption cell with OCS assuming $\mu = 0.7124\text{D}$ resulted in a cell constant of $1.112 \text{ Mc/s}^2 \text{ volts}^{-2} \text{ debye}^{-2}$.

Assuming $\mu_a^2 = 18.75 \text{ D}^2$ then, from (25) $\mu_c = 0.86 \text{ D}$ in both cases.

5. The Energy Levels in ND_2CN

There was now sufficient information available on the energy levels for the relative positions of the $v = 0, K_{-1} = 2$ and $v = 1, K_{-1} = 1$ levels to be calculated quite precisely. This was carried out as follows.



Energy level Diagram for ND_2CN .

fig.12.

The separations x and x' can be obtained from fig. 5 as 4007.50 Mc/s and 2406.24 Mc/s and y can be readily calculated from the μ_a R - branch data as 70842.67 Mc/s. z and z' have been measured experimentally and thus Y and δ are easily calculated

$$\delta = 18.94 \text{ Mc/s.}$$

$$Y = 45160.75 \text{ Mc/s.}$$

Now from Polo's expressions it can be shown that for the $K_{-1} = 2$ energy levels,

$$\delta \sim [J^2(J+1)^2 - 2J(J+1)] \frac{B-C}{8} \epsilon$$

Hence $\frac{B-C}{8} \epsilon$ was calculated as 0.0526 for the $J = 4, K_{-1} = 2$ levels.

This value was used to evaluate the $K_{-1} = 2$ splittings for the remaining energy levels with $J = 2$ to 5.

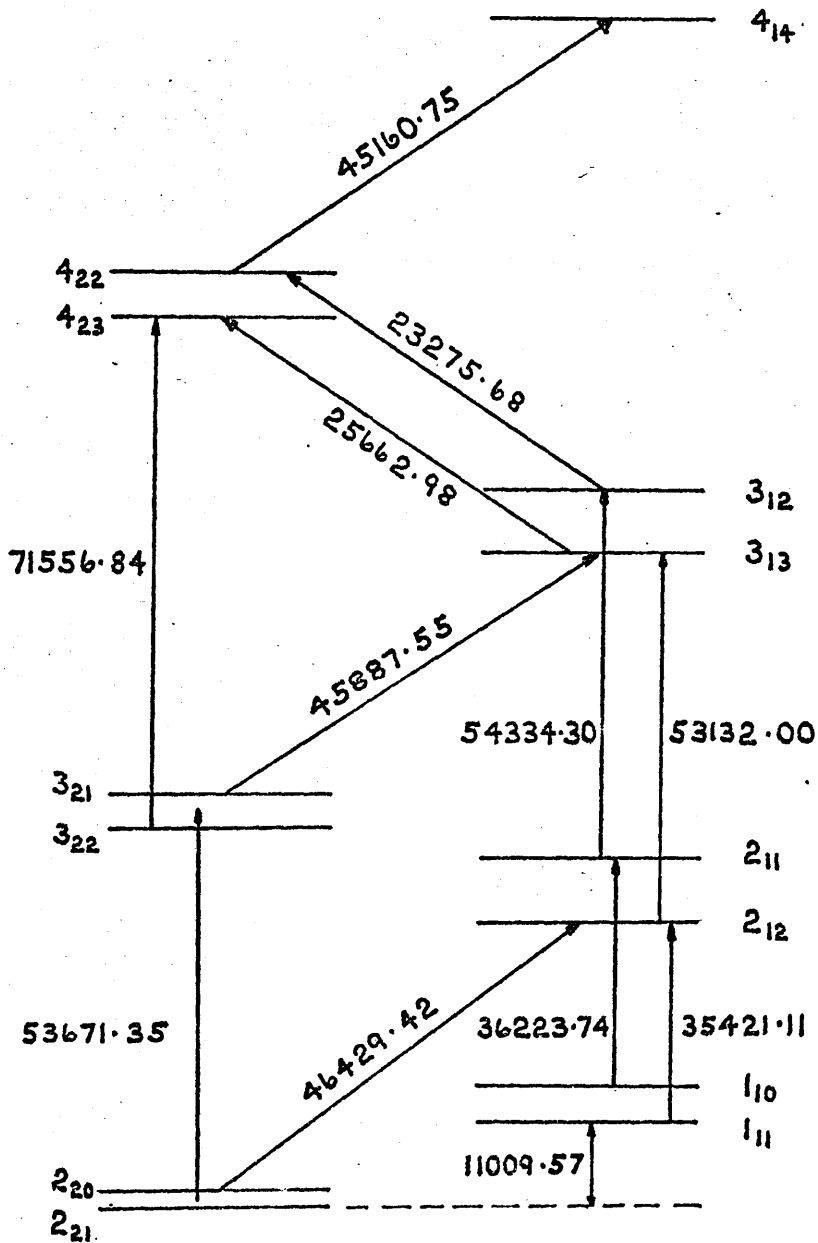
It can be shown that the frequency separation $\Delta\nu$ between the $J = 2$ and $J = 3 \mu_c$ Q - branch transitions is given by

$$\Delta\nu \sim \frac{1}{2} \delta_3 - \frac{1}{2} \delta_1 + \nu_{K=2} - \nu_{K=1} \quad (26)$$

where δ_3 and δ_1 are the separations of the $J = 3, K_{-1} = 2$ and $J = 2, K_{-1} = 2$ levels respectively and $\nu_{K=2}$ is the frequency of the previously measured μ_a transition $J = 3, K_{-1} = 2 - J = 2, K_{-1} = 2$ where the $K_{-1} = 2$'s were not resolved. $\nu_{K=1}$ is the transition frequency $\nu = 1 \ 3_{13} - 2_{12}$. Thus $\Delta\nu = 541.83 \text{ Mc/s}$. using this fact together with the $J = 4 \mu_c$ Q - branch frequency of 45160.75 Mc/s . the lower section of the graph shown in fig.8 was reconstructed in such a way that, starting from the frequency of the $J = 2 \mu_c$ Q - branch transition and using fig. 8, the experimentally measured Q - branch lines ($J = 9 - 13$) were predicted exactly. The points on this graph which satisfy this requirement are given in the table in appendix C.

Calculating the energy level separations in this way the resulting lower section of the energy level manifold is as shown in fig. 13. From this figure it can be seen that $\Delta = 11009.57 \text{ Mc/s}$.

Using this value of Δ and the energy level separations as given in fig.13, the Stark effect calculation for the $1_{11} - 2_{12}$ transition was repeated. The revised expression for the Stark



The Energy levels of ND₂ CH. (Mc/s).

fig.13.

shift of the $M = 0$ component is

$$\Delta\nu = 0.7829 \mu_a^2 v^2 - 4.2450 \mu_c^2 v^2 \quad (27)$$

Using the slopes as given in fig. 2 equation (27) gives μ_c as 0.89 D. This value is in close agreement with that obtained from the μ_c R - branch transitions.

6. Discussion.

Despite the fact that the $K_{-1} = 1$ section of the $v = 1$ energy level manifold has now been located exactly relative to the $K_{-1} = 2$ section of the $v = 0$ manifold the large rotational constant A is still poorly determined. Thus the inversion frequency Δ' cannot be evaluated to much greater accuracy than has been done previously^{1,3}. The original estimate of 14.7 cm^{-1} was calculated on the assumption that the $v = 0, J = 2, K_{-1} = 2$ and $v = 1, J = 2, K_{-1} = 1$ levels were degenerate and used a value of $A = 155965 \text{ Mc/s}$ determined from a model. Fig. 13 suggests that this estimate will be low by $\sim 46500 \text{ Mc/s}$. or $\sim 1\frac{1}{2} \text{ cm}^{-1}$. Thus Δ' is expected to be about 16.2 cm^{-1} .

The results obtained here show clearly that the energy levels of the two lowest vibrational states in ND_2CN cannot be obtained by perturbation techniques and therefore a more complete calculation is necessary. In order to set up and diagonalise the complete energy matrix resulting from (1) for reasonable J values a

knowledge is required of nine parameters, Δ' , A_v , B_v , C_v , $e_{vv'}$, $d_{vv'}$, where v refers to the vibrational state involved. Gwinn⁴ has carried out a similar calculation for trimethylene sulphide and trimethylene oxide and obtained values of these unknowns by a least squares fitting procedure on observed line frequencies. He obtained the interesting result that the frequencies of certain ground state lines were strongly dependent on the rotational constants of the first excited state and vice versa. A similar effect may well be found from an energy level calculation on ND_2CN , the reason being that any small change in Δ' or any of the rotational constants will produce a shift in the relative positions of the energy levels connected by vibration - rotation matrix elements. This will therefore change the magnitude of the perturbing effect and hence the frequency of the line.

There are a few points worth consideration regarding the accuracy of the energy separations as given in fig. 13. Although the energy level separations cycle perfectly their reliability is very strongly interdependent. The calculated splittings of the $v = 0$, $K_{-1} = 2$ levels have been derived from the value of $\frac{B-C}{8}\epsilon$ obtained from the splitting of the $J = 4$, $K_{-1} = 2$ levels. While it is felt that this splitting is fairly accurately determined the value of $\frac{B-C}{8}\epsilon$ is again only

an "effective" parameter and owing to the change in (B-C) with J it will not in fact be constant for each pair of $K_{-1} = 2$ energy levels.

Since however the value of (B-C)^{*} for the $v = 1, K_{-1} = 1$ μ_a Q - branch transitions converges on the unperturbed value of (B-C) at low J values (see fig.6) it seems reasonable to assume that the same will apply to the effective (B-C) for the $v = 0, K_{-1} = 2$ levels. Thus the $K_{-1} = 2$ splittings are not expected to be excessively in error for low J values. The value of Δ as given in fig. 13 is therefore expected to be quite close to the true value.

A direct consequence of the expected error in the $K_{-1} = 2$ splittings for higher J values is that the $K_{-1} = 2 \mu_a$ Q - branch lines expected to occur in the 8 - 40 Gc/s region ($J \sim 27 - 30$) will be very seriously perturbed making their identification and assignment very difficult.

At no stage in this work has any account been taken of centrifugal distortion corrections to line frequencies or energy levels. While for high J values this may well introduce some small errors into calculated quantities in most cases the shifts are small compared to the vibration - rotation perturbations and can thus readily be absorbed into "effective" parameters as have been used throughout this treatment.

It is interesting to note that the graph of $\frac{\Delta\nu}{J+1} / (J+1)^2$ for the μ_c Q - branch transitions has its intercept at 179.20 Mc/s. From equation (21) it can be shown that this corresponds to a value of $G' = 3.84$ Mc/s as compared to 3.20 Mc/s from the R - branch data. A small discrepancy of this nature may be the result of a number of factors however in view of the fact that second order perturbation theory is inadequate for this molecule it seems likely that G' will vary depending on the transitions from which it is determined.

The fact that the μ_c dipole moment of ND_2CN has been determined to an accuracy of ± 0.05 D from four transitions is good evidence for the validity of the energy separations of fig.13 and for the value of Δ obtained. The value of 0.86 D is much lower than that for ammonia (1.47 D). In the case of ammonia the dipole moment is largely due to the contribution from the lone-pair electrons of the nitrogen and, since in ND_2CN these electrons are certainly involved in π -bonding with the rest of the molecule, the value of the μ_c dipole moment would be expected to reflect this as indeed it does. The total dipole moment vector for ND_2CN is therefore 4.41 D lying within $\sim 10^\circ$ of the \underline{a} inertial axis.

REFERENCES

1. D. J. Millen, G. Topping and D.R. Lide Jr., J. Mol. Spec. 8, 153 (1962)
2. D.R. Lide Jr., J. Mol. Spec., 8, 142 (1962)
3. J.K. Tyler, Ph.D. Thesis, University of Birmingham (1960)
4. D.O. Harris, H.W. Harrington, A.C. Lunz and W.D. Gwinn, J. Chem. Phys., 44, 3467 (1966)
5. C.H. Townes and A.L. Shawlow, "Microwave Spectroscopy", McGraw Hill, New York, (1955)
6. S.R. Polo, Canad. J. Phys., 35, 880 (1957)
7. J.K. Tyler, Private communication.
8. Neilsen, Rev. Mod. Phys., 23, 90 (1951)

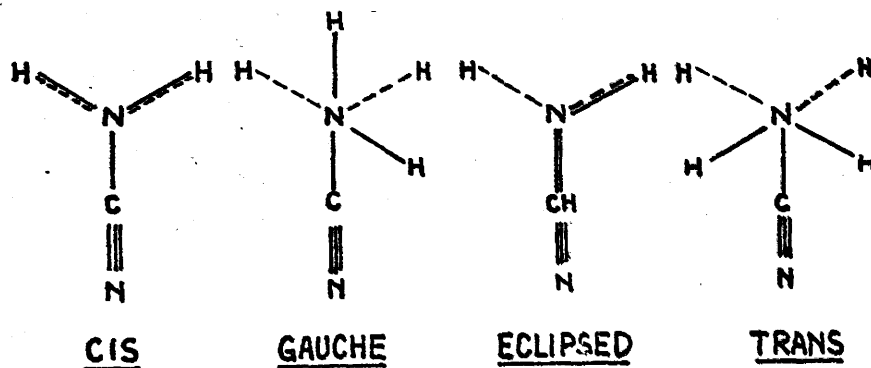
CHAPTER 5.

The Conformation of Aminoacetonitrile

1. Introduction.

In this chapter some preliminary conclusions are drawn regarding the preferred conformation of aminoacetonitrile ($\text{NH}_2\text{CH}_2\text{CN}$).

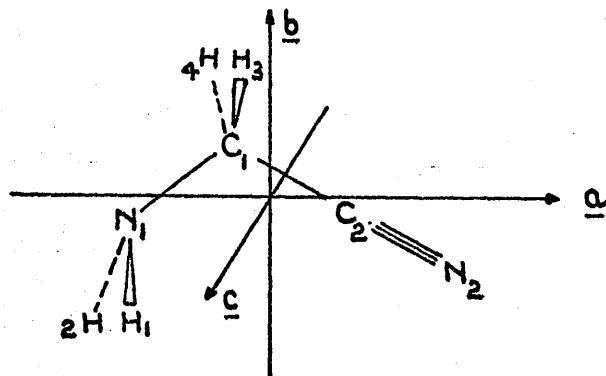
Some of the possible conformations for this type of molecule are shown in Newmann projection along the $\text{C} - \text{N}_1$ bond in fig. 1. (The numbering system and inertial axis system are shown in fig. 2.).



The conformations of aminoacetonitrile.

fig. 1.

The dotted lines in fig. 1. represent the $\text{C}_1 - \text{H}$ bonds of the molecule.



The inertial axis system for $\text{NH}_2\text{CH}_2\text{CN}$

fig. 2.

Whether the molecule can exist in more than one conformation will depend on the form of the potential function for internal rotation of the amine group about the $\text{C}_1 - \text{N}_1$ bond. Qualitative consideration of fig. 1 suggests that the minima in the potential function will correspond to the gauche and trans conformers. It is interesting to note that an inversion of the amino group from either of these conformations places the molecule in a conformation corresponding to a maximum in the potential function and will therefore be accompanied by a rotation to return it to a potential minimum.

Three isotopic species of the molecule have been studied, $\text{NH}_2\text{CH}_2\text{CN}$, NHDCH_2CN and $\text{ND}_2\text{CH}_2\text{CN}$. While for each species there are several vibrational satellites associated with the ground state lines there is no evidence for any very low frequency vibration which may be identified with an inversion or torsional mode.

Both μ_a and μ_b type transitions have been observed and analysis of the spectra leads to the conclusion that amino acetonitrile exists primarily in the trans form, no spectra due to molecules in any other form having been observed.

The μ_a and μ_b components of the dipole moment for the ground vibrational state of the normal species have been determined from Stark effect measurements as 2.55 ± 0.02 D and 0.30 ± 0.02 D respectively. The dipole moment for the molecule is therefore 2.57 ± 0.03 D.

2. Analysis of the Spectra.

The model used for the preliminary calculation of line frequencies for aminoacetonitrile was based on the structure of ethyl cyanide¹ with the methyl group replaced by an amino fragment with geometry similar to that in methylamine². The structure is given in table I.

TABLE I
Preliminary Model for Aminoacetonitrile (\AA)

C = N	1.160	C - N	1.474
N - H	1.011	CNH	112°
C - H	1.093	HNH	106°
C - C	1.460	HCH	109°

Both the trans and gauche conformers of the normal species are prolate slightly asymmetric tops with $\kappa \sim -0.960$. Owing to the effect of the highly polar nitrile group the μ_a component of the dipole moment for these molecules is expected to be fairly large and the μ_b component somewhat smaller. It was decided therefore to search first for the $J = 4 - 3 \mu_a$ R - branch transition predicted in the region 35 - 40 Gc/s.

The vapour pressure of aminoacetonitrile is ~ 0.2 m.m. of mercury at room temperature which is more than adequate for microwave spectroscopy. Samples of the vapour were readily introduced into the cell and the pressure reduced by pumping to a normal working value of ~ 0.010 m.m. of mercury. All observations were made with the absorption cell at room temperature.

For the normal species a number of strong lines with well defined Stark effects were observed centred at ~ 36200 Mc/s. Wavemeter measurements of the line frequencies together with the characteristic Stark patterns suggested that these lines belonged, as expected, to the $J = 4 - 3 \mu_a$ R - branch transitions. The assignment was confirmed by locating the $J = 3 - 2$ and $J = 2 - 1$ patterns centred at 27200 Mc/s and 18100 Mc/s respectively. The $1_{01} - 0_{00}$ transition was also identified at 9071.87 Mc/s.

The analysis of the accurately measured lines was based on the treatment of the energy levels of a non-rigid slightly asymmetric top molecule given by Polo³ (see also chapter 4 section 3). It can be shown that for a molecule with the asymmetry of aminoacetonitrile it is a satisfactory approximation to truncate Polo's expansion at terms including ϵ^3 at least for the levels of importance here. The expressions used for the energy levels of aminoacetonitrile were therefore identical with these used in the analysis of the cyanamide spectrum⁴, i.e.,

$$\underline{J + 1}_{0,J+1} - J_{0,J}$$

$$\frac{\nu}{J+1} = B + C - 8R_6 - J(J+2) \frac{B-C}{2} \epsilon - 4D_J(J+1)^2 \quad (1)$$

$$\underline{J + 1}_{1,J+1} - J_{1,J}$$

$$\begin{aligned} \frac{\nu}{J+1} = B + C - \frac{B-C}{2} - 8R_6 - 4R_5 - 2D_{JK} - (J-1)(J+3) \frac{B-C}{8} \epsilon \\ - 4(D_J - \delta_J)(J+1)^2 \end{aligned} \quad (2)$$

$$\underline{J + 1}_{1,J} - J_{1,J-1}$$

$$\begin{aligned} \frac{\nu}{J+1} = B + C + \frac{B-C}{2} - 8R_6 + 4R_5 - 2D_{JK} - (J-1)(J+3) \frac{B-C}{8} \epsilon \\ - 4(D_J + \delta_J)(J+1)^2 \end{aligned} \quad (3)$$

$$\frac{J + 1_{2,J-1} - J_{2,J-2}}{J+1}$$

$$\begin{aligned} \frac{\nu}{J+1} = & B + C - 12R_6 - 8D_{JK} + (5J^2 + 10J + 8) \frac{B-C}{12} \epsilon \\ & - 4(D_J - R_6)(J+1)^2 \end{aligned} \quad (4)$$

$$\frac{J + 1_{2,J} - J_{2,J-1}}{J+1}$$

$$\begin{aligned} \frac{\nu}{J+1} = & B + C - 4R_6 - 8D_{JK} - (J-2)(J+4) \frac{B-C}{12} \epsilon \\ & - 4(D_J + R_6)(J+1)^2 \end{aligned} \quad (5)$$

$$\frac{J + 1_{3,J-2} - J_{3,J-3} \text{ and } J + 1_{3,J-1} - J_{3,J-2}}{J+1}$$

$$\begin{aligned} \frac{\nu}{J+1} = & B + C - 8R_6 - 18D_{JK} + (J^2 + 2J + 9) \frac{B-C}{16} \epsilon \\ & - 4D_J (J+1)^2 \end{aligned} \quad (6)$$

From equation (1) it can be seen that for $K_{-1} = 0$ lines, a graph of $\frac{\nu}{J+1}$ against $J(J+2)$ is expected to be linear with slope $4D_J + \frac{B-C}{2} \epsilon$ and intercept $B + C - 8R_6 - 4D_J$. Using the mean of the frequencies of two $K_{-1} = 1$ lines in the manner described below a good estimate of $B - C$ may be obtained. Also ϵ may be determined quite accurately using the final set of rotational constants, A having been obtained from the μ_0 Q - branch series of lines. Thus from the slope of the $K_{-1} = 0$ plot an estimate

of D_J may be obtained. For all species the term $4D_J$ is of the order 0.01 Mc/s therefore the intercept of the $K_{-1} = 0$ plot gives a good estimate of $B + C$ assuming $8R_6$ to be negligible.

Using equations (2) - (6) a number of further expressions may be derived which enable the rotational constants B and C and the larger centrifugal distortion terms to be estimated graphically from the μ_2 R - branch lines. It is found that a graph of $\frac{K_0 - \langle K_2 \rangle}{J + 1}$ against $(J + 1)^2$ provides a good estimate of D_{JK} from the intercept and gives an approximate value for $(B - C)\epsilon$ from the slope. (In the notation used here K_n is the frequency of a line with $K_{-1} = n$ and $\langle K_n \rangle$ is the mean of the frequencies of the two such lines for a given J). A further check on D_{JK} may be obtained from equation (6) which is strongly dependent on this constant.

It can be readily seen from (2) and (3) that the difference in frequency between the two $K_{-1} = 1$ lines for a given J is given by

$$\frac{\Delta\nu}{J+1} = B - C + 8R_5 - 8(J+1)^2 \delta_J \quad (7)$$

Thus from (7) assuming $8R_5$ to be negligible the quantity $B - C$ can be derived from the measured $K_{-1} = 1$ lines and an estimate of the order of magnitude of δ_J obtained.

Using the procedures outlined above the rotational constants

B and C and the centrifugal distortion constants D_{JK} , D_J and δ_J were estimated for the species $\text{NH}_2\text{CH}_2\text{CN}$, $\text{NHD CH}_2\text{CN}$ and $\text{ND}_2\text{CH}_2\text{CN}$.

While from the μ_a R - branch transitions accurate values of B and C may be obtained, it is not possible to obtain an accurate value of the large rotational constant A from these transitions. In order to obtain a good value of A the μ_b Q - branch series $J_{1,J-1} - J_{0,J}$ was located and assigned for the species $\text{NH}_2\text{CH}_2\text{CN}$ and $\text{NHD CH}_2\text{CN}$. In particular the frequency of the transition $l_{10} - l_{01}$ gives a very good estimate of the quantity $A - C$ assuming D_K is negligible. Using the values of C obtained from the μ_a transitions values of A were obtained in this way for the two species mentioned above.

The observed and calculated line frequencies for all species are given in tables II - VI, and the rotational constants for each species in table VII.

It can be seen from tables II, III and IV that the fit obtained between the observed and calculated μ_a R - branch line frequencies for all species is not very good especially for lines with $K_{-1} = 2$. It is surprising that the fit to these lines is poor for all the species studied suggesting that it is a systematic and not random effect.

TABLE II

Observed and Calculated Line frequencies for $\text{NH}_2\text{CH}_2\text{CN}$ μ_a R - branch transitions (Mc/s.)

	observed	calculated
$1_{01} - 0_{00}$	9071.87	9071.87
$2_{02} - 1_{01}$	18137.61	18137.70
$2_{12} - 1_{11}$	17693.57	17693.57
$3_{03} - 2_{02}$	27191.56	27191.51
$3_{13} - 2_{12}$	26536.60	26536.43
$3_{12} - 2_{11}$	27887.14	27887.09
$3_{22} - 2_{21}$	27217.06	27216.26
$3_{21} - 2_{20}$	27238.67	27239.87
$4_{04} - 3_{03}$	36227.27	36227.30
$4_{14} - 3_{13}$	35374.63	35374.57
$4_{13} - 3_{12}$	37175.21	37175.44
$4_{23} - 3_{22}$	36283.73	36283.30
$4_{22} - 3_{21}$	36342.37	36342.34
$4_{32} - 3_{31}$ } $4_{31} - 3_{30}$ }	36302.17	36301.50

TABLE III

Observed and Calculated Line frequencies for NHD CH₂CN μ_a R - branch transitions (Mc/s.)

	observed	calculated
$1_{01} - 0_{00}$	8820.17	8820.17
$2_{02} - 1_{01}$	17633.58	17633.80
$2_{11} - 1_{10}$	18082.69	18082.22
$3_{03} - 2_{02}$	26434.43	26434.47
$3_{13} - 2_{12}$	25792.01	25792.12
$3_{12} - 2_{11}$	27120.16	27120.21
$3_{22} - 2_{21}$	26462.46	26461.06
$3_{21} - 2_{20}$	26484.87	26486.41
$4_{04} - 3_{03}$	35215.92	35215.66
$4_{14} - 3_{13}$	34382.06	34381.93
$4_{13} - 3_{12}$	36152.11	36151.77
$4_{23} - 3_{22}$	35276.37	35273.35
$4_{22} - 3_{21}$	35339.12	35339.18

TABLE IV

Observed and Calculated Line frequencies for $\text{ND}_2\text{CH}_2\text{CN}$

μ_a R - branch transitions (Mc/s.)

	observed	calculated
$3_{03} - 2_{02}$	25736.18	25736.26
$3_{13} - 2_{12}$	25123.09	25122.80
$3_{12} - 2_{11}$	26391.95	26392.48
$3_{22} - 2_{21}$	25764.82	25762.92
$3_{21} - 2_{20}$	25786.43	25788.26
$4_{04} - 3_{03}$	34284.97	34284.88
$4_{14} - 3_{13}$	33490.31	33490.34
$4_{13} - 3_{12}$	35181.19	35181.68
$4_{23} - 3_{22}$	34344.91	34345.07
$4_{22} - 3_{21}$	34408.59	34408.43
$4_{32} - 3_{31}$ } $4_{31} - 3_{30}$ }	34364.97	34364.87

TABLE V

Observed Line frequencies of μ_b $J_{1,J-1} - J_{0,J}$
series for $\text{NH}_2\text{CH}_2\text{CN}$ (Mc/s.)

$1_{10} - 1_{01}$	25935.46
$2_{11} - 2_{02}$	26391.53
$3_{12} - 3_{03}$	27087.14
$4_{13} - 4_{04}$	28035.21
$5_{14} - 5_{05}$	29252.73
$6_{15} - 6_{06}$	30760.84
$7_{16} - 7_{07}$	32583.51
$8_{17} - 8_{08}$	34747.95

TABLE VI

Observed Line frequencies of $\mu_b J_{1,J-1} - J_{0,J}$
 series for NHD CH₂CN (Mc/s.)

$1_{10} - 1_{01}$	23391.83
$2_{11} - 2_{02}$	23841.41
$3_{23} - 3_{03}$	24526.46
$4_{13} - 4_{04}$	25462.45
$5_{14} - 5_{05}$	26667.65
$6_{15} - 6_{06}$	28163.63
$7_{16} - 7_{07}$	29976.84
$8_{17} - 8_{08}$	32134.23
$9_{18} - 9_{09}$	34665.46
$10_{19} - 10_{010}$	37596.97

TABLE VII

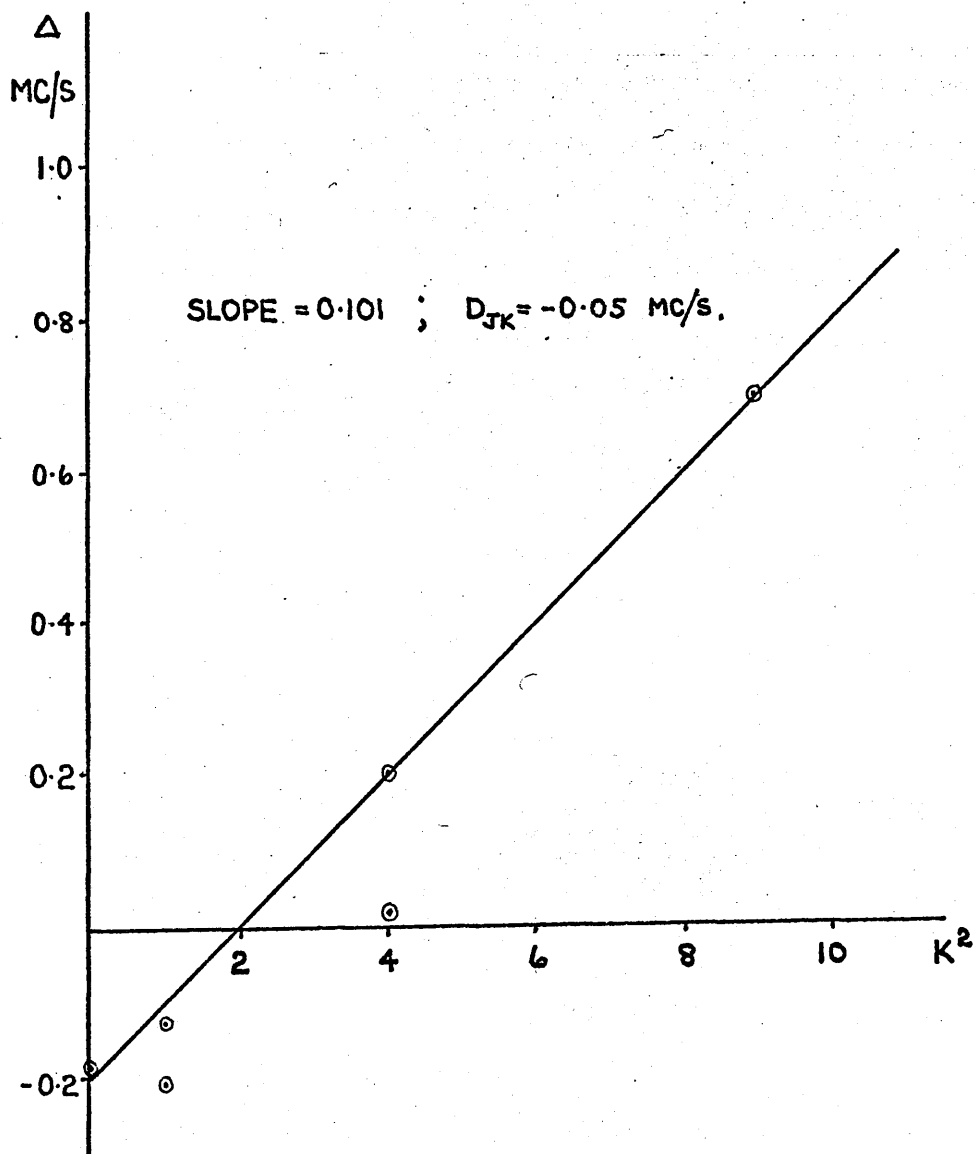
Ground State Rotational constants for the various
species of Aminoacetonitrile (Mc/s.)

	$\text{NH}_2\text{CH}_2\text{CN}$	NHDCH_2CN	$\text{ND}_2\text{CH}_2\text{CN}$
A	30247.43	27580.43	25496
B	4761.05	4631.57	4505.24
C	4310.83	4188.60	4082.02
D_{JK}	- 0.045	- 0.050	- 0.055
D_{J}	0.004	0.006	0.007
δ_{J}	-	0.004	0.004

It was felt that these discrepancies may be due to poorly determined centrifugal distortion constants and that in particular the largest constant D_{JK} may be considerably in error. To check this the line frequencies of, for example, the $J = 4 - 3$ transition of $\text{NH}_2\text{CH}_2\text{CN}$ as given by equations (1) - (6) were corrected for all terms on the right hand side of these equations excepting those terms in D_{JK} . A graph of K^2 against the corrected left hand sides of these equations will now have slope $-2D_{JK}$. This plot is shown in fig. 3. The slope gives a value of -0.050 for D_{JK} in good agreement with that obtained by the methods described above. However it can be seen that while this value will satisfy all the transitions falling on or close to the line, it will not satisfy the two transitions which fall well away from this line. One of these transitions has $K_{-1} = 1$ ($4_{13} - 3_{12}$) and the other has $K_{-1} = 2$ ($4_{22} - 3_{21}$).

If similar plots are constructed for the other transitions and the other species the scatter of the points is in general worse than that shown in fig. 3. The same general effect remains, however, that it apparently is not possible to obtain a value of D_{JK} which will give a good fit to all the observed R - branch lines of a given species.

The reason for these discrepancies is not at present clear and some further investigation of the effect is required in order



D_{JK} plot for $J = 4 - 3$ transition of $\text{NH}_2\text{CH}_2\text{CN}$

fig. 3.

to definitely establish it as genuine and to determine the cause.

Hyperfine structure due to ^{14}N - quadrupole coupling was observed on the $1_{01} - 0_{00}$ transition of the normal species. As in the case of cyanamide (chapter 3) the quadrupole interactions in aminoacetonitrile are complicated by the presence of two ^{14}N nuclei. The observed pattern for the $1_{01} - 0_{00}$ transition is shown in fig. 4.

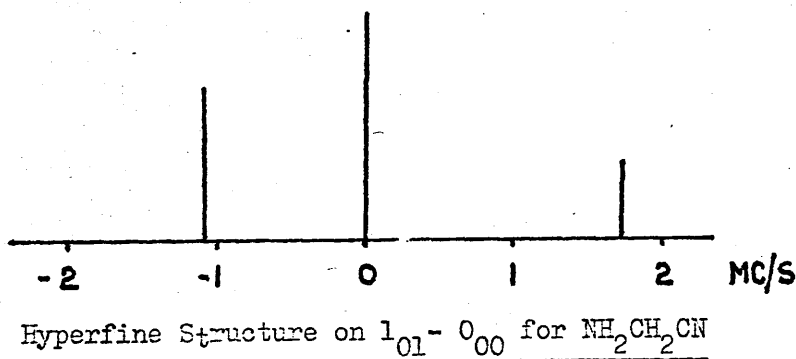


fig. 4.

The ratio of the observed splittings of this line is ~ 1.59 which is slightly greater than that normally associated with the splitting caused by the ^{14}N of a nitrile group alone (~ 1.50). The fact that only a triplet is observed suggests that the χ_{aa} coupling constants for both nitrogen atoms in aminoacetonitrile have the same negative sign and comparable magnitude. Before a more quantitative analysis of the quadrupole coupling effects

can be carried out further experimental data, preferably measurements on some other lines, is required.

3. The Dipole Moment

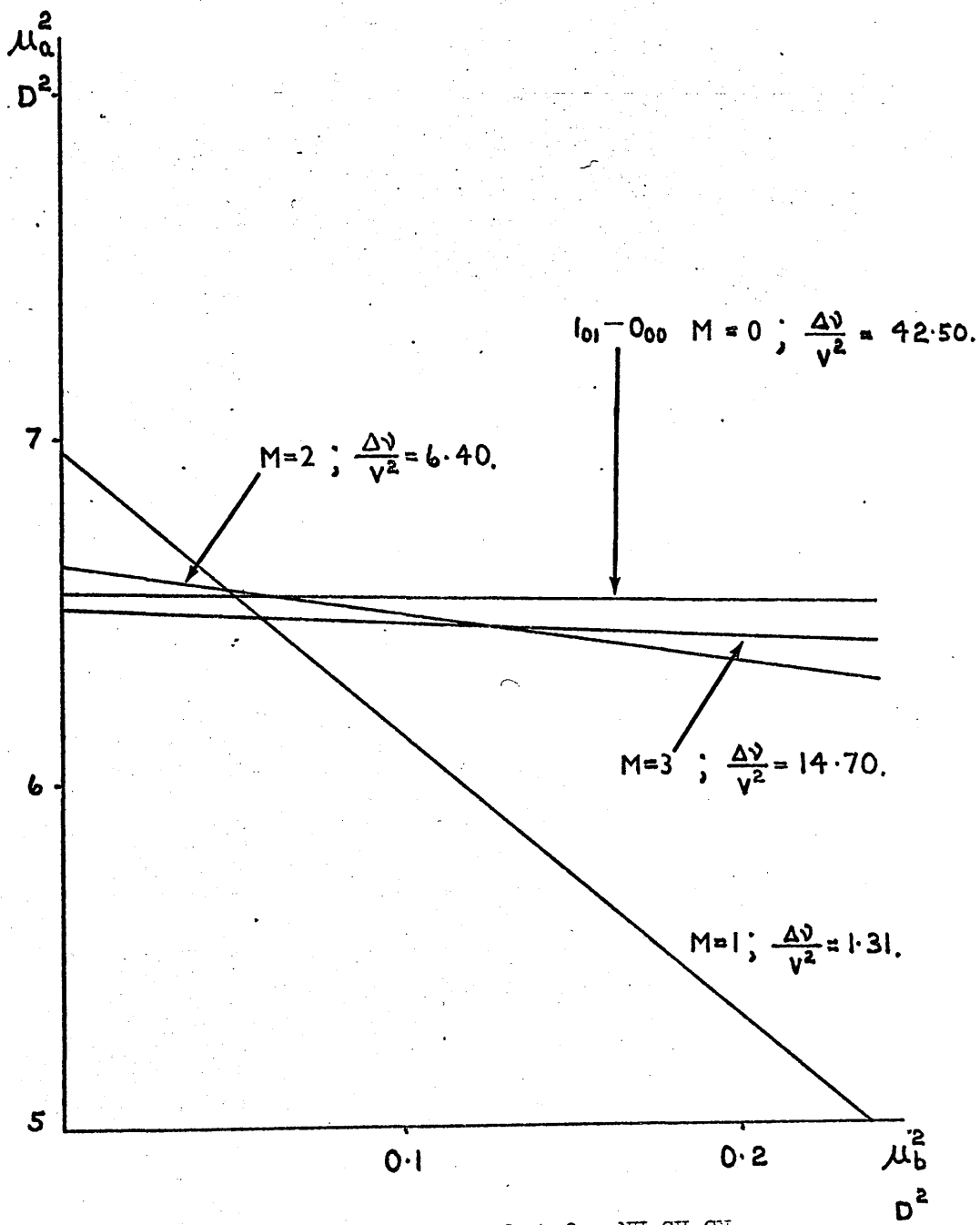
Stark effect measurements were carried out on the $1_{01} - 0_{00}$ and $4_{14} - 3_{13}$ transitions. The cell was calibrated in each case with OCS assuming its dipole moment as 0.7124D, resulting in a value of $1.103 \text{ Mc/s}^2 \text{ volts}^{-2} \text{ debye}^{-2}$ for the cell constant.

The analysis of the Stark effect was based on the standard treatment of the energy levels by second order perturbation theory, and, since this has been discussed in detail elsewhere in this thesis it will not be repeated here.

The expressions for the Stark energies of the transitions studied are :

$$\begin{aligned}
 1_{01} - 0_{00} \quad M = 0 \quad \Delta\nu &= 6.4845 \mu_a^2 v^2 - 0.5556 \mu_b^2 v^2 \\
 4_{14} - 3_{13} \quad M = 1 \quad \Delta\nu &= 0.1883 \mu_a^2 v^2 + 0.7735 \mu_b^2 v^2 \\
 &M = 2 \quad \Delta\nu = 0.9642 \mu_a^2 v^2 + 0.6898 \mu_b^2 v^2 \\
 &M = 3 \quad \Delta\nu = 2.2573 \mu_a^2 v^2 + 0.5502 \mu_b^2 v^2
 \end{aligned} \tag{8}$$

where all the terms have their usual meanings. Equations (8) were solved graphically for μ_a^2 and μ_b^2 the graph of μ_a^2/μ_b^2 being shown in fig. 5.



Dipole Moment plot for $\text{NH}_2\text{CH}_2\text{CN}$

fig. 5.

$$\mu_a^2 = 6.51 \pm 0.05 \text{ D}$$

$$\mu_a = 2.55 \pm 0.02 \text{ D}$$

$$\mu_b^2 = 0.09 \pm 0.05 \text{ D}$$

$$\mu_b = 0.30 \pm 0.02 \text{ D}$$

$$\mu^2 = 6.60 \pm 0.07 \text{ D}$$

$$\mu = 2.57 \pm 0.03 \text{ D}$$

The error on the results was estimated from the intersection in fig. 5.

4. Conformation of the Molecule

The moments of inertia and inertial defects of the three species of aminoacetonitrile which have been studied are given in table VIII.

TABLE VIII

Ground State Moments of Inertia and inertial defects of the various species of aminoacetonitrile (a.m.u. \AA^2).

	I_A	I_B	I_C	Δ
$\text{NH}_2\text{CH}_2\text{CN}$	16.7131	106.1805	117.2700	- 5.6238
$\text{NHD CH}_2\text{CN}$	18.3293	109.1489	120.6921	- 6.7862
$\text{ND}_2\text{CH}_2\text{CN}$	19.8278	112.2096	123.8433	- 8.1941

The coordinates of the amino hydrogen atoms were located in the principal axis system of $\text{NH}_2\text{CH}_2\text{CN}$ by using the differences in moments of inertia of the species $\text{NH}_2\text{CH}_2\text{CN}$ and $\text{NHD CH}_2\text{CN}$, and

Kraitchman's equations for a non-planar asymmetric top⁵. The resulting coordinates are :

$$\begin{aligned} a_H &= -1.5367 \text{ \AA} \\ b_H &= -1.0134 \text{ \AA} \\ c_H &= \pm 0.8182 \text{ \AA} \end{aligned}$$

A check on these coordinates was obtained by using the differences in moments of inertia between $\text{NH}_2\text{CH}_2\text{CN}$ and $\text{ND}_2\text{CH}_2\text{CN}$. It is convenient to express these differences in the following way :

$$\begin{aligned} \Delta I_a' &= \Delta I_a - 2\Delta M C_H^2 \\ \Delta I_b' &= \Delta I_b - 2\Delta M C_H^2 \\ \Delta I_c' &= \Delta I_a' + \Delta I_b' \end{aligned} \quad (9)$$

where ΔI_i are the observed differences in moments of inertia, $\Delta M = M_D - M_H$, and C_H is the C coordinate of the amino hydrogen atom. The $\Delta I_i'$ may now be used with Kraitchman's equations for a planar asymmetric top to evaluate the hydrogen atom coordinates with the following results :

$$\begin{aligned} a_H &= -1.5464 \text{ \AA} \\ b_H &= -0.9782 \text{ \AA} \\ c_H &= \pm 0.7989 \text{ \AA} \end{aligned}$$

Since no μ_b transitions have been assigned for the species $\text{ND}_2\text{CH}_2\text{CN}$ the value of I_a for this species can only be considered accurate to ± 0.02 a.m.u. \AA^2 . This leads to a large error on ΔI_a in equations (9) and thus to rather poorly determined coordinates. The error in these coordinates can be as large as ± 0.02 \AA .

It is clear therefore that the most reliable set of coordinates for the amino hydrogen atoms is that obtained from the combination $\text{NH}_2\text{CH}_2\text{CN} - \text{NHD CH}_2\text{CN}$.

Calculation of the coordinates of these hydrogen atoms in the principal axis system of the trans conformer of the model given in table I leads to the results :

$$\begin{aligned} a'_H &= -1.5900 \text{ \AA} \\ b'_H &= -1.0088 \text{ \AA} \\ c'_H &= \pm 0.8113 \text{ \AA} \end{aligned}$$

The agreement with the experimental results is fairly good. The coordinates of these atoms for the corresponding cis and gauche conformers are clearly very different from those given above. It is therefore concluded that the observed microwave spectra are those resulting from the trans conformer.

This conclusion is in accord with the nature of the observed spectra. If the molecule existed in the gauche form the two

amino hydrogen atoms would be non-equivalent and the spectrum of the mono-deuterated species would have been correspondingly more complicated.

Confirmation for the deduced conformation is found in the qualitative analysis of the quadrupole hyperfine pattern of the $1_{01} - 0_{00}$ transition shown in fig. 2. The fact that χ_{aa} for the amino nitrogen atom appears to have a negative sign suggests that the lone pair electrons of this atom are approximately aligned along the a inertial axis of the molecule. This could only arise for the trans conformer of fig. 1.

It is instructive to compare these results with the almost identical conclusions of Bolton, Owen and Sheridan regarding the conformation of propargylamine⁶. Although only the normal species has been studied the indications are clear that the molecule occupies what has been defined in fig. 1. as the trans conformation.

In the microwave spectrum of ethyl cyanide¹ it was found that perturbations resulting from a Coriolis interaction between the C - C - N bend and the methyl torsional mode produced an anomalous pattern of vibrational satellites. From a very brief investigation of the vibrational satellite pattern of the normal species of aminoacetonitrile it seems likely that a similar effect

is operating in this molecule. An investigation of any line splitting which may be present in the excited state lines may lead to information regarding torsional motion of the amine group.

REFERENCES

1. V.W. Laurie, J. Chem. Phys., 31, 1500, (1959)
2. D.R. Lide, Jr., J. Chem. Phys., 27, 343, (1957)
3. S.R. Polo, Canad. J. Phys., 35, 880, (1957)
4. J.K. Tyler, Ph.D. Thesis, University of Birmingham, (1960)
5. J. Kraitchman, Am. J. Phys., 21, 17 (1953)
6. K. Bolton, N.L. Owen and J. Sheridan, Nature, 217, 164, (1968).

CHAPTER 6.

Chemical Preparations

In this chapter details are given of the preparation of the compounds and their isotopic species whose microwave spectra have been discussed earlier in this thesis. For precise details of reaction conditions and precautions the original papers should be consulted.

Only preparations which have been carried out by the author are included.

1. Cyanamide.

a) NH_2CN^1

Cyanamide was prepared from crude calcium cyanamide which has been previously washed with ether. 10 gms. of calcium cyanamide was placed in a beaker containing 30 ml. of ether. The beaker was placed in an ice bath and 1:1 sulphuric acid slowly added until the solution became slightly acidic (pH~5).



The solution was filtered, dried over anhydrous sodium sulphate and cleaned with animal charcoal. On evaporation of the ether under reduced pressure white crystalline cyanamide was obtained.

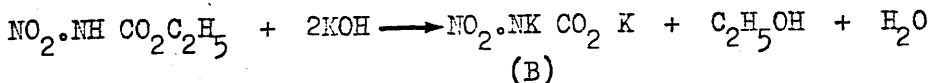
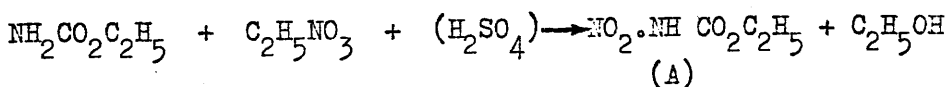
Cyanamide dimerises in acid or alkaline solution and at temperatures above 70°C but it may be effectively stored in a vacuum desiccator over calcium chloride for long periods without deterioration.

b) ND₂CN²

It is possible to obtain an almost 100% deuterated sample of ND₂CN simply by dissolving 0.2 g of NH₂CN in 2 mls of D₂O and evaporating the resulting solution to dryness under vacuum.

2. Nitramide.

Nitramide was prepared by the method of Marlies, La Mer, and Greenspan³. The reaction sequence is as follows:



It should be noted that slight variations in procedure markedly affect the yield and that purity of the solvents used

used is essential. For details of the essential precautions the original paper should be consulted.

To a beaker immersed in an ice/salt bath were added 125 ml of concentrated sulphuric acid and 25 gms of ethyl carbamate. After stirring, the mixture was cooled to -5°C and 28 gm of ethyl nitrate were added. The mixture was stirred for $1\frac{1}{2}$ hours and then poured over 0.4 Kgms of crushed ice. The solution was extracted with 200 ml portions of ether.

The ethereal extract was added to 25 mls of concentrated ammonium hydroxide diluted with 50 mls of water and 25 mls of crushed ice. The aqueous layer was then drawn off, and checked for the required alkalinity.

A mixture of 25 mls of concentrated sulphuric acid and 75 gms of crushed ice was added to the ammoniacal solution and the resulting solution extracted with alcohol free ether. The combined extracts were dried over calcium chloride. This solution, after filtration, was diluted with 75 mls of ether and treated with excess liquid ammonia. Ammonium nitrourethane (A) was precipitated, filtered off, and dried.

15 gm of powdered ammonium nitrourethane were added to a mixture of 25 mls of water and 25 mls of methanol. After cooling to 5°C this solution was poured into a cooled solution

of 125 gms of potassium hydroxide in 500 mls of methanol with continuous stirring. The mixture was kept in an ice bath for two hours and stirred continuously.

The mixture was then filtered and the solid washed with cold ethanol. The precipitate was then dried by drawing air through it, in the filter funnel. Since the filtrate will still contain some alcohol and tends to decompose under these circumstances, all the alcohol must be removed by evaporation in a vacuum desiccator.

The potassium nitrocarbamate (B) thus obtained is very unstable being affected by moisture, heat and carbon dioxide. It should therefore be used immediately after its preparation if possible.

2 gms of potassium nitrocarbamate were added slowly to cooled dilute sulphuric acid the solution being stirred continuously. 3 mls of water were then added followed by 15 mls of ether. The flask was then immersed in a cold bath until the water layer was completely frozen and the ether layer was decanted off.

The ether was then slowly evaporated off until nitramide precipitated. The precipitate was filtered and washed with pet-ether and the product dried by drawing air through the

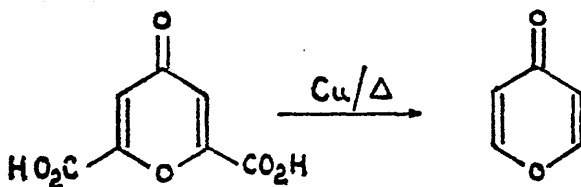
filter funnel. The yield of nitramide was ~0.1g and could be stored in a desiccator over phosphorous pentoxide for a considerable time without decomposition.

3. Y-Pyrone.

a) 4H - Y Pyrone.

Of the preparations of Y-Pyrone^{4,5} by far the simplest and quickest is that described in ref. 5.

A 1:2 weight/weight mixture of dry chelidonic acid and precipitated black copper powder was dry distilled in a retort from a Wood's metal bath. The temperature of the metal bath was raised to 340°C over a period of one hour. The crude distillate was then refluxed in benzene in a Dean and Stark apparatus to remove traces of water.



After removal of the benzene under vacuum the residue was distilled at 108°C/12 m.m. of mercury to give a clear liquid which, on cooling, crystallises to give white crystalline Y-Pyrone. (m.p. 31°C, yield 33%).

γ - Pyrone is extremely deliquescent and must at all times be stored under vacuum in a desiccator.

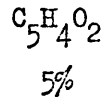
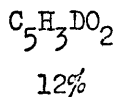
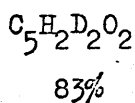
b) 3:5 d₂ γ - Pyrone.

The sample of 3:5 d₂ γ - Pyrone was prepared by the following method^{6,7,8}.

0.4 gm of γ - Pyrone were added to 2.4 gms of 98% enriched D₂O and the solution made slightly acidic (pH ~ 6 - 7) with dilute hydrochloric acid. The solution was then refluxed for 36 hours at 95°C.

After extracting the γ - Pyrone from the aqueous solution into ether, the ethereal solution was dried over anhydrous magnesium sulphate. On removal of the ether under vacuum ~0.2 gms of product were obtained.

The expected composition of the product was

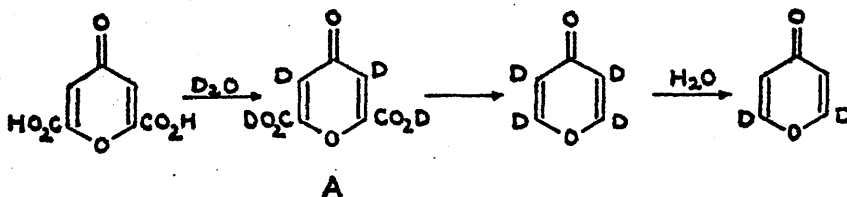


The microwave spectrum of the sample showed no sign of any lines arising from the mono-deuterated species suggesting that very little of this species had in fact been formed.

c) 2:6 d₂ γ - Pyrone.

Although the 3:5 hydrogen atoms α to the carbonyl group in γ - Pyrone are sufficiently labile to be exchanged directly with deuterium as described in (b), the 2:6 hydrogen atoms cannot be replaced so directly, The method used here is that suggested by Lord and Phillips⁷.

Chelidonic acid was recrystallised several times from water and finally from 98% D₂O. The sample was dried at 110° for 24 hours in an atmosphere of nitrogen. 10 gms of this material were dissolved in a mixture of 98% D₂O (150g) and dioxan in a closed system under a positive pressure of nitrogen. The resulting solution was warmed for 72 hours at 85°C. The D₂O was removed by vacuum distillation and the residue obtained dried at 100°C in a stream of nitrogen to give 10 gms of product A.



The deuterated chelidonic acid (A) thus obtained was then converted to γ - Pyrone d₄ by the method described in section a.

0.037 moles of γ -Pyrone d_4 were then heated with one equivalent of water for 24 hours at 95°C . This replaced most of the d -atoms α to the carbonyl group by hydrogen atoms. The yield from this latter stage is low (2.2 gm) due to hydrolysis of the γ -Pyrone on heating with water.

d) O^{18} γ -Pyrones.

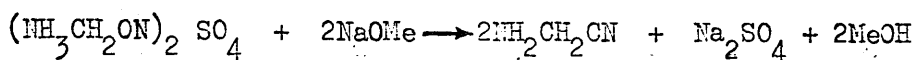
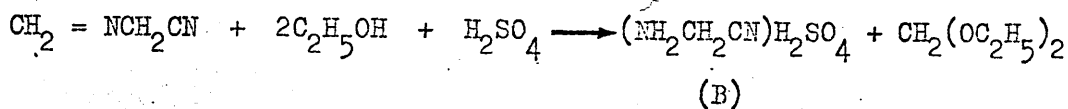
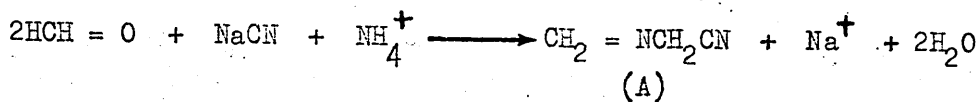
The preparation of O^{18} substituted γ -Pyrones is again described in ref. 6.

0.234 gms of γ -Pyrone were dissolved in 1 gm of 62% enriched H_2O^{18} and dilute hydrochloric acid added until $\text{pH} \sim 3$. The solution was refluxed for 26 hours at 98°C . The work-up was identical with that described above for the deuterated species and gave 0.1 gm of product with the expected composition, $C_5H_4O_2$ (86%) and $C_5H_4O^{16}O^{18}$ (13%). The microwave spectra of the two mono-substituted O^{18} species were of similar intensity suggesting equal distribution of O^{18} between the two most probable species.

4. Aminoacetonitrile.

a) NH_2CH_2CN ^{9,10,11.}

The reaction sequence for the preparation of this compound is as follows.



In this preparation there are again a number of precautions which must be observed. These are given in detail in ref. 9.

The preparation of the intermediate methylene aminoacetonitrile (a) was carried out by the method given in ref. 9. In a flask immersed in an ice/salt bath were placed 375 mls of technical formaldehyde and 135 gms of ammonium chloride. The temperature of the contents of the flask was maintained at 0°C throughout the reaction. Stirring was commenced and a solution of 120 gms of sodium cyanide in 210 mls of water was slowly dropped into the solution.

When one half of the sodium cyanide solution had been added, the addition of 95 mls of glacial acetic acid was begun in such a way that the addition of acid and sodium cyanide solution were completed at the same time.

After about two hours continuous stirring the methylene aminoacetonitrile was filtered off. (yield 80 gms.)(m.p.129°).

For the preparation of aminoacetonitrile the procedure of ref.11 was followed in favour of that of ref.10.

50 mls of concentrated sulphuric acid was added to 250 mls of ethanol and the solution maintained at a temperature of 45°C. 70 gms of methylene aminoacetonitrile were rapidly added and the flask shaken vigorously until it dissolved. After a short period of cooling crystals separated and were filtered off and washed with ethanol. These are crystals of the salt $(\text{NH}_2\text{CH}_2\text{CN}) \text{H}_2\text{SO}_4 \cdot (\text{B})$.

The product was dissolved in water (10 mls) and the solution run into 30 mls of stirred 95% ethanol. The neutral sulphate $(\text{NH}_3\text{CH}_2\text{CN})_2 \text{SO}_4$ was precipitated. The sulphate was finely powdered, covered with methanol containing a trace of phenolphthalein and neutralised by adding a solution of 3 gms of sodium in 80 mls of methanol to the mixture under an atmosphere of nitrogen. Sodium sulphate was filtered off and the filtrate evaporated at room temperature under vacuum. The resulting aminoacetonitrile is a colourless liquid which may be distilled easily in a vacuum system and may be stored for long periods under nitrogen and at 0°C.

b) NHD CH₂CN

A sample of 0.3 gms of aminoacetonitrile was mixed with an equal volume of 98.8% CH₃OD, the flask evacuated and left for 48 hours. The methanol was then evaporated off under vacuum. The infra-red spectrum of the product had strong peaks corresponding to the ND stretching and bending modes. The product obtained by this method contains NH₂CH₂CN and NHD CH₂CN.

c) ND₂CH₂CN

This compound is most readily prepared simply by mixing a small sample of D₂O vapour and NH₂CH₂CN vapour in the waveguide absorption cell. The microwave spectrum of the product shows both NHD CH₂CN and ND₂CH₂CN in about equal concentrations.

REFERENCES.

1. Colucci, Chem. Abs., 2396⁹ (1947)
2. J. K. Tyler, Ph.D. Thesis, University of Birmingham (1960)
3. C. A. Marlies, V. K. La Mer and J. Greenspan, "Inorganic Sythesis", vol. I, 68, McGraw Hill, New York (1939)
4. E. R. Reigel and F. Zwillgneyer, "Organic Synthesis", vol. II, 126, J. Wiley & Sons (1943)

References (Cont'd.)

5. N.M.D. Brown, Private communication.
6. P. Beak and G.A. Carls, J. Org. Chem., 29, 2678, (1964)
7. R. C. Lord and W. D. Phillips, J. Am. Chem. Soc., 74, 2429 (1952)
8. D. W. Mayo, P. J. Sapienza, R. C. Lord and W. D. Phillips, J. Org. Chem., 29, 2682 (1964)
9. R. Adams and W. D. Langley, "Organic Synthesis" vol. I, p.298, J. Wiley & Sons (1932)
10. W. K. Anslow and H. King, "Organic Synthesis" vol.I, p.298, J. Wiley & Sons (1932)
11. A. H. Cook, I. Heilbron and A. L. Lewy, J. Chem. Soc., 1, 201, (1948)

APPENDIX A.

The Secular Determinants for ^{14}N - Quadrupole Coupling Energies
in molecules containing two Nitrogen Atoms.

Since the determinants are symmetrical about the leading diagonal the off - diagonal elements are listed once only, Where appropriate the elements are labelled as elements of an array A [i , j] .

$$F = |J + 2|$$

$$C(J + 1, J + 1)^2 E_2(J + 1) + E_1(J + 1) - E$$

$$F = |J + 1|$$

$$C(J, J)^2 E_2(J) + C(J, J + 1)^2 E_2(J + 1) + E_1(J) - E \quad 1,1$$

$$C(J, J) C(J + 1, J) E_2(J) + C(J, J + 1) C(J + 1, J + 1) \\ \times E_2(J + 1) \quad 1,2$$

$$C(J + 1, J + 1)^2 E_2(J + 1) + C(J + 1, J)^2 E_2(J) \\ + E_1(J + 1) - E. \quad 2,2$$

$$F = |J|$$

$$C(J-1, J-1)^2 E_2(J-1) + C(J-1, J)^2 E_2(J) + C(J-1, J+1)^2 \\ \times E_2(J + 1) + E_1(J - 1) - E. \quad 1,1$$

$$C(J-1, J-1) C(J, J-1) E_2(J-1) + C(J-1, J) C(J, J) E_2(J) \\ + C(J-1, J+1) C(J, J+1) E_2(J+1) \quad 1,2$$

Appendix A (Cont'd.)

$$C(J-1, J-1)C(J+1, J-1)E_2(J-1) + C(J-1, J)C(J+1, J)E_2(J) \\ C(J+1, J+1)C(J-1, J+1)E_2(J+1) \quad 1,3$$

$$C(J, J-1)^2 E_2(J-1) + C(J, J)^2 E_2(J) + C(J, J+1)^2 E_2(J+1) \\ + E_1(J) - E. \quad 2,2$$

$$C(J, J-1)C(J+1, J-1)E_2(J-1) + C(J, J)C(J+1, J)E_2(J) + C(J, J+1)C(J+1, J+1) \\ \times E_2(J+1) \quad 2,3$$

$$C(J+1, J-1)^2 E_2(J-1) + C(J+1, J)^2 E_2(J) + C(J+1, J+1)^2 E_2(J+1) \\ + E_1(J+1) - E. \quad 3,3$$

$$\underline{F = |J - 1|}$$

$$C(J, J)^2 E_2(J) + C(J, J-1)^2 E_2(J-1) + E_1(J) - E. \quad 1,1$$

$$C(J, J)C(J-1, J)E_2(J) + C(J, J-1)C(J-1, J-1)E_2(J-1) \quad 1,2$$

$$C(J-1, J)^2 E_2(J) + C(J-1, J-1)^2 E_2(J-1) + E_1(J-1) - E. \quad 2,2$$

$$\underline{F = |J - 2|}$$

$$C(J-1, J-1)^2 E_2(J-1) + E_1(J-1) - E.$$

The significance of the symbols used is explained in the

text of chapter 3.

A computer program was written in KDF9 Algol which sets up and diagonalises the energy matrices listed above for any given set of coupling constants. It will then output the coupling energies labelled by the appropriate F value for any selected energy level.

The diagonalisation procedure used is that due to Jacobi. Although this procedure is basically a slow one in terms of computer time taken for a given size of matrix, this is not a serious disadvantage in this case since the largest matrix to be diagonalised is 3×3 . The procedure does have the considerable advantage that the matrices are not in any way disordered in the diagonalisation process, thus the eigenvalues can be readily assigned the appropriate F value.

The program may be used to predict line splittings in the spectrum of any molecule containing up to two nitrogen atoms. If only one nitrogen atom is present then one of the other sets of coupling constants is simply set to zero.

APPENDIX B.

Extended Perturbation Treatment of the Stark Effect in γ -Pyrone.

As described in chapter 2 a computer program was written which sets up and diagonalises a rather special form of the Stark energy matrix for an asymmetric top molecule. On the diagonal of the energy matrix are unperturbed rigid rotor energies for the levels under consideration, and the off-diagonal elements are the Stark connections applicable to a particular case.

In the program, which is written in KDF9 Algol, the rigid rotor energies are computed by the method described in chapter 1 and the off-diagonal Stark connections are calculated by the method outlined in chapter 2.

The diagonalisation procedure used is that of Jacobi, although, in terms of computing time taken for a diagonalisation this is highly inefficient in the case of γ -Pyrone. For most energy level manifolds it is fairly obvious which levels are mainly responsible for the breakdown of second order perturbation theory and thus, since only these levels need be included in the matrix, the size of the matrix can be kept quite small. However for γ -Pyrone where this is not at all obvious the size of the matrix can become very large (50 x 50 would not be unusual) and the time taken in diagonalisation becomes correspondingly large.

Appendix B (Cont'd.)

Since a great many of the elements of the matrix are in fact zero the Jacobian diagonalisation procedure takes much longer than is really necessary. Once again however the advantage of keeping the matrix ordered in the diagonalising process enables the eigenvalues for the perturbed levels to be readily associated with their counterparts for the unperturbed levels.

For selected values of the quantum number M , the dipole moment and the applied field the program will output the perturbed and unperturbed energies of all the levels included in the matrix.

APPENDIX. C.

Points on the graph of $\frac{\Delta\nu}{J+1} / (J+1)^2$ for the μ_c Q - branch series

$J_{1,J} - J_{2,J-2}$ (Mc/s)		
<u>ND₂CN</u>		
J	$\Delta\nu$	$\frac{\Delta\nu}{J+1}$
2	541.87	180.62
3	726.80	181.70
4	916.10	183.22
5	1108.70	184.78
6	1305.80	186.54
7	1508.30	188.53
8	1715.15	190.56
9	1927.20	192.75
10	2144.20	194.93
11	2364.03	197.00
12	2585.41	198.88
13		